

**CHARACTERIZATION OF CAVITY-BACKED FOLDED SLOT  
ANTENNAS**

By

María Fernanda Córdoba-Erazo

A thesis submitted in partial fulfillment of the requirements for the degree of

**MASTER OF SCIENCE**

in

**ELECTRICAL ENGINEERING**

**UNIVERSITY OF PUERTO RICO  
MAYAGÜEZ CAMPUS**

June, 2009

Approved by:

\_\_\_\_\_  
José Colóm Ustariz, Ph.D.  
Member, Graduate Committee

\_\_\_\_\_  
Date

\_\_\_\_\_  
Henrick Mario Ierkic Vidmar, Ph.D.  
Member, Graduate Committee

\_\_\_\_\_  
Date

\_\_\_\_\_  
Rafael Rodríguez Solís, Ph.D.  
President, Graduate Committee

\_\_\_\_\_  
Date

\_\_\_\_\_  
Anand D. Sharma, Ph.D.  
Representative of Graduate Studies

\_\_\_\_\_  
Date

\_\_\_\_\_  
Isidoro Couvertier, Ph.D.  
Chairperson of the Department

\_\_\_\_\_  
Date

Abstract of Dissertation Presented to the Graduate School  
of the University of Puerto Rico in Partial Fulfillment of the  
Requirements for the Degree of Master of Science

## **CHARACTERIZATION OF CAVITY-BACKED FOLDED SLOT ANTENNAS**

By

María Fernanda Córdoba-Erazo

June 2009

Chair: Rafael Rodríguez Solís

Major Department: Electrical and Computer Engineering

In this thesis, two Cavity-Backed Folded-Slot Antennas (CBFSA's) are characterized through the Design Of Experiments technique (DOE) to study the influence that the Folded-Slot Antennas (FSA) and cavity dimensions of each CBFSA have on the following responses: resistance, frequency, reflection coefficient and gain in the substrate and cavity side. The antennas characterized were: the CPW-capacitively fed CBFSA and the CPW-inductively fed CBFSA. Two  $2^k$  factorial DOE's are proposed for performing the characterization of each antenna. The designs proposed in the DOE's are simulated in the High Frequency Structure Simulator (HFSS) and the results obtained were statistically analyzed. Linear regression models for each response of the CBFSA's are presented. Some CBFSA designs were fabricated in order to validate the simulations. The CPW-inductively fed CBFSA achieves gain of 4.28 dB and reflection coefficient  $< 0.33$  or VSWR  $< 2$  at 4.5 GHz, whereas

the CPW-capacitively fed CBFSAs achieve a gain of 4.63 dB and reflection coefficient  $< 0.33$  or VSWR  $< 2$  at 4.5 GHz. The radiation patterns of the antennas are uni-directional and Front-to-Back-Ratio (FBR) about 15 dB is obtained.

Resumen de Disertación Presentado a Escuela Graduada  
de la Universidad de Puerto Rico como requisito parcial de los  
Requerimientos para el grado de Maestría en Ciencias

## **CARACTERIZACIÓN DE ANTENAS DE RANURA PLEGADA CUBIERTAS POR UNA CAVIDAD**

Por

María Fernanda Córdoba-Erazo

Junio 2009

Consejero: Rafael Rodríguez Solís  
Departamento: Ingeniería Eléctrica y Computadoras

En esta tesis, dos antenas de ranura cubiertas por una cavidad (CBFSA's) son caracterizadas usando la técnica de Diseño de Experimentos (DOE) con el fin de estudiar la influencia que tienen las dimensiones de la antena de ranura plegada (FSA) y la cavidad sobre las siguientes respuestas: resistencia, frecuencia, coeficiente de reflexión y ganancia en el lado del sustrato y de la cavidad. Las antenas que serán caracterizadas son: la antena de ranura cubierta por una cavidad alimentada capacitivamente por una CPW y la antena de ranura cubierta por una cavidad alimentada inductivamente por una CPW. Dos diseños factoriales  $2^k$  se proponen para caracterizar cada una de las antenas. Los diseños propuestos en el DOE fueron simulados en el simulador de estructuras de alta frecuencia (HFSS) y los resultados obtenidos fueron analizados estadísticamente. Se presentan modelos de regresión lineal para cada una de las respuestas de las CBFSA's. Algunos diseños de antenas fueron fabricados con el fin de validar las simulaciones. La antena de ranura plegada cubierta por una cavidad alimentada inductivamente por una CPW obtuvo una

ganancia de 4.28 dB y un coeficiente de reflexión  $< 0.33$  o  $VSWR < 2$  a 4.5 GHz, mientras que la antena de ranura plegada cubierta por una cavidad alimentada capacitivamente por una CPW obtuvo una ganancia de 4.63 dB y un coeficiente de reflexión  $< 0.33$  o  $VSWR < 2$  a 4.5 GHz. Los patrones de radiación de las antenas son uni-direccionales y la razón de radiación frontal a la posterior obtenida es aproximadamente 15 dB.

Copyright © 2009

by

María Fernanda Córdoba-Erazo

*A la memoria de mi amadísima madre.*

## ACKNOWLEDGMENTS

I would like to say thanks to my advisor, Dr. Rafael Rodríguez Solís, for giving me the opportunity to learn about electromagnetics since I started my M.S.E.E studies, for teaching me how the amazing microwave equipments work, for trusting me and for his guidance during this thesis work. Special thanks to Dr. José Colóm Ustariz for giving me the opportunity to be his teaching assistant and for providing me the economical support during this last year.

I also express my gratitude to my committee professors: Dr. José Colóm Ustariz and Dr. Henrick Mario Ierkic Vidmar. I would also like to thank Sandra Montalvo, because she made me feel comfortable since I arrive to Puerto Rico. Thanks for all the encouraging words and advice. To the Electrical Engineering Department for giving me the opportunity to carry out graduate studies at the UPRM campus, which had not been possible without their support.

Thanks to my uncle Edgar, for giving me his unconditional support and love from the distance. To Jaime Di Cristina, for his advice and comments, to Leidy, for her friendship and for sharing with me all difficult and great moments during this time and through the last nine years.

Finally, I would like to express my gratitude to Horacio for his love, patience and advice.

## TABLE OF CONTENTS

	<u>page</u>
ABSTRACT ENGLISH . . . . .	ii
ABSTRACT SPANISH . . . . .	iv
ACKNOWLEDGMENTS . . . . .	viii
LIST OF TABLES . . . . .	xi
LIST OF FIGURES . . . . .	xiii
<b>1 INTRODUCTION . . . . .</b>	<b>1</b>
1.1 Objectives . . . . .	2
1.2 Work organization . . . . .	2
<b>2 LITERATURE REVIEW AND BACKGROUND . . . . .</b>	<b>4</b>
2.1 Coplanar waveguide . . . . .	4
2.2 CPW-fed folded-slot antenna . . . . .	9
2.3 Cavity-baked slot antenna . . . . .	14
2.4 Rectangular resonant cavity . . . . .	24
2.5 Design of experiments . . . . .	25
2.5.1 Design of experiments applied to characterization of antennas	26
<b>3 METHODOLOGY . . . . .</b>	<b>28</b>
3.1 Design procedure . . . . .	28
3.1.1 Substrate selection . . . . .	32
3.1.2 Cavity selection . . . . .	32
3.1.3 CPW feed design . . . . .	33
3.2 CPW-inductively fed cavity-backed folded-slot antenna structure .	33
3.3 CPW-capacitively fed cavity-backed folded-slot antenna structure	37
<b>4 SIMULATION AND EXPERIMENTAL RESULTS . . . . .</b>	<b>47</b>
4.1 Results . . . . .	47
4.1.1 DOE I simulation results . . . . .	50
4.1.2 DOE II simulation results . . . . .	67
4.1.3 DOE III simulation results . . . . .	82
4.1.4 DOE IV simulation results . . . . .	94
4.2 Examples of CBFSA's designs with $\Gamma < 0.33$ at 5 GHz . . . . .	104

4.3	Experimental results . . . . .	107
5	CONCLUSION AND SUGGESTIONS FOR FUTURE WORK . . . . .	120
5.1	Suggestions for future work . . . . .	122
	APPENDIX A . . . . .	123

LIST OF TABLES

Table	page
3-1 Factors and levels for DOE I . . . . .	34
3-2 Resonant Frequencies for the $TE_{mnp}$ modes . . . . .	34
3-3 Design matrix and dimensions of the experiments ( $2_V^{5-1}$ fractional factorial design) . . . . .	35
3-4 Coded factors of the experiments ( $2_V^{5-1}$ fractional factorial design, using I=ABCDE) . . . . .	36
3-5 Factors and levels for DOE II . . . . .	37
3-6 Design matrix and dimensions of the experiments ( $2_{VII}^{7-1}$ fractional factorial design) . . . . .	38
3-6 Design matrix and dimensions of the experiments ( $2_{VII}^{7-1}$ fractional factorial design) . . . . .	39
3-6 Design matrix and dimensions of the experiments ( $2_{VII}^{7-1}$ fractional factorial design) . . . . .	40
3-7 Coded factors of the experiments ( $2_{VII}^{7-1}$ fractional factorial design) . . . . .	40
3-7 Coded factors of the experiments ( $2_{VII}^{7-1}$ fractional factorial design) . . . . .	41
3-7 Coded factors of the experiments ( $2_{VII}^{7-1}$ fractional factorial design) . . . . .	42
3-8 Factors and levels for DOE III and DOE IV . . . . .	44
3-9 Design matrix and dimensions of the experiments ( $2^3$ factorial design) . . . . .	44
3-10 Coded factors of the experiments ( $2^3$ factorial design) . . . . .	45
3-11 Resonant Frequencies for the $TE_{mnp}$ modes . . . . .	46
4-1 Simulation results for DOE I ( $2_V^{5-1}$ fractional factorial design) . . . . .	51
4-2 Predicted and simulated interest responses for DOE I . . . . .	66
4-3 Simulation results for DOE II ( $2_{VII}^{7-1}$ fractional factorial design) . . . . .	67
4-3 Simulation results for DOE II ( $2_{VII}^{7-1}$ fractional factorial design) . . . . .	68
4-3 Simulation results for DOE II ( $2_{VII}^{7-1}$ fractional factorial design) . . . . .	69

4-4	Predicted and simulated interest responses for DOE II . . . . .	82
4-5	Simulation results for DOE III ( $2^3$ factorial design) . . . . .	83
4-6	Simulation results for DOE IV ( $2^3$ factorial design) . . . . .	94
4-7	Measured Gain and Radiated far fields of the fabricated CBFSA's . . .	118

## LIST OF FIGURES

<u>Figure</u>	<u>page</u>
2-1 Schematic of a CPW with substrate of finite thickness . . . . .	4
2-2 Electric field distribution in the cross section of the CPW . . . . .	5
2-3 Magnetic field distribution of the CPW for the odd mode . . . . .	5
2-4 Schematic of a CPW sandwiched between two dielectric substrates with a cover shield. . . . .	8
2-5 Geometry of the FSA. . . . .	9
2-6 Calculated impedance for a folded-slot and a simple slot design . . . . .	10
2-7 Double FSA design . . . . .	11
2-8 E- and H- radiation patterns of the FSA simulated and fabricated on Alumina substrates . . . . .	12
2-9 Layout of the multiple-slots design and simulation-measurement re- sults of the impedance scaling . . . . .	13
2-10 CPW-capacitively fed FSA . . . . .	14
2-11 Resistance and Reactance of the dielectric filled CBSA . . . . .	16
2-12 Slot geometry . . . . .	18
2-13 Slot backed by a rectangular cavity . . . . .	19
2-14 Cavity backed wide slot antenna . . . . .	21
2-15 Geometry of the CBSA . . . . .	22
2-16 Topology of the reduced-size CBSA . . . . .	23
2-17 Geometry of a rectangular cavity. . . . .	24
3-1 CPW-inductively fed CBFSA . . . . .	29
3-2 CPW-capacitively fed CBFSA . . . . .	30
3-3 CPW-capacitively fed CBFSA . . . . .	31
3-4 Graphical representation of the design matrix of DOE I . . . . .	37

3-5	Graphical representation of the design matrix of DOE II . . . . .	43
3-6	Graphical representation of the design matrix of DOE III and DOE IV . . . . .	45
4-1	Input impedance of a CBFSAs vs Frequency (3 GHz - 6 GHz) . . . . .	48
4-2	Input impedance of a CBFSAs vs Frequency (4.7 GHz - 5 GHz) . . . . .	49
4-3	Reference plane for measurements . . . . .	50
4-4	Normal probability plot of the effects for Rmax in DOE I . . . . .	52
4-5	Normal plot of residuals and residuals versus predicted values for Rmax model of DOE I . . . . .	54
4-6	Normal probability plot of the effects for the frequency at maximum resistance in DOE I . . . . .	55
4-7	Impedance of the CDE design . . . . .	57
4-8	Normal probability plot of the effects for the reactance at $F_R$ in DOE I . . . . .	57
4-9	Normal probability plot of the effects for the magnitude of the reflection coefficient at $F_R$ in DOE I . . . . .	58
4-10	Normal probability plot of the effects for the magnitude of the reflection coefficient at 5 GHz in DOE I . . . . .	60
4-11	Normal probability plot of the effects for the gain in the substrate side at $F_R$ in DOE I . . . . .	61
4-12	2-D and 3-D Radiation patterns plots for CDE design . . . . .	62
4-13	Normal probability plot of the effects for the gain in the cavity side at $F_R$ in DOE I . . . . .	63
4-14	Normal probability plot of the effects for the gain in the substrate side at 5 GHz in DOE I . . . . .	64
4-15	Normal probability plot of the effects for the gain in the cavity side at 5 GHz in DOE I . . . . .	65
4-16	Normal probability plot of the effects for the maximum resistance in DOE II . . . . .	70
4-17	Normal probability plot of the effects for the frequency at maximum resistance in DOE II . . . . .	71
4-18	Impedance plots for CDF, BCD and ABD designs of DOE II . . . . .	72

4-19 Normal probability plot of the effects for the reactance at $F_R$ in DOE II . . . . .	73
4-20 Normal probability plot of the effects for the reflection coefficient at $F_R$ in DOE II . . . . .	74
4-21 Normal probability plot of the effects for the reflection coefficient at 5 GHz in DOE II . . . . .	76
4-22 Normal probability plot of the effects for the gain in the substrate side at $F_R$ in DOE II . . . . .	77
4-23 Normal probability plot of the effects for the gain in the cavity side at $F_R$ in DOE II . . . . .	79
4-24 Normal probability plot of the effects for the gain in the substrate side at 5 GHz in DOE II . . . . .	80
4-25 Normal probability plot of the effects for the gain in the cavity side at 5 GHz in DOE II . . . . .	81
4-26 Normal probability plot of the effects for the maximum resistance in DOE III . . . . .	84
4-27 Normal probability plot of the effects for the frequency at maximum resistance in DOE III . . . . .	85
4-28 Impedance plots of B and AB designs of DOE III . . . . .	86
4-29 Normal probability plot of the effects for the reactance at $F_R$ in DOE III . . . . .	87
4-30 Normal probability plot of the effects for the reflection coefficient at $F_R$ in DOE III . . . . .	88
4-31 Normal probability plot of the effects for the reflection coefficient at 5 GHz in DOE III . . . . .	89
4-32 Normal probability plot of the effects for the gain in the substrate side at $F_R$ in DOE III . . . . .	90
4-33 Normal probability plot of the effects for the gain in the cavity side at $F_R$ in DOE III . . . . .	91
4-34 Normal probability plot of the effects for the gain in the substrate side at 5 GHz in DOE III . . . . .	92
4-35 Normal probability plot of the effects for the gain in the cavity side at 5 GHz in DOE III . . . . .	93

4-36 Normal probability plot of the effects for the maximum resistance in DOE IV . . . . .	95
4-37 Normal probability plot of the effects for the frequency at maximum resistance in DOE IV . . . . .	96
4-38 Impedance plots of B and AB designs of DOE IV . . . . .	97
4-39 Normal probability plot of the effects for the reactance at $F\_R$ in DOE IV . . . . .	98
4-40 Normal probability plot of the effects for the reflection coefficient at $F\_R$ in DOE IV . . . . .	99
4-41 Normal probability plot of the effects for the reflection coefficient at 5 GHz in DOE IV . . . . .	100
4-42 Normal probability plot of the effects for the gain in the substrate side at $F\_R$ in DOE IV . . . . .	101
4-43 Normal probability plot of the effects for the gain in the cavity side at $F\_R$ in DOE IV . . . . .	102
4-44 Normal probability plot of the effects for the gain in the substrate side at 5 GHz in DOE IV . . . . .	103
4-45 Normal probability plot of the effects for the gain in the cavity side at 5 GHz in DOE IV . . . . .	104
4-46 $\Gamma_{5GHz}$ plot for the ABCDE design of DOE I . . . . .	105
4-47 $\Gamma_{5GHz}$ plot for the ABCDE design with $W_{a_2} = 1.6\text{mm}$ . . . . .	106
4-48 $\Gamma_{5GHz}$ plot for the BDEFG design . . . . .	107
4-49 CBFSA's fabricated without adding the cavities . . . . .	108
4-50 CBFSA's fabricated . . . . .	108
4-51 Reflection coefficient measured and simulated for the CDE antenna design. . . . .	109
4-52 Resistance measured and simulated for the CDE antenna design. . . . .	110
4-53 Reactance measured and simulated for the CDE antenna design. . . . .	110
4-54 Reflection coefficient measured and simulated for the BCDFG antenna design. . . . .	111
4-55 Resistance measured and simulated for the BCDFG antenna design. . . . .	112

4-56	Reactance measured and simulated for the BCDFG antenna design. . . . .	112
4-57	Reflection coefficient measured and simulated for the AC antenna design. . . . .	113
4-58	Resistance measured and simulated for the AC antenna design. . . . .	114
4-59	Reactance measured and simulated for the AC antenna design. . . . .	114
4-60	Radiation pattern measured and simulated for the CDE antenna design	116
4-61	Radiation pattern measured and simulated for the BCDFG antenna design . . . . .	116
4-62	Radiation pattern measured and simulated for the BCDFG antenna design . . . . .	117
5-1	Normal plot of residuals and residuals versus predicted values for $F_R$ model of DOE I . . . . .	124
5-2	Normal plot of residuals and residuals versus predicted values for $X_{F_R}$ model of DOE I . . . . .	124
5-3	Normal plot of residuals and residuals versus predicted values for $\Gamma_{F_R}$ model of DOE I . . . . .	125
5-4	Normal plot of residuals and residuals versus predicted values for $\Gamma_{5GHz}$ model of DOE I . . . . .	125
5-5	Normal plot of residuals and residuals versus predicted values for $G_{S_{F_R}}$ model of DOE I . . . . .	126
5-6	Normal plot of residuals and residuals versus predicted values for Rmax model of DOE II . . . . .	126
5-7	Normal plot of residuals and residuals versus predicted values for $F_R$ model of DOE II . . . . .	127
5-8	Normal plot of residuals and residuals versus predicted values for $X_{F_R}$ model of DOE II . . . . .	127
5-9	Normal plot of residuals and residuals versus predicted values for $G_{S_{F_R}}$ model of DOE II . . . . .	128
5-10	Normal plot of residuals and residuals versus predicted values for $G_{C_{F_R}}$ model of DOE II . . . . .	128
5-11	Normal plot of residuals and residuals versus predicted values for $G_{C_{5GHz}}$ model of DOE II . . . . .	129

5-12 Normal plot of residuals and residuals versus predicted values for Rmax model of DOE III . . . . .	129
5-13 Normal plot of residuals and residuals versus predicted values for $F_R$ model of DOE III . . . . .	130
5-14 Normal plot of residuals and residuals versus predicted values for $X_{F_R}$ model of DOE III . . . . .	130
5-15 Normal plot of residuals and residuals versus predicted values for $\Gamma_{F_R}$ model of DOE III . . . . .	131
5-16 Normal plot of residuals and residuals versus predicted values for $G_{S_{5GHz}}$ model of DOE III . . . . .	131
5-17 Normal plot of residuals and residuals versus predicted values for $G_{C_{5GHz}}$ model of DOE III . . . . .	132
5-18 Normal plot of residuals and residuals versus predicted values for Rmax model of DOE IV . . . . .	132
5-19 Normal plot of residuals and residuals versus predicted values for $F_R$ model of DOE IV . . . . .	133
5-20 Normal plot of residuals and residuals versus predicted values for $X_{F_R}$ model of DOE IV . . . . .	133
5-21 Normal plot of residuals and residuals versus predicted values for $\Gamma_{F_R}$ model of DOE IV . . . . .	134
5-22 Normal plot of residuals and residuals versus predicted values for $\Gamma_{5GHz}$ model of DOE IV . . . . .	134
5-23 Normal plot of residuals and residuals versus predicted values for $G_{S_{F_R}}$ model of DOE IV . . . . .	135
5-24 Normal plot of residuals and residuals versus predicted values for $G_{C_{F_R}}$ model of DOE IV . . . . .	135
5-25 Normal plot of residuals and residuals versus predicted values for $G_{S_{5GHz}}$ model of DOE IV . . . . .	136
5-26 Normal plot of residuals and residuals versus predicted values for $G_{C_{5GHz}}$ model of DOE IV . . . . .	136

# CHAPTER 1

## INTRODUCTION

Advances in portability and miniaturization in microwave antennas have occurred for the past century. These advances have been influenced by the progress in computer technology and electronic circuits fabrication, which have allowed the integration of the antennas in communication radar systems, and Radio Frequency IDentification (RFID). Slot and folded-slot antennas are part of these promising antennas due to their light weight, low volume, low cost, conformal configuration and compatibility with integrated circuits, which make them suitable for applications in portable communication systems, Monolithic Microwave Integrated Circuits (MMICs), aircraft, spacecraft and satellites.

Folded slot antennas (FSA's) offer some of the attractive characteristics of the slot antennas, such as small size, light weight, and the capability to be flush-mounted on surfaces. They also present an input impedance about four times lower than the slot antenna at the first useful resonance ( $f_0$ ) [1], facilitating the matching to  $50 \Omega$  and providing a wider bandwidth. However, FSA's, as well as slot antennas, are free to radiate from both sides of the substrate. This could limit their applications in multilayer circuits, near metallic objects or even near the earth.

Placing a cavity behind the slot focuses the antenna radiation on one side of the substrate, suppressing backward radiation. This configuration is known as a cavity backed slot antenna (CBSA). Although there are many works related with CBSA's, to the knowledge of the author, studies about Cavity-Backed Folded-Slot antennas CBFSA's have not been reported and there is no information about their input

impedance, bandwidth and radiation characteristics. Since FSA's have the aforementioned desirable characteristics, CBFSA's with shallow cavities (thickness  $< \frac{\lambda_d}{4}$ ), could be of great interest in antennas miniaturization, wireless devices, active and passive arrays, ground penetrating radars and airborne devices due to their compact size, flush-mounting capability, light weight and unidirectional pattern.

### 1.1 Objectives

The main goal of this work is to characterize a CPW-fed CBFSA through the study of the influence that the dimensions of the FSA and cavity have on the radiation pattern, reflection coefficient  $\Gamma$ , gain on the substrate and cavity side and input impedance. It is desirable for most of the applications that the antenna is matched to  $50 \Omega$ . Therefore, once the characterization of the antenna is performed, CBFSA designs that achieve the goal  $\Gamma < 0.33$  at the operation frequency of 5 GHz are presented. Simulation and experimental results will be compared in order to validate the simulations.

### 1.2 Work organization

This thesis is organized as follows. Theory about the operation and characteristics of coplanar waveguide (CPW) transmission lines, CPW-fed folded-slot antennas, rectangular cavities, Design of Experiments (DOE) techniques, as well as, a literature review about previous works related to the cavity-backed slot antennas are presented in Chapter 2.

Chapter 3 presents how the CPW-fed CBFSA is designed and the designs of experiments used to determine the influence that the FSA and cavity dimensions have on the responses of interest.

Chapter 4 presents and discusses the simulation results of the experiments proposed, as well as a study about the parameters that affect the antenna responses. Details about simulation, fabrication and testing of the antennas are included.

The last chapter includes the conclusions and recommendations for future work.

# CHAPTER 2

## LITERATURE REVIEW AND BACKGROUND

This chapter begins with a review about the Coplanar Waveguide (CPW) transmission line, which is the antenna feed used in this work and is one of most popular transmission lines used in microwave circuits and antennas. Later, a literature review about previous work related with CPW-FSA's and CBSA's is presented. These works summarize the state of the art on the cavity-backed slot antennas which could serve as starting point in the understanding and design of CBFSA'. Information about rectangular cavities as well as design of experiments is presented at the end of this chapter.

### 2.1 Coplanar waveguide

The CPW was introduced by C.Wen in 1969 [2], and consists of three conductors printed on a dielectric substrate with thickness  $h$ ; the central conductor width is denoted by  $S$  and corresponds to the signal line, and the others correspond to ground. The slots width are denoted by  $W$  as shown in the Figure 2-1.

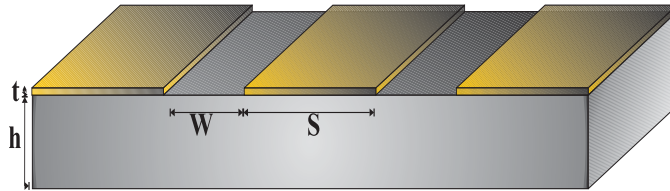


Figure 2-1: Schematic of a CPW with substrate of finite thickness

The equations of the components of the electric and magnetic fields expressions were found by R. N. Simmons and R. K. Arora in 1982 [3]. The distribution of the electric and magnetic fields shown in Figure 2-2 and Figure 2-3 are also presented

in [3]. There are two propagation modes supported by the CPW: an odd mode and an even mode, also called CPW-mode and coupled slot-line mode, respectively. The slot-line mode is excited in the CPW when discontinuities or asymmetries are present in the geometry.

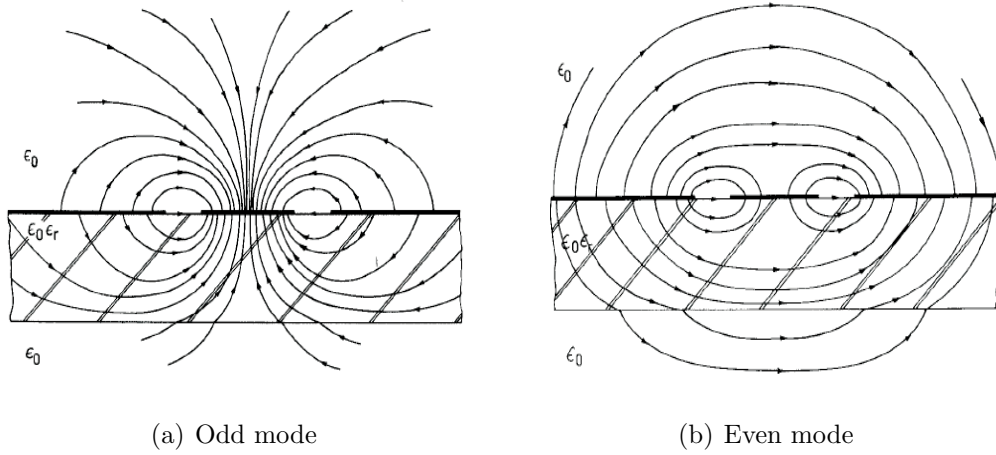


Figure 2-2: Electric field distribution in the cross section of the CPW for the: (a) odd mode; and (b) even mode [3].

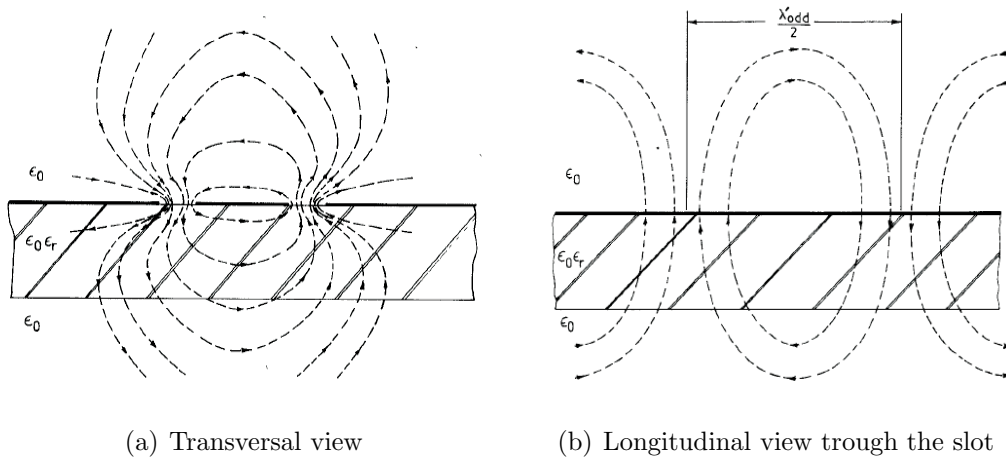


Figure 2-3: Magnetic field distribution of the CPW for the odd mode: (a) transversal view; (b) longitudinal view [3].

Although the Wen's approach assumed an infinitely thick substrate and zero conductor thickness, which ignores possible dispersion effects, good results were obtained and practical applications were experimentally demonstrated.

The localization of ground planes in same plane as the signal strip is one of the most interesting characteristics of the CPW because it allows easy connections of external shunt elements such as active devices. It is also ideal for connecting various elements in microwave integrated circuits (MIC's) and MMIC's which can be built on semiconductor substrates.

### **CPW with substrate of finite thickness**

The CPW can be studied by quasi-static analysis in which the nature of propagation is considered to be TEM and phase velocity and characteristic impedance are calculated from the electrostatic capacitance of the structure. The quasi-static analysis can be conducted by using the conformal mapping method, which takes into account effects of substrate thickness, finite width of the ground planes and conductor backing. Conformal mapping allows the transformation of one geometry into another more convenient for the analysis. Nevertheless, in the conformal mapping approach, the effects of frequency on the phase velocity and characteristic impedance are ignored. A detailed explanation about this analysis for CPW is available in [4] and [5].

The capacitance of the CPW of Figure 2-1, is obtained through conformal mapping by using two *Schwarz-Christoffel* transformations. The capacitance of the CPW is related to the impedance through the phase velocity. The substrate is assumed of finite thickness and the metalization is assumed negligible ( $t = 0$ ). The characteristic impedance of the CPW is:

$$Z_0 = \frac{30\pi K(k')}{\sqrt{\epsilon_{re}}K(k)} \quad (2.1)$$

Where  $e_{re}$  is the effective dielectric constant given by (2.2), which can be interpreted as the dielectric constant of a homogeneous medium that replaces the air and dielectric regions of the coplanar waveguide.

$$e_{re} = 1 + \frac{e_r - 1}{2} \frac{K(k_2)}{K(k'_2)} \frac{K(k')}{K(k)} \quad (2.2)$$

$k$  and  $k_2$  are called the modules of the complete elliptical integral of the first kind  $K$ , and are obtained from

$$k = \frac{S}{S + 2W} \quad (2.3)$$

and

$$k_2 = \frac{\sinh\left(\frac{\pi S}{2h}\right)}{\sinh\left(\frac{\pi(S+2W)}{2h}\right)} \quad (2.4)$$

$K'$  is the complement of  $K$  and they are related through (2.5) and (2.6). The complete elliptical integral can be resolved by computational resources such as MATLAB or by using tables available from literature.

$$K'(k) = K(k') \quad (2.5)$$

$$K'(k_2) = K(k'_2) \quad (2.6)$$

$k'$  and  $k'_2$  are called the complementary modules of the complete elliptical integral of the first kind and they are related to  $k$  and  $k_2$  through

$$k' = \sqrt{1 - k^2} \quad (2.7)$$

$$k'_2 = \sqrt{1 - k_2^2} \quad (2.8)$$

### CPW sandwiched between two dielectric substrates with a cover shield

This structure is schematically illustrated in Figure 2–4, and consists in a CPW covered by a dielectric piece with thickness  $h_2$ , which is metalized in the top side.

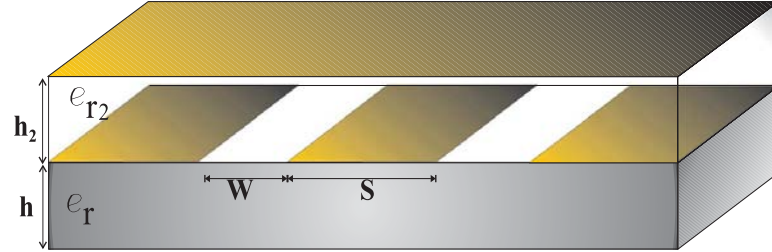


Figure 2–4: Schematic of a CPW sandwiched between two dielectric substrates with a cover shield.

The dielectric effective constant of this structure is given by Equation (2.9)

$$e_{re} = \frac{(er - 1) \frac{K(k_1)}{K(k'_1)} + (er_2 - 1) \frac{K(k_2)}{K(k'_2)} + \frac{K(k)}{K(k')} + \frac{K(k_3)}{K(k'_3)}}{\frac{K(k)}{K(k')} + \frac{K(k_3)}{K(k'_3)}} \quad (2.9)$$

Where  $k_1$ ,  $k_3$ , and their complementary modules  $k'_1$ ,  $k'_3$  are given by Equations (2.10), (2.11) and (2.12), respectively. The modulus  $k$  and  $k_2$  are the same as the earlier case.

$$k_1 = \frac{\sinh\left(\frac{\pi S}{2h_2}\right)}{\sinh\left(\frac{\pi(S+2W)}{2h_2}\right)} \quad (2.10)$$

$$k_3 = \frac{\tanh\left(\frac{\pi S}{2h_2}\right)}{\tanh\left(\frac{\pi(S+2W)}{2h_2}\right)} \quad (2.11)$$

$$k'_1 = \sqrt{1 - k_1^2} \quad (2.12)$$

$$k'_3 = \sqrt{1 - k_3^2} \quad (2.13)$$

In this structure the characteristic impedance of the CPW is given by Equation (2.14), and depends on the dielectric effective constant, as well as, the complete elliptical integrals  $K(k)$ ,  $K(k_3)$ ,  $K(k')$  and  $K(k'_3)$ .

$$Z_0 = \frac{60\pi}{\sqrt{\epsilon_{re}} \left( \frac{K(k)}{K(k')} + \frac{K(k_3)}{K(k'_3)} \right)} \quad (2.14)$$

## 2.2 CPW-fed folded-slot antenna

Although the FSA could be microstrip-fed [6], the CPW-feed is the more popular feeding technique because in the CPW all conductors are located on the same side, avoiding vias through the substrate and allowing easy connection of external shunt elements as well as series surface mounting of active and passive devices. A CPW inductively-fed FSA is shown in the Figure 2-5.

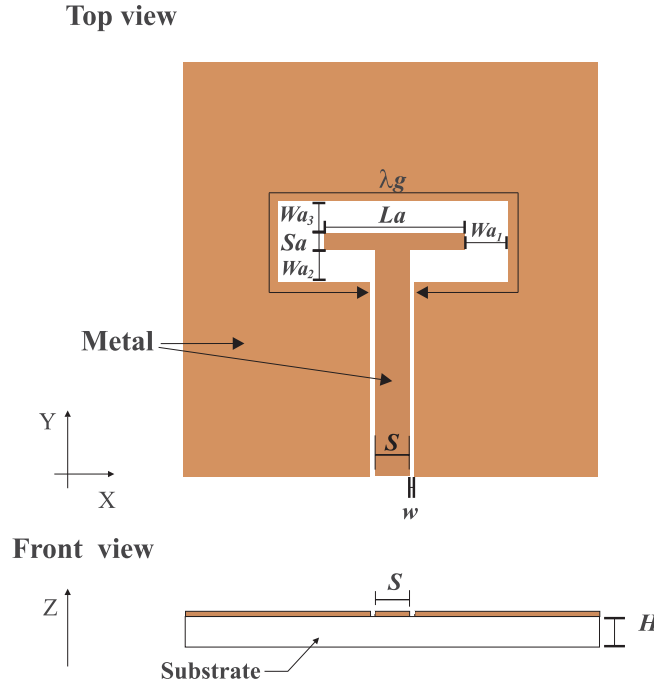


Figure 2-5: Geometry of the FSA.

In Figure 2-1,  $S_a$  and  $L_a$  are the width and length of the conductor between the slots of the antenna, respectively.  $W_{a1}$ ,  $W_{a2}$  and  $W_{a3}$  are the width of the slots

and  $S$  and  $w$  are the width of the signal strip and slots of the CPW. The conductors are placed above a dielectric substrate with thickness  $H$  and dielectric constant  $\epsilon_r$ .

In 1995, T. Weller *et al.* [1], presented design guidelines for single and double FSA, in which it is shown that the impedance of the single-FSA is four times lower than the impedance of a simple slot antenna at the first useful resonance. Figure 2–6 shows the calculated impedances for the single-FSA compared with a simple slot antenna in a range of frequencies from 2.5 GHz to 12.5 GHz. The parameters of the FSA and slot antenna were:  $\epsilon_r=11.7$ ,  $W=0.10\text{mm}$ ,  $S=0.40\text{mm}$ ,  $Wa_1=0.10\text{mm}$ ,  $Wa_2=0.20\text{mm}$ ,  $Wa_3=0.10\text{mm}$ ,  $L_a=10\text{mm}$  and  $W_a/L_a=0.02\text{mm}$ .

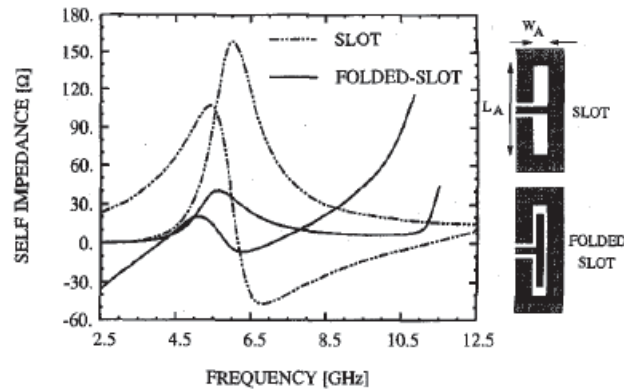


Figure 2–6: Calculated impedance for a folded-slot and a simple slot design [1].

The first useful resonance of the FSA, which is actually the second resonance, occurs when the perimeter is close to  $\lambda_g$ , where  $\lambda_g$  is the guided wavelength of the propagating CPW mode at  $f_0$ . This resonance is commonly used because at the first and third resonances the impedances are associated with a short-circuit and an open-circuit, respectively. In Figure 2–6, the first useful resonance occurs at 5.0 GHz.

The double-FSA proposed in this work is intended to provide a directional E-plane pattern and consists in two folded slot elements connected through a meandered half-wavelength CPW, as shown in Figure 2–7. The connecting line feeds

each FSA in phase and maximize the main beam efficiency. It was found that the first useful resonant frequency of the double-FSA occurs when the perimeter is close to  $0.8\lambda_g$ , which is not very different from the one obtained for the single FSA. The radiated patterns obtained are symmetric and the sidelobes levels are below -12 dB over 8-10% bandwidth.

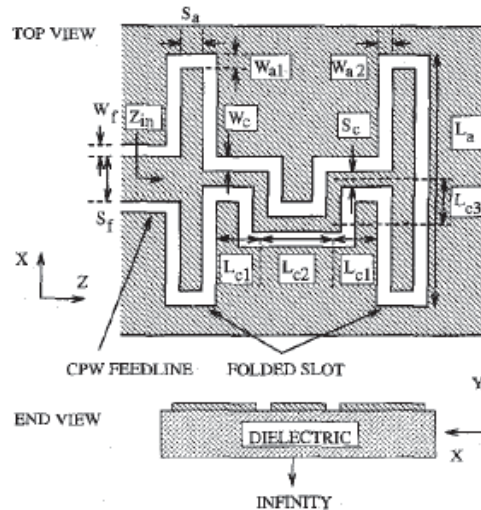


Figure 2-7: Double FSA design [1].

Other work related with double-FSA was published in 1999 by G. Gauthier *et al.* [7]. They presented a double-FSA designed to operate at 90 - 100 GHz. The design was similar to the one presented previously, and the substrate used was silicon. The input impedance obtained was close to  $20 \Omega$  over the range of interest. The radiation patterns obtained were symmetric and the sidelobes maintain below -15 dB from 90 to 100 GHz.

A very interesting study related with the resonant frequency, bandwidth and radiation properties of the CPW-fed FSAs was presented in 1996 by H. Tsai and R. York [8]. This work is based on the finite-difference time domain (FDTD) method and provides design guidelines for the CPW-fed FSAs. The substrates used in this study were Duroid 5880 with  $\epsilon_r=2.2$ , Duroid 6010 with  $\epsilon_r=10.8$  and Alumina with

$\epsilon_r=9.8$ . The radiation patterns obtained for the FSA designed on the last substrate mentioned are shown in the Figure 2-8.

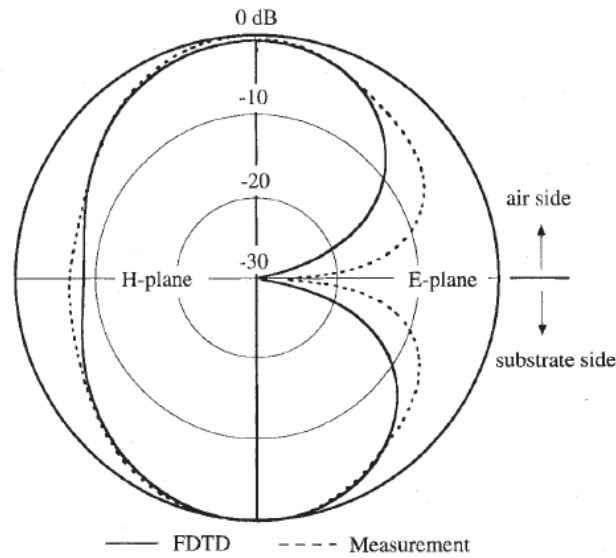
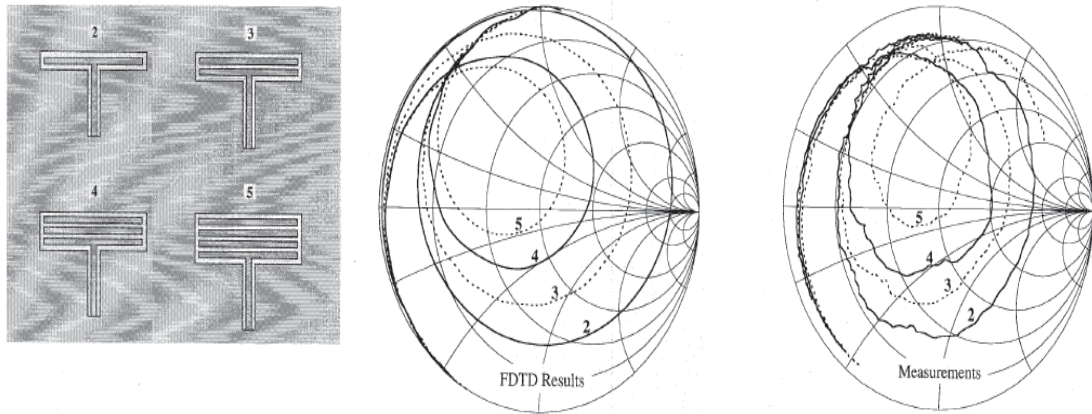


Figure 2-8: E- and H- radiation patterns of the FSA simulated and fabricated on Alumina substrates [8].

It is observed that the E-plane radiation pattern has a peak at broadside and is quite similar to the radiation patterns of a slot antenna. The resonant frequency and antenna bandwidth showed a strong influence of the layout antennas. The resonant frequency of the FSA fabricated on Duroid 5880 decreases as the thickness increases. Regarding the antenna bandwidth for the FSA fabricated on Duroid 6010, it is shown that the separation of the slots has a negligible effect on the antenna bandwidth. However, it was observed that the bandwidth increases as the slot widths increases.

A study about the input impedance of the FSA is also included in [8] and [9]. In these works a multiple-slot antenna design is proposed. This structure consists in adding parasitic slots to the antenna to reduce the input impedance without employing any matching network. The impedance manipulation is achieved whenever the electric fields in the slots are in phase, which is only possible if the number of parasitic slots is not too large. In [9], the input impedance of a FSA fabricated on

a Alumina substrate ( $\epsilon_r=9.8$ ), was successfully engineered from  $\approx 300 \Omega$  to  $50 \Omega$  when 5 parasitic slots were used. Figure 2-9, shows the multiple-slots antennas fabricated on an alumina substrate and the variation of the input impedance with the number of parasitic slots. It was also demonstrated that increasing in the number of parasitic slots do not alter the resonant frequency of the antenna.



(a) Layout of the multiple-slot antennas and simulation results of the impedance scaling. (b) Experimental results of the impedance scaling.

Figure 2-9: Layout of the multiple-slots design and simulation-measurement results of the impedance scaling: (a) Layout of the multiple-slot antennas and simulation results; and (b) Experimental results [8].

One disadvantage of the multi-slot antenna design is that it could require a noticeable increment in the antenna dimensions produced by the parasitic slots added. One simpler technique for controlling the input impedance of the FSA's that overcomes the disadvantages of the multi-slots design was presented in 2002 by N. López-Rivera and R. Rodríguez-Solís [10]. In this work, several CPW-fed FSA's, which use different substrates, were designed and simulated to study the behavior of the antennas as  $Wa_3$  increases. It was noted that the input impedance of the antennas with  $\epsilon_r=10.2$  and  $\epsilon_r=6.15$  decreases exponentially as  $Wa_3$  increases. The input impedance of the antennas with lower dielectric constant ( $\epsilon_r=2.33$ ) decreases almost

linearly as  $Wa_3$  increases. The widths  $Wa_3$  required for matching the antennas to  $50 \Omega$  are wider for substrates with higher dielectric constants.

So far, CPW-inductively fed FSA's have been discussed. However, W. Liu and Z.Hu designed a CPW-fed capacitive FSA for RFID applications at 5.8 GHz [11]. The antenna is shown in Figure 2–10 and was fabricated on a FR-4 substrate with  $\epsilon_r=4.3$ .

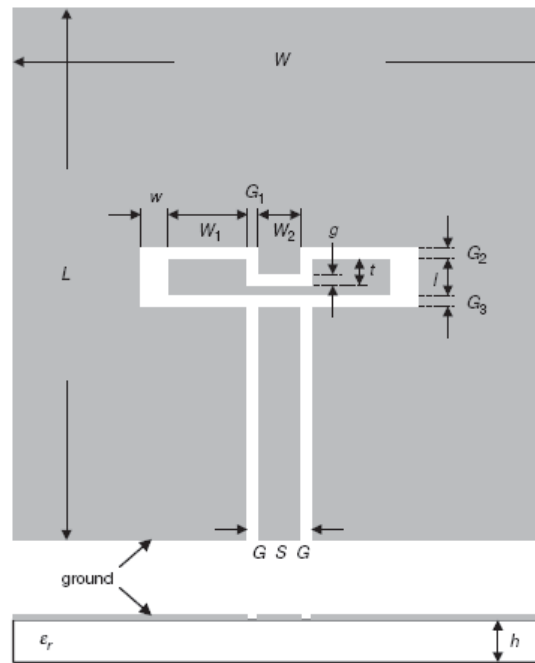


Figure 2–10: CPW-capacitively fed FSA [11].

The impedance matching is achieved by increasing  $w$  and protruding inwards the upper slot of the antenna. The impedance bandwidth obtained was close to 7.5% for return loss  $< 10$  dB. The antenna obtained a measured gain of 4.7 dBi and radiation patterns which were bidirectional in the E-plane and a almost omnidirectional in the H-plane.

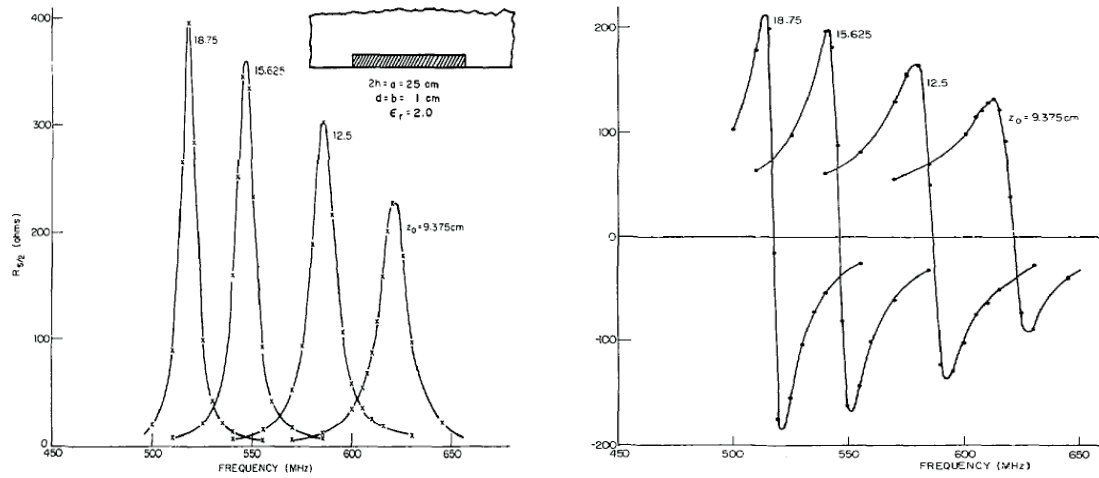
### 2.3 Cavity-backed slot antenna

One of the earliest works about CBSAs was presented by Galejs in 1963 [12], who performed a theoretical study about the input admittance of a cavity backed

narrow slot radiator which is excited across its center by a current delta source. In the geometry considered, the cavity was assumed to be a short-circuited waveguide. The work begins finding the tangential magnetic fields inside and outside of the slot. These magnetic fields are expressed in terms of the transversal and longitudinal electric fields components and Green's functions. Then, the magnetic fields are related to the current source which can be expressed in terms of voltage and admittance. Thus, the admittance of the slot is expressed in terms of integral equations of the transversal and longitudinal electric fields distributions. The longitudinal contribution was obtained by using variational techniques and the transversal contribution was approximated by the static solution. If the slot is considered narrow (slot width  $\ll \lambda$ ), then the longitudinal component can be neglected and only the transversal component contributes to the solution of the integrals and therefore to the input impedance. The results obtained by calculations showed good agreement with measurements. Effects of the slot and cavity dimensions on the input admittance and bandwidth were studied. However, this work is restricted to narrow slots and the position of the source in the slot and radiation responses were not considered.

In 1975, Long [13], carried out an experimental study about the impedance of the CBSA. The work study the input impedance of an open slot antenna without a cavity and three different designs of CBSA, which consist in a dielectric filled CBSA, a CBSA with continuously adjustable depth cavity and a CBSA with a cavity terminated in a inductive post. The antennas were fabricated and tested. In the first design, a slot of 25 cm was backed by cavities with depth incrementally varied from  $\frac{3}{16}\lambda$  to  $\frac{3}{8}\lambda$ . The material that fills the cavity was teflon ( $\epsilon_r = 2.0$ ), which according with the cavity dimension and dielectric constant allows only the fundamental mode ( $TE_{10}$ ) propagation inside the cavity over the frequency range (450-800 MHz). Figure 2-11 shows plots of resistance and reactance against frequency. The values of

the Y axis corresponds to the resistance/reactance of a half part of the slot, because only half of the CBSA was analyzed.



(a) Resistance of the dielectric filled CBSA.

(b) Reactance of the dielectric filled CBSA.

Figure 2-11: Resistance and Reactance of the dielectric filled CBSA: (a) Resistance of the dielectric filled CBSA ; and (b) Reactance of the dielectric filled CBSA [13].

Results obtained show that the resistance decreases and the resonance frequency increases as the cavity depth decreases. In the second design, the height and width of the cavity were increased and the material that fills the cavity was replaced by air. Thus, the resonance frequency is kept similar to that of the first design. In this design, the cavity depth variation was done continuously without disconnecting the feed or cavity assemblies. In the third design, the cavity was filled with a dielectric material and the short-circuited termination was replaced by movable vertical posts.

A novel theoretical approach was proposed by Cockrell in 1976[14], who presented a theoretical investigation about the input admittance, relative bandwidth and quality factor of a CBSA. The study was based on the change in the stored energy in the slot due to the addition of the cavity. For obtaining this energy change, the cavity backed slot antenna was divided into two parts: an internal and an external part. The internal part consists in a cavity and the external part is

the half space. Solutions of both parts (cavity and half space) are combined by using the complex Poynting vector theorem, which is a power balance equation, and is expressed as [15]:

$$P_i = P_t + P_l + P_s \quad (2.15)$$

where

$$P_i = -\frac{1}{2} \int_V (\bar{E} \cdot \bar{J}_s^* + \bar{H}^* \cdot \bar{M}_s) dv \quad (2.16)$$

$$P_t = \frac{1}{2} \oint_S (\bar{E} \times \bar{H}^*) \cdot d\bar{s} \quad (2.17)$$

$$P_l = \frac{\sigma}{2} \int_V |\bar{E}|^2 dv + \frac{\omega}{2} \int_V (\epsilon'' |\bar{E}|^2 + \mu'' |\bar{H}|^2) dv \quad (2.18)$$

$$P_s = 2j\omega (W_m - W_e) = \frac{j\omega}{2} \int_V (\mu' |\bar{H}|^2 - \epsilon' |\bar{E}|^2) dv \quad (2.19)$$

$P_i$  is the complex power delivered by the sources  $J_s$ ,  $M_s$  and the conduction current ( $\sigma \cdot E$ ).  $P_t$  is the complex power transmitted through a surface  $S$  that encloses the volume  $V$  and contains the sources.  $P_l$  is the time average power dissipated in the volume  $V$ , and  $P_s$  is the contribution of the time average electric and magnetic stored energies in the volume  $V$ .

Cockrell applied equation (2.15) to the volume  $V''$  of figure 2-14, to combine the internal and external parts of the cavity backed slot antenna. The volume  $V''$  consists in a slot with a thickness  $\delta$  and a voltage source connected through it.

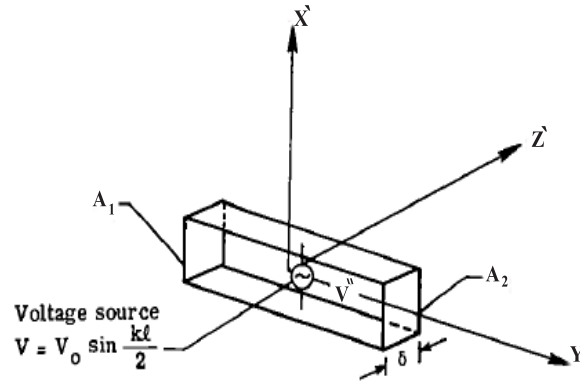


Figure 2-12: Slot geometry [14].

The walls  $A_1$  and  $A_2$  are the surfaces through which the complex power flows into the half space and the cavity respectively. For this analysis the losses were not taken into account because the metallic surfaces were considered to be perfect conductors and the material inside the cavity was assumed to be vacuum, thus  $P_l$  was omitted. The power balance equation that combines the internal and external parts is obtained when the thickness  $\delta$  is considered negligible, therefore  $P_s$  is ignored and only  $P_i$  and  $P_t$  are present in Equation (2.15).

$$-\frac{1}{2} \int_{V''} (\bar{E} \cdot \bar{J}_s^*) dv'' = \frac{1}{2} \iint_{A_1} (\bar{E} \times \bar{H}^*)(-\hat{z}) \cdot dx' dy' + \frac{1}{2} \iint_{A_2} (\bar{E} \times \bar{H}^*)(\hat{z}) \cdot dx' dy' \quad (2.20)$$

The first term in the right part of the equation corresponds to the power flow into the half space and the second term corresponds to the power flow into the cavity, which is assumed as a short-circuited waveguide. The solution for the half space had been proposed by Rhodes in 1966 in terms of time average electric and magnetic stored energies [16]. The solution for the internal part was determined by Cockrell also in terms of stored energy by finding the fields within a narrow slot



Afterwards, in 1977, S. Long published a mathematical model for the impedance of the CBSA as function of frequency and cavity depth [17]. Nevertheless, the model is somewhat restricted because it uses certain previous experimental results of [13], which are related to impedance measurements of the open slot and the CBSA with continuously adjustable cavity depth. The procedure for obtaining the functions that model this CBSA begins with the assumption that the impedance of the antenna could not be considered as the half of the open slot, and that some additional term must be taken into account. To find this term, and to establish a relationship between the open slot and the CBSA, the admittance is preferred over the impedance in the equations because of the cavity was modeled by a short-circuited transmission line, which is connected in parallel with a slot. The final expression for the admittance of the CBSA is:

$$Y_{\frac{s}{2}} = \frac{Y_2}{2} + Y_D(z_0, a, b, f_{MHz}) \quad (2.22)$$

Where  $z_0$ ,  $a$ ,  $b$  are the cavity depth, width and height, respectively.  $Y_{\frac{s}{2}}$  is the admittance of the CBSA,  $\frac{Y_2}{2}$  is the admittance of the open slot without the cavity and  $Y_D$  is the difference between the open slot and the CBSA, which is expressed as a complex quantity. The real component ( $Y_{DR}$ ) was neglected.

$$Y_D = Y_{DR} + j \cdot Y_{DI} \quad (2.23)$$

$$= j \cdot Y_{DI} = j \cdot (Y_{IF} - Y_{IO} \cdot \cot(\beta_g z_0)) \quad (2.24)$$

$Y_{IF}$  and  $Y_{IO}$  are the constants obtained from the previous experimental results. Replacing the equation (2.23) into (2.22); the admittance of the CBSA is obtained as a function of the cavity depth and frequency. Results show similarity between the curves obtained by experiments performed by [14] and [12] and the curves modeled.

Additional theoretical studies have been developed to provide some design guidelines of the CBSA. In 1989, Hadidi *et al.*[18], developed integral equations of the electric fields in the slot of the CBSA with the current source placed across the slot. The equations are similar that proposed by Galejs [12], but they were solved by using the moments method instead of variational techniques. In earlier works, the influence of the feed position along the slot on the radiation properties and circuit parameters had not been studied. Numerical results shows that better radiation resistance is obtained when the source is placed in the middle of the slot. However, this parameter has little effect on the resonance frequency and bandwidth. Additional results present the main parameters (slot and cavity dimensions) of a CBSA with a narrow slot, which affect the resonance frequency, radiation resistance, radiation quality factor and bandwidth.

So far, the works mentioned employ a source across the slot to excite it, however, it is possible to excite the slot by using microstrip lines which are very useful in microwave designs. J.Hirokawa *et al.*[19], proposed a wide slot cavity backed slot antenna (slot width=  $\frac{3}{10}$  slot length), which is excited by a microstrip line as shown in figure 2-14.

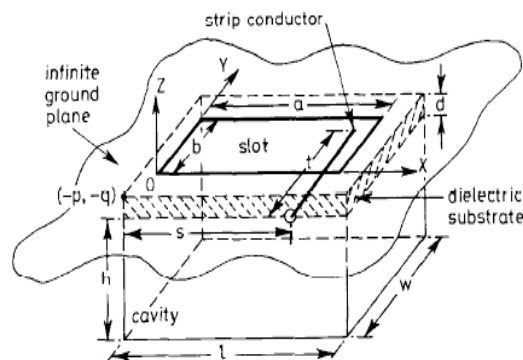


Figure 2-14: Cavity backed wide slot antenna [19].

For this design, equations for the current distribution of the feed line and integral equations for the electric field distribution along and across the slot were obtained and solved. The design proposed obtained a bandwidth of 35% ( $VSWR \leq 2$ ), and a characteristic impedance of  $50\Omega$  because an offset-feed was used. In this work the cavity was placed in the same side as the microstrip line but the cavity also can be located in the slot side of the substrate [6]. This configuration, in which the radiating side is located in the microstrip side is called inverted configuration and was used to enhance the radiation of the microstrip-fed cavity backed wide slot antenna. One single antenna and an array of eight elements were simulated and fabricated. The single CBSA was simulated and fabricated with the same characteristics that [19] to compare results. The bandwidth obtained was 43% which is 8% wider than obtained previously, at the same center frequency, and the gain was 6.1 dBi which is 0.5dBi more than the non inverted microstrip-fed CBSA.

Other technique employed to enhance the gain of the CBSA, consists in placing a superstrate above the substrate[20]. In 2005, W.Tan *et al.*[21], used the inverted configuration of the CBSA proposed by [6], but placed a superstrate with high dielectric constant ( $\epsilon_r=10.2$ ) above the microstrip feed of the antenna. The geometry of the structure is presented in figure 2–15.

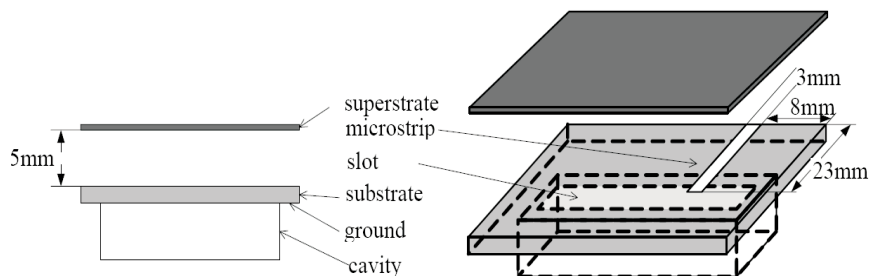


Figure 2–15: Geometry of the CBSA [21].

The walls that cover the structure have a low dielectric constant ( $\epsilon_r \approx 1$ ) and the distance between the substrate and superstrate was carefully selected as 5mm.

Simulated and measured results showed an enhancement of the gain of 11 dBi at the center frequency of 5.8 GHz, in comparison with the antenna without superstrate. On the other hand, the bandwidth measured decreased almost 10%, but the antenna still maintains the broadband behaviour.

Besides gain enhancement, the size reduction of the CBSA also has been recently studied by W.Hong *et al.* [22] in 2006. The reduction in size of the microstrip-fed CBSA is attained by replacing the metallic conductor around the slot with a metallic loop and parallel meander metallic strips placed perpendicular to the loop as depicted in figure 2–16.

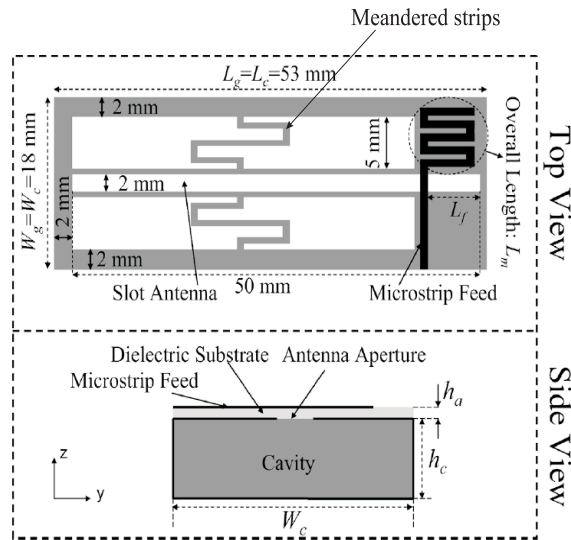


Figure 2–16: Topology of the reduced-size CBSA [22].

Therefore, the size of the antenna, together with the cavity undergo a width reduction of almost 65% compared with the CBSA without the bent lines. Simulations and experiments show that the reduced CBSA with more meander lines obtained the maximum gain of 3.5%, but no gain was obtained when few meander lines were used. Although this work presents acceptable gain values for the reduced-CBSA with many meandered strips and the deepest cavity, the case when there are many

meandered strips but the cavity is shallow, was not considered. This could allow additional size reduction of the CBSA.

Miniaturization and size reduction also have been explored by Adams [23] and Paryani *et al.* in [24]. In this last approach a shallow dielectric cavity with depth of  $(\frac{\lambda_0}{10})$  was used in the design of a wide-band dual-polarized CBSA

## 2.4 Rectangular resonant cavity

The rectangular cavity is the most popular cavity among cylindrical or spherical cavities. Figure 2-17 shows the geometry of a rectangular cavity which can be constructed by closing with metal plates the front and back sides of a rectangular waveguide. Thus, all walls of the cavity are metalized and it can be filled with air or with a dielectric.

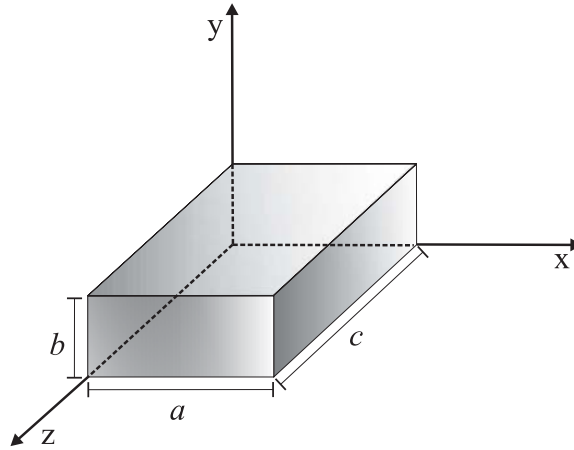


Figure 2-17: Geometry of a rectangular cavity.

Similar to the rectangular waveguide, the cavity does not support Transversal Electromagnetic Fields ( $TEM^z$ ) but supports either Transversal Electric ( $TE^z$ ) or Transversal Magnetic ( $TM^z$ ) modes. Modes refers to the field configuration. In the  $TE^z$  and  $TM^z$  modes the direction of the electric and magnetic fields are transverse to the Z-direction, respectively. Contrary to the rectangular waveguide, in the cavity there is no wave propagation along Z. In cavities only standing waves are allowed along all axis.

If the  $TE_{mnp}^z$  mode is excited, the resonant frequency is given by:

$$(f_r)_{mnp}^{TE} = \frac{1}{2\pi\sqrt{\mu\epsilon}} \sqrt{\left(\frac{m\pi}{a}\right)^2 + \left(\frac{n\pi}{b}\right)^2 + \left(\frac{p\pi}{c}\right)^2} \quad (2.25)$$

for

$$m = 0, 1, 2, 3, \dots$$

$$n = 0, 1, 2, 3, \dots$$

$$p = 1, 2, 3, 4, \dots$$

$$m = n \neq 0$$

If the convention  $c > a > b$  is used, the lowest order is ( $TE_{101}^z$ ) and the resonant frequency is reduced to:

$$(f_r)_{101}^{TE} = \frac{1}{2\pi\sqrt{\mu\epsilon}} \sqrt{\left(\frac{1\pi}{a}\right)^2 + \left(\frac{1\pi}{c}\right)^2} \quad (2.26)$$

A complete derivation of the resonant frequency and modes supported by the rectangular cavity could be obtained in [25].

## 2.5 Design of experiments

According with [26], Design of Experiments (DOE) is the process of planning an experiment so that the obtained data can be analyzed by statistical methods, resulting in valid and objective conclusions.

Thus, the DOE becomes in a efficient and powerful tool for an experimenter who is interested in organize a set of observations in order to investigate the influence that the variables, also called factors, have on the output responses of the experiment. The influence of the factors becomes difficult to be established without help of DOE techniques because the intuitive best-guess approach used by a experimenter could not consider the influence of the interaction between these factors.

The factorial design consider all of possible combinations of factors and gives information about the influence of the individual factors (main effects) as well as the influence of their interactions on the responses. In this design all factors are varied together. In a  $2^k$  factorial design,  $k$  is the number of factors and 2 is the number of the levels, which are usually low and high. These levels could be quantitative or qualitative. In this work only quantitative levels are used. The number of observations needed to complete a  $2^k$  design are called also treatments or runs. For example, for performing a  $2^4$  factorial design, it is needed 16 treatments or runs. Thus, the higher the number of factors, the higher the number of runs.

A fractional factorial design is used to decrease the number of runs required when there are many factors involved in the experiment. In the fractional factorial design only a subset (fraction) of the treatments are performed. For example, in a  $2^{3-1}$  design only 4 runs are required whereas the full design requires 8 runs. The number  $3$  describes the number of factors and the resolution of the design, which is III in this example and 1 describe the faction of the design, and corresponds to the number of independent generators.

### 2.5.1 Design of experiments applied to characterization of antennas

In 2003, N. López-Rivera employed DOE to characterize a FSA [27]. A  $2^{16}$  design was proposed to study the effects of the antenna dimensions  $Wa_1$ ,  $Wa_2$ ,  $Wa_3$  and  $Sa$  on the input impedance, directivity, and resonant frequency of the antennas, for different values of  $La$ . Results showed that the input impedance of the FSA decreases as the upper slot width  $Wa_3$  increases. This procedure provides a simpler technique to match the antenna to  $50 \Omega$ , than used in the multiple-slots design.

In 2008, P. Lozada used  $2^{6-2}$  fractional factorial designs for studying CPW-fed and microstrip-fed log-periodic rectangular slot ring antennas [28]. The influence that the geometrical factors of both antennas have on the input impedance, return

loss and radiation pattern were studied in this work. It was found that decreasing the scaling factor  $\tau$ , the responses improve.

$2^k$  factorial designs also have been used to characterize other antennas, such as a tunable folded-slot antenna with thin film ferroelectric material [29], broadband and multi-band slot ring antennas [30] and asymmetric-annular-slot antennas with ferroelectric material [31].

## CHAPTER 3

# METHODOLOGY

This chapter begins with the design procedure of the CBFSA, which includes substrate selection, cavity selection and feed design. Two structures are proposed to be characterized: CPW-inductively fed cavity-backed folded-slot antenna (CPW-inductively fed CBFSA) and CPW-capacitively fed cavity-backed folded-slot antenna (CPW-capacitively fed CBFSA). Four design of experiments (DOE I, DOE II, DOE III, DOE IV) are proposed to perform the characterization of the structures. In DOE I and DOE II, the cavity dimensions are kept constant whereas the FSA dimensions of the CPW-inductively fed CBFSA and CPW-capacitively fed CBFSA are varied. In DOE III and DOE IV, the cavity dimensions are varied whereas the FSA dimensions of the both structures remain constant.

### 3.1 Design procedure

The characterization of the CBFSA consists in the study about the influence of the dimensions of the FSA and cavity on the radiation pattern, reflection coefficient, gain on the substrate and cavity sides and input impedance of the antenna. To characterize the antenna two structures are proposed: CPW-inductively fed CBFSA and CPW-capacitively fed CBFSA. Both structures consist of a shallow ( $< \frac{\lambda_d}{4}$ ) rectangular dielectric-filled cavity, placed on a folded-slot antenna (FSA), which are fed through CPW. The difference in the structures is the coupling of the CPW to the CBFSA. The geometry of both structures is shown in the Figure 3-1 - 3-2. The structure in the Figure 3-1 corresponds the CPW-inductively-fed CBFSA and the structure of the Figure 3-2 corresponds to the CPW-capacitively fed CBFSA.

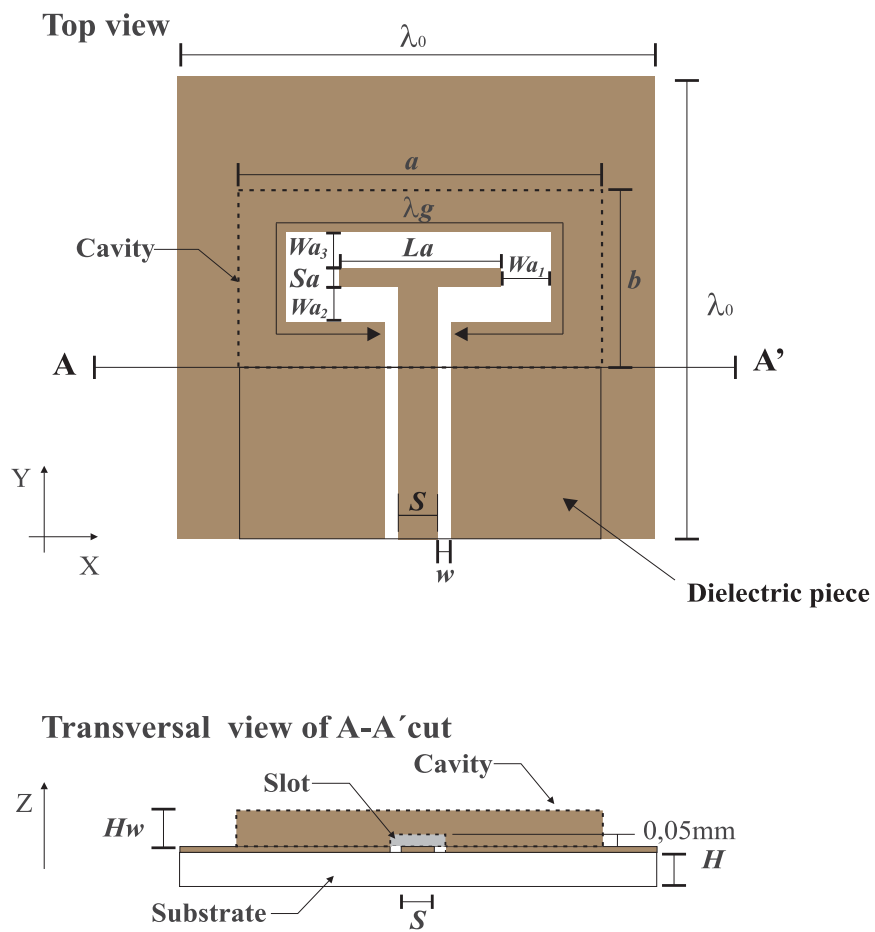


Figure 3-1: CPW-inductively fed CBFSA

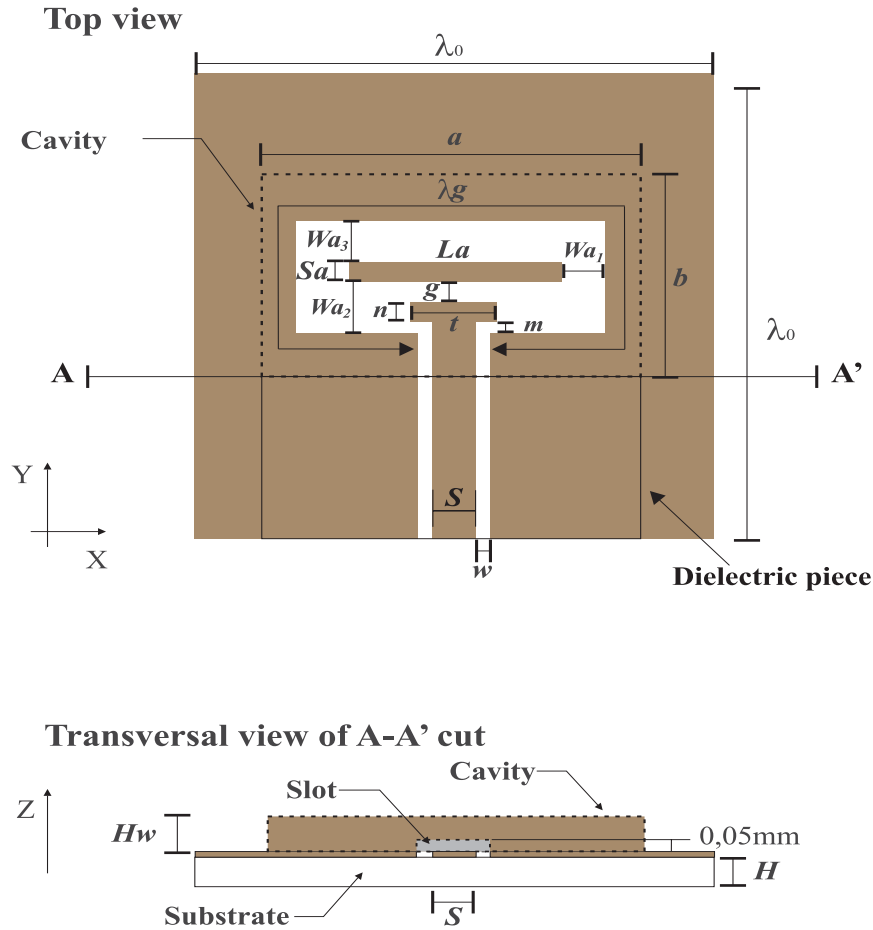


Figure 3-2: CPW-capacitively fed CBFSA

In the top view and the transversal view across A-A', the dotted lines correspond to the rectangular cavity that is placed on the FSA side. The cavity is located in this side, to avoid drilling the substrate to keep the ground of the FSA and cavity together. Additionally, this inverted arrangement was previously used in inverted microstrip-fed cavity-backed slot antennas and provided wider impedance bandwidths and higher antenna gains than conventional microstrip-fed antennas [6].

In addition to the cavity, a dielectric piece is placed on the FSA in the section of the CPW which is not covered by the cavity, in order to preserve constant the characteristic impedance of the CPW along the feed. The cavity is metalized on all sides and the dielectric piece is only covered on the lateral sides as shown in Figure

3–3, which shows a 3D geometry of a CBFSA geometry in which the metalization of the FSA, cavity and dielectric piece is explained. The cavity and dielectric piece were adhered to the FSA with silver paint.

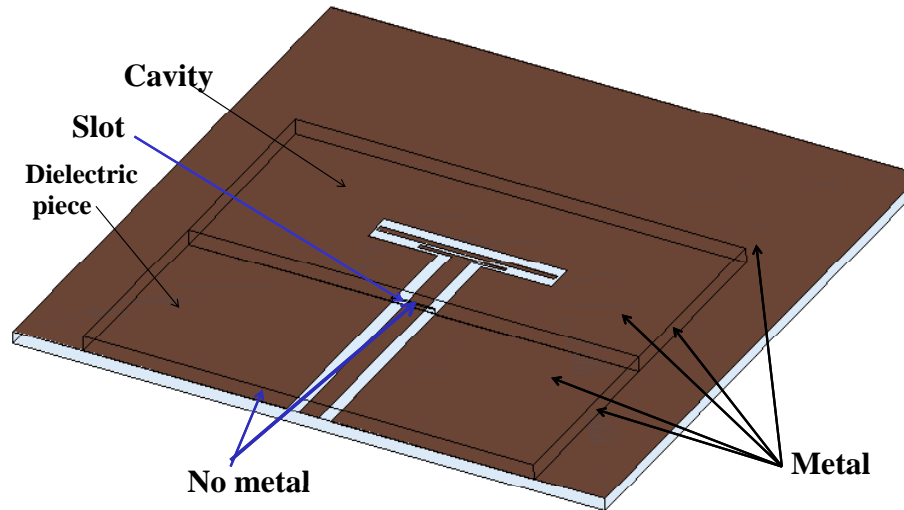


Figure 3–3: CPW-capacitively fed CBFSA

A small slot of  $0.05\text{mm} * (S + 2w)$  was cut in the front wall of the cavity to avoid an electrical short in the CPW when the cavity is placed on the FSA. Therefore there is no metal in this slot as shown in Figure 3–3. The cavity and FSA are aligned through the center of the substrate and the position remains constant for all designs. The width and length of the substrate was chosen  $\lambda_0$  for an operation frequency of 5 GHz.

The FSA is designed to operate at its second impedance resonance, in which the antenna perimeter is approximately one guided wavelength,  $\lambda_g$ , at 5 GHz. FSA are usually designed at this resonance [32], [33], [11]. The outer perimeter was selected to determine the antenna perimeter instead of the inner or average, because in [27]

it was found that the outer perimeter minimizes the sum of the square errors for different values of  $La$ .

Details about each structure, the selection of the substrates for FSA and cavity, the CPW feed design and the DOE's proposed for characterize each structure are discussed in the rest of the chapter.

### 3.1.1 Substrate selection

The design of the CBFSA involves the substrate selection for the FSA, cavity and dielectric piece. There are a variety of substrates commercially available that offer a wide range of values of dielectric constant, thickness, thermal coefficient and dissipation factor. Among the substrates available, the RO3006 from Roger Corp. was selected for the FSA because it is rigid enough to avoid deformations in the substrate and consequently, variations in the antenna responses. Additionally, this substrate has a high dielectric constant ( $e_r = 6.15$ ), gives rise to smaller circuit dimensions than ones obtained with low dielectric constant substrates, such as ( $e_r = 2.2$ ). Thus, the antenna feed can be made narrow, reducing its effects on the antenna performance.

### 3.1.2 Cavity selection

A rectangular dielectric cavity is used for suppressing the radiation from one side of the FSA. The rectangular geometry is selected because it is the most common geometry used in cavities and offer simplicity of fabrication.

The substrate employed for the cavity is the RO4350B (with  $e_r = 3.48$ ), instead of RO3006 (with  $e_r = 6.5$ ), because it is mechanically rigid and previous simulations showed that the CBFSA's, that used cavities filled with low dielectric constants undergo higher gains and better unidirectional patterns than the ones that employed higher dielectric constants such as ( $e_r = 6.15$ ).

The resonant frequency of the cavity depends on the modes and the cavity dimensions. The relation  $a > b > Hw$  is maintained for all designs. Thus, the resonant frequency of the cavity is determined by the Equation (2.26), for the  $TE_{mnp}$  modes.

### 3.1.3 CPW feed design

This feeding is selected because in the CPW all conductors are located on the same side, avoiding vias through the substrate, it reduces the radiation loss and it is easy to fabricate. The selection of the widths  $S = 2\text{mm}$  and  $w = 1.2\text{mm}$  of the CPW of Figure 2-1, is performed by using the Equation (2.14) for a characteristic impedance of  $50 \Omega$ ,  $H = 1.28 \text{ mm}$ ,  $H = 1.52$ , ( $\epsilon_{r2} = 3.48$ ), operation frequency of  $5\text{GHz}$  and ( $\epsilon_r = 6.15$ ). These dimensions were calculated and confirmed through the Estimate calculator of Designer. The dimensions of the CPW are the same for both CBFSA's structures.

## 3.2 CPW-inductively fed cavity-backed folded-slot antenna structure

### DOE I

A top and transversal view across A-A' of this structure is presented in Figure 3-1. In this structure, only the FSA dimensions are varied and the cavity and dielectric piece dimensions remain constant. The design parameters that will be considered of interest factors are 5:  $La$ ,  $Wa_2$ ,  $Wa_1$ ,  $Wa_3$  and  $Sa$ . DOE is used for characterize the antenna because it provides an efficient way of designing a experiment to study the effects that each factor (or main effect) and its interactions with other factors have on the responses. Since there are more than two factors, it is convenient to use a  $2^k$  factorial design, in which  $k$  are the factors and 2 refers to the levels of the factors, which are a high and a low level. Thus, the total runs or simulations required to complete the experiment are  $2^5 = 32$ . To reduce the number of runs, which means to reduce the time of simulation, a fractional factorial design is used. Table 3-1 shows the factors and their low and high values.

Table 3–1: Factors and levels for DOE I

Factor	$Wa_3(\text{mm})$	$Wa_2(\text{mm})$	$Wa_1(\text{mm})$	$Sa(\text{mm})$	$La(\text{mm})$
High	0.30	0.30	0.30	0.30	14.00
Low	1.00	1.20	1.20	1.20	18.00

The low and high levels of  $Wa_1$ ,  $Wa_2$ ,  $Wa_3$  and  $Sa$  correspond to  $\frac{\lambda_0}{200} \approx \frac{\lambda_g}{100}$  and  $\frac{\lambda_0}{50} \approx \frac{\lambda_g}{25}$ , respectively. The levels for  $La$  were selected to provide an outer perimeter of  $\lambda_g$  in order to keep the resonance of the FSA around 5 GHz. Previous experiences showed that the levels proposed provide meaningful results.

The cavity dimensions  $a=45.72\text{mm}$  and  $b=20.32\text{mm}$  were chosen as twice the aperture of a X-band standard rectangular waveguide. The cavity thickness  $H_w$  is selected to be shallow 1.52mm, ( $\frac{\lambda_0}{40} \approx \frac{\lambda_d}{22}$ ), which is more shallow than cavity-backed antennas commonly proposed. This thickness corresponds to the biggest thickness offered for a RO4350B substrate. The resonance frequency of the cavity is determined by the Equation (2.26), and the dimensions of the cavity  $a$ ,  $b$  and  $H_w$ .

Table 3–2: Resonant Frequencies for the  $TE_{mnp}$  modes

Mode	Resonant Frequency (GHz)
$TE_{101}$	4.33
$TE_{102}$	5.29
$TE_{103}$	6.59

The dielectric piece dimensions are  $a=45.72\text{mm}$ ,  $H_d=1.52\text{mm}$  and  $c=19.84\text{mm}$ .  $c$  is considered as the distance required to cover the portion of the CPW that is not covered by the cavity.

Table 3–3 shows the design matrix and the physical dimensions of the  $2_V^{5-1}$  fractional factorial design. The combination treatments are named by a capital letter as shown in the first column. The experiments have only one replica because there is available only one 3D simulation software.

Table 3–3: Design matrix and dimensions of the experiments ( $2_{V}^{5-1}$  fractional factorial design)

Design	$Wa_3$ (mm)	$Wa_2$ (mm)	$Wa_1$ (mm)	$Sa$ (mm)	$La$ (mm)
E	0.30	0.30	0.30	0.30	18.00
A	1.00	0.30	0.30	0.30	14.00
B	0.30	1.20	0.30	0.30	14.00
ABE	1.00	1.20	0.30	0.30	18.00
C	0.30	0.30	1.20	0.30	14.00
ACE	1.00	0.30	1.20	0.30	18.00
BCE	0.30	1.20	1.20	0.30	18.00
ABC	1.00	1.20	1.20	0.30	14.00
D	0.30	0.30	0.30	0.60	14.00
ADE	1.00	0.30	0.30	0.60	18.00
BDE	0.30	1.20	0.30	0.60	18.00
ABD	1.00	1.20	0.30	0.60	14.00
CDE	0.30	0.30	1.20	0.60	18.00
ACD	1.00	0.30	1.20	0.60	14.00
BCD	0.30	1.20	1.20	0.60	14.00
ABCDE	1.00	1.20	1.20	0.60	18.00

Table 3–4 presents the coded factors levels of the  $2_{V}^{5-1}$  fractional factorial design. Coding is a linear transformation of the original measurement scale and it is useful because allows to the statistical software to find the independent contribution of each effect. Thus, the lower levels are represented by -1 and the higher levels by 1. The capital letters A,B,C,D and E of the first row are the coded factors that represent the factors  $Wa_3$ ,  $Wa_2$ ,  $Wa_1$ ,  $Sa$  and  $La$  of the design. The resolution of the fractional factorial design is V because it is intended to obtain the effects of the main factors, as well as, the two factor interactions. In resolution V designs no main effect or two-factor interaction is aliased with any other main factor or two-factor interaction [26]. The fractional factorial design was constructed by writing down the basic having 16 runs (a  $2^4$  design in  $A$ ,  $B$ ,  $C$  and  $D$ ), selecting ABCDE as the generator, and then setting the levels of the fifth factor as the multiplication of the other factors  $E = ABCD$ .

Table 3-4: Coded factors of the experiments ( $2_{V}^{5-1}$  fractional factorial design, using I=ABCDE)

Design	A	B	C	D	E=A*B*C*D
E	-1	-1	-1	-1	1
A	1	-1	-1	-1	-1
B	-1	1	-1	-1	-1
ABE	1	1	-1	-1	1
C	-1	-1	1	-1	-1
ACE	1	-1	1	-1	1
BCE	-1	1	1	-1	1
ABC	1	1	1	-1	-1
D	-1	-1	-1	1	-1
ADE	1	-1	-1	1	1
BDE	-1	1	-1	1	1
ABD	1	1	-1	1	-1
CDE	-1	-1	1	1	-1
ACD	1	-1	1	1	-1
BCD	-1	1	1	1	-1
ABCDE	1	1	1	1	1

Figure 3-4 shows a graphical representation of DOE I. Each corner of the cubes represents a run and there are 4 cubes and 8 corners, for a total of 32 runs. The 16 runs proposed for the factorial design are represented by a red point in the corners.

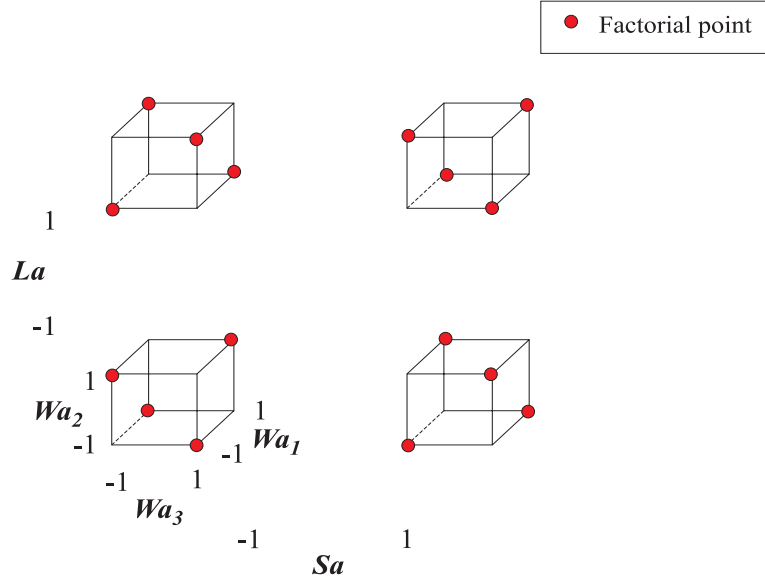


Figure 3–4: Graphical representation of the design matrix of DOE I

### 3.3 CPW-capacitively fed cavity-backed folded-slot antenna structure DOE II

The top and transversal view across the A-A'cut is presented in Figure 3–2. This structure is also CPW-fed, but the coupling to the FSA is capacitive. In this structure, the dimensions of the cavity and the dielectric piece are the same as the CPW-inductively fed CBFSA and remain constant for all treatments. The factors of interest for the structure are:  $Wa_3$ ,  $g$ ,  $t$ ,  $m$ ,  $n$ ,  $La$  and  $Sa$ . The factor  $Wa_1$  is fixed at 0.3mm in order to reduce the complexity in the analysis of the factorial design. Table 3–5 presents the factors and their low and high levels.

Table 3–5: Factors and levels for DOE II

Factor	$Wa_3$ (mm)	$g$ (mm)	$t$ (mm)	$m$ (mm)	$n$ (mm)	$La$ (mm)	$Sa$ (mm)
High	0.30	0.10	4.40	0.1	0.1	14.00	0.30
Low	1.20	0.40	8.80	0.4	0.4	18.00	0.60

Previous experience shows that the high and low levels chosen provided meaningful results.

The complete factorial design consists in  $2^7=128$  treatments and a VII resolution fractional design is used for reduce the runs and the simulation time. For this resolution, each main effect is aliased with a single 6-factor interaction, each 2-factor interaction is aliased with a 5-factor interaction and each 3-factor interaction is aliased with a 4-factor interaction [26]. The fractional factorial design was constructed by writing down the basic having 32 runs (a  $2^6$  design in  $A, B, C, D, E$  and  $F$ ), selecting ABCDEF as the generator, and then setting the levels of the seventh factor as the multiplication of the other factors  $G = ABCDEF$ .

Table 3–6 shows the design matrix and dimensions of the  $2_{VII}^{7-1}$  fractional factorial design and Table 3–8 presents the coded values of the factors levels.

Table 3–6: Design matrix and dimensions of the experiments ( $2_{VII}^{7-1}$  fractional factorial design)

Design	$Wa_3(\text{mm})$	$g(\text{mm})$	$t(\text{mm})$	$m(\text{mm})$	$n(\text{mm})$	$La(\text{mm})$	$Sa(\text{mm})$
G	0.30	0.10	4.40	0.10	0.10	14.00	0.60
A	1.20	0.10	4.40	0.10	0.10	14.00	0.30
B	0.30	0.40	4.40	0.10	0.10	14.00	0.30
ABG	1.20	0.40	4.40	0.10	0.10	14.00	0.60
C	0.30	0.10	8.80	0.10	0.10	14.00	0.30
ACG	1.20	0.10	8.80	0.10	0.10	14.00	0.60
BCG	0.30	0.40	8.80	0.10	0.10	14.00	0.60
ABC	1.20	0.40	8.80	0.10	0.10	14.00	0.30
D	0.30	0.10	4.40	0.40	0.10	14.00	0.30
ADG	1.20	0.10	4.40	0.40	0.10	14.00	0.60
BDG	0.30	0.40	4.40	0.40	0.10	14.00	0.60
ABD	1.20	0.40	4.40	0.40	0.10	14.00	0.30
CDG	0.30	0.10	8.80	0.40	0.10	14.00	0.60
ACD	1.20	0.10	8.80	0.40	0.10	14.00	0.30
BCD	0.30	0.40	8.80	0.40	0.10	14.00	0.30
ABCDG	1.20	0.40	8.80	0.40	0.10	14.00	0.60
E	0.30	0.10	4.40	0.10	0.40	14.00	0.30
AEG	1.20	0.10	4.40	0.10	0.40	14.00	0.60

Continued ...

Table 3-6: (continued)

Design	$Wa_3(\text{mm})$	$g(\text{mm})$	$t(\text{mm})$	$m(\text{mm})$	$n(\text{mm})$	$La(\text{mm})$	$Sa(\text{mm})$
BEG	0.30	0.40	4.40	0.10	0.40	14.00	0.60
ABE	1.20	0.40	4.40	0.10	0.40	14.00	0.30
CEG	0.30	0.10	8.80	0.10	0.40	14.00	0.60
ACE	1.20	0.10	8.80	0.10	0.40	14.00	0.30
BCE	0.30	0.40	8.80	0.10	0.40	14.00	0.30
ABCEG	1.20	0.40	8.80	0.10	0.40	14.00	0.60
DEG	0.30	0.10	4.40	0.40	0.40	14.00	0.60
ADE	1.20	0.10	4.40	0.40	0.40	14.00	0.30
BDE	0.30	0.40	4.40	0.40	0.40	14.00	0.30
ABDEG	1.20	0.40	4.40	0.40	0.40	14.00	0.60
CDE	0.30	0.10	8.80	0.40	0.40	14.00	0.30
ACDEG	1.20	0.10	8.80	0.40	0.40	14.00	0.6
BCDEG	0.30	0.40	8.80	0.40	0.40	14.00	0.60
ABCDE	1.20	0.40	8.80	0.40	0.40	14.00	0.30
F	0.30	0.10	4.40	0.10	0.10	18.00	0.30
AFG	1.20	0.10	4.40	0.10	0.10	18.00	0.60
BFG	0.30	0.40	4.40	0.10	0.10	18.00	0.60
ABF	1.20	0.40	4.40	0.10	0.10	18.00	0.30
CFG	0.30	0.10	8.80	0.10	0.10	18.00	0.60
ACF	1.20	0.10	8.80	0.10	0.10	18.00	0.30
BCF	0.30	0.40	8.80	0.10	0.10	18.00	0.30
ABCFG	1.20	0.40	8.80	0.10	0.10	18.00	0.60
DFG	0.30	0.10	4.40	0.40	0.10	18.00	0.60
ADF	1.20	0.10	4.40	0.40	0.10	18.00	0.30
BDF	0.30	0.40	4.40	0.40	0.10	18.00	0.30
ABDFG	1.20	0.40	4.40	0.40	0.10	18.00	0.60
CDF	0.30	0.10	8.80	0.40	0.10	18.00	0.30
ACDFG	1.20	0.10	8.80	0.40	0.10	18.00	0.60
BCDFG	0.30	0.40	8.80	0.40	0.10	18.00	0.60
ABCDF	1.20	0.40	8.80	0.40	0.10	18.00	0.30
EFG	0.30	0.10	4.40	0.10	0.40	18.00	0.60
AEF	1.20	0.10	4.40	0.10	0.40	18.00	0.30
BEF	0.30	0.40	4.40	0.10	0.40	18.00	0.30
ABEFG	1.20	0.40	4.40	0.10	0.40	18.00	0.60

Continued ...

Table 3-6: (continued)

Design	$Wa_3(\text{mm})$	$g(\text{mm})$	$t(\text{mm})$	$m(\text{mm})$	$n(\text{mm})$	$La(\text{mm})$	$Sa(\text{mm})$
CEF	0.30	0.10	8.80	0.10	0.40	18.00	0.30
ACEFG	1.20	0.10	8.80	0.10	0.40	18.00	0.60
BCEFG	0.30	0.40	8.80	0.10	0.40	18.00	0.60
ABCEF	1.20	0.40	8.80	0.10	0.40	18.00	0.30
DEF	0.30	0.10	4.40	0.40	0.40	18.00	0.30
ADEFG	1.20	0.10	4.40	0.40	0.40	18.00	0.60
BDEFG	0.30	0.40	4.40	0.40	0.40	18.00	0.60
ABDEF	1.20	0.40	4.40	0.40	0.40	18.00	0.30
CDEFG	0.30	0.10	8.80	0.40	0.40	18.00	0.60
ACDEF	1.20	0.10	8.80	0.40	0.40	18.00	0.30
BCDEF	0.30	0.40	8.80	0.40	0.40	18.00	0.30
ABCDEF	1.20	0.40	8.80	0.40	0.40	18.00	0.60

Table 3-7: Coded factors of the experiments ( $2_{VII}^{7-1}$  fractional factorial design)

Design	A	B	C	D	E	F	G=ABCDEF
G	-1	-1	-1	-1	-1	-1	1
A	1	-1	-1	-1	-1	-1	-1
B	-1	1	-1	-1	-1	-1	-1
ABG	1	1	-1	-1	-1	-1	1
C	-1	-1	1	-1	-1	-1	-1
ACG	1	-1	1	-1	-1	-1	1
BCG	-1	1	1	-1	-1	-1	1
ABC	1	1	1	-1	-1	-1	-1
D	-1	-1	-1	1	-1	-1	-1
ADG	1	-1	-1	1	-1	-1	1
BDG	-1	1	-1	1	-1	-1	1
ABD	1	1	-1	1	-1	-1	-1
CDG	-1	-1	1	1	-1	-1	1
ACD	1	-1	1	1	-1	-1	-1
BCD	-1	1	1	1	-1	-1	-1

Continued ...

Table 3-7: (continued)

Design	A	B	C	D	E	F	G=ABCDEF
ABCDG	1	1	1	1	-1	-1	1
E	-1	-1	-1	-1	1	-1	-1
AEG	1	-1	-1	-1	1	-1	1
BEG	-1	1	-1	-1	1	-1	1
ABE	1	1	-1	-1	1	-1	-1
CEG	-1	-1	1	-1	1	-1	1
ACE	1	-1	1	-1	1	-1	-1
BCE	-1	1	1	-1	1	-1	-1
ABCEG	1	1	1	-1	1	-1	1
DEG	-1	-1	-1	1	1	-1	1
ADE	1	-1	-1	1	1	-1	-1
BDE	-1	1	-1	1	1	-1	-1
ABDEG	1	1	-1	1	1	-1	1
CDE	-1	-1	1	1	1	-1	-1
ACDEG	1	-1	1	1	1	-1	1
BCDEG	-1	1	1	1	1	-1	1
ABCDE	1	1	1	1	1	-1	-1
F	-1	-1	-1	-1	-1	1	-1
AFG	1	-1	-1	-1	-1	1	1
BFG	-1	1	-1	-1	-1	1	1
ABF	1	1	-1	-1	-1	1	-1
CFG	-1	-1	1	-1	-1	1	1
ACF	1	-1	1	-1	-1	1	-1
BCF	-1	1	1	-1	-1	1	-1
ABCFG	1	1	1	-1	-1	1	1
DFG	-1	-1	-1	1	-1	1	1
ADF	1	-1	-1	1	-1	1	-1
BDF	-1	1	-1	1	-1	1	-1
ABDFG	1	1	-1	1	-1	1	1
CDF	-1	-1	1	1	-1	1	-1
ACDFG	1	-1	1	1	-1	1	1
BCDFG	-1	1	1	1	-1	1	1
ABCDF	1	1	1	1	-1	1	-1
EFG	-1	-1	-1	-1	1	1	1

Continued ...

Table 3-7: (continued)

Design	A	B	C	D	E	F	G=ABCDEF
AEF	1	-1	-1	-1	1	1	-1
BEF	-1	1	-1	-1	1	1	-1
ABEFG	1	1	-1	-1	1	1	1
CEF	-1	-1	1	-1	1	1	-1
ACEFG	1	-1	1	-1	1	1	1
BCEFG	-1	1	1	-1	1	1	1
ABCEF	1	1	1	-1	1	1	-1
DEF	-1	-1	-1	1	1	1	-1
ADEFG	1	-1	-1	1	1	1	1
BDEFG	-1	1	-1	1	1	1	1
ABDEF	1	1	-1	1	1	1	-1
CDEFG	-1	-1	1	1	1	1	1
ACDEF	1	-1	1	1	1	1	-1
BCDEF	-1	1	1	1	1	1	-1
ABCDEF	1	1	1	1	1	1	1

The graphical representation of the matrix design of the experiments is shown in Figure 3-5. Similar to the representation of DOE I, the red points represent the treatments.

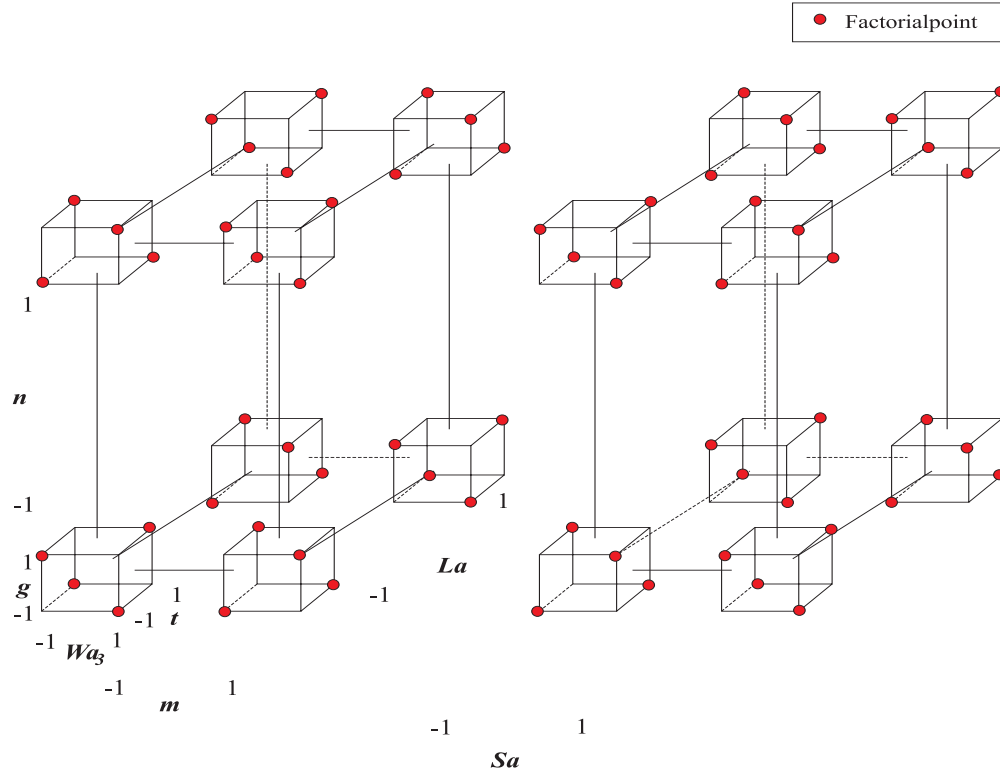


Figure 3-5: Graphical representation of the design matrix of DOE II

### DOE III and DOE IV

In the last two approaches the cavity was maintained constant. However, it is also desired to study the influence that the dimensions of the cavity have on the desired responses for the structures previously proposed. The approach used for performing this study is as follows. It is selected one treatment of each structure previously presented. For these treatments, the dimensions of the FSA will remain constant but the cavity dimensions  $Hw$ ,  $b$  and  $a$  will be varied. The low and high levels for  $Hw$  are selected to preserve a shallow cavity. Thus, the cavity thickness are varied between 1.52 mm ( $\frac{\lambda_0}{40} \approx \frac{\lambda_d}{22}$ ) and 0.72 mm ( $\frac{\lambda_0}{80} \approx \frac{\lambda_d}{44}$ ). The high and low levels of  $a$  and  $b$  were chosen because in previous simulations was observed that they provide meaningful results in frequency ranges close to 5 GHz.

The factorial designs for DOE III and IV are  $2^3$  full factorial designs. The low and high levels of the interest factors are detailed in the Table 3-8.

Table 3-8: Factors and levels for DOE III and DOE IV

Factor	$Hw(\text{mm})$	$b(\text{mm})$	$a(\text{mm})$
High	0.76	17.00	40
Low	1.52	25.00	50

Because of the cavity thickness varies from 1.52mm to 0.76mm, the dimensions  $S$  and  $w$  of the CPW should also vary according with the design. Thus, for a cavity thickness of  $Hw=0.76$  mm, the CPW dimensions obtained through Equation (2.14) for a characteristic impedance of  $50 \Omega$  are  $S=1.5$  mm and  $w= 2.7$  mm.

In DOE III, the treatment selected from the Table 3-3 is BCE, where  $Wa_3=0.30\text{mm}$ ,  $Wa_2=1.20\text{mm}$ ,  $Wa_1=1.20\text{mm}$ ,  $Sa=0.30\text{mm}$  and  $La=18.00\text{mm}$ . In DOE IV, the treatment selected from the Table 3-6 is DEF, where  $Wa_3=0.30\text{mm}$ ,  $g=0.10\text{mm}$ ,  $t=4.40\text{mm}$ ,  $m=0.40\text{mm}$ ,  $n=0.40\text{mm}$ ,  $La=18.00\text{mm}$  and  $Sa=0.30\text{mm}$ . Table 3-9 shows the design matrix of the DOE III and DOE IV.

Table 3-9: Design matrix and dimensions of the experiments ( $2^3$  factorial design)

Design	$Hw(\text{mm})$	$b(\text{mm})$	$a(\text{mm})$
1	0.76	17.00	40.00
A	1.52	17.00	40.00
B	0.76	25.00	40.00
AB	1.52	25.00	40.00
C	0.76	17.00	50.00
AC	1.52	17.00	50.00
BC	0.76	25.00	50.00
ABC	1.52	25.00	50.00

Table 3-10 presents the coded values of the factors levels for the  $2^3$  factorial design of DOE III and IV.

Table 3–10: Coded factors of the experiments ( $2^3$  factorial design)

Design	A	B	C
1	-1	-1	-1
A	1	-1	-1
B	-1	1	-1
AB	1	1	-1
C	-1	-1	1
AC	1	-1	1
BC	-1	1	1
ABC	1	1	1

The graphical representation of the  $2^3$  factorial design of DOE III and IV is shown in Figure 3–6.

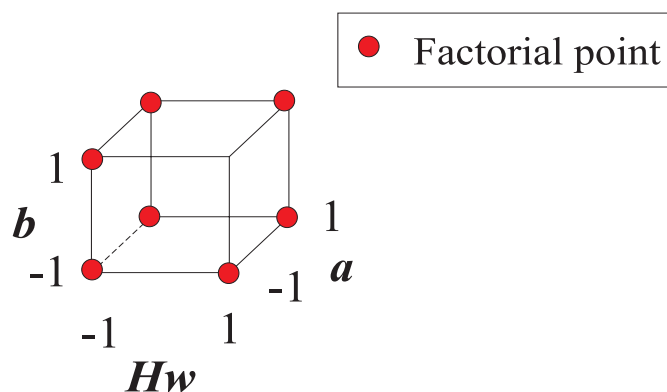


Figure 3–6: Graphical representation of the design matrix of DOE III and DOE IV

In DOE III and IV designs, the cavity resonant frequencies are different from DOE I and II and there are eight different resonant frequencies, one for each treatment. Table 3–11 presents the resonant frequencies for the first resonant modes of the cavity for DOE III and DOE IV.

Table 3–11: Resonant Frequencies for the  $TE_{mnp}$  modes

Design	$(f_r)_{101}^{TE}$	$(f_r)_{102}^{TE}$	$(f_r)_{103}^{TE}$
1	5.13	6.20	7.66
A	5.13	6.20	7.66
B	3.79	5.14	6.83
AB	3.79	5.14	6.83
C	4.99	5.71	6.75
AC	4.99	5.71	6.75
BC	3.59	4.54	5.79
ABC	3.59	4.54	5.79

# CHAPTER 4

## SIMULATION AND EXPERIMENTAL RESULTS

This Chapter presents the simulation results of the designs of experiments DOE I, DOE II, DOE III and DOE IV proposed in chapter 3. These results are statistically analyzed to determine the influence that the FSA and cavity dimensions have on the resistance, frequency, magnitude of reflection coefficient and gain of the CPW-inductively fed CBFSA and the CPW-capacitively fed CBFSA. The chapter is divided into three sections. The first section presents the simulation results as well as the analysis of the data. This section is divided into four subsections, one subsection for each design of experiments. The second section presents two designs of CBFSA's that achieve the goal  $\Gamma < 0.33$  at 5GHz. In the last section, the simulation and experimental results are compared in order to validate the simulations.

### 4.1 Results

The designs proposed in DOE I, DOE II and DOE III are simulated in the the High Frequency Simulator Software (HFSS<sup>®</sup>) V.11. This software employs the finite element method to generate the electromagnetic behavior of the structure. Thus, HFSS is able to compute the characteristic port impedance of the structure, S-parameters and the radiated near and far fields, which make it suitable for studying the electrical and radiation properties of the CBFSA's.

The responses to be studied in all design of experiments are: maximum resistance (Rmax), frequency at Rmax (F\_R), reactance at F\_R ( $X_{F_R}$ ), reflection coefficient at F\_R ( $\Gamma_{F_R}$ ) and reflection coefficient at 5 GHz ( $\Gamma_{5GHz}$ ), gain in the

side of the substrate at  $F_{R}$  ( $G_{s_{F_{R}}}$ ) and at 5 GHz ( $G_{s_{5GHz}}$ ) and gain in the side of the cavity at  $F_{R}$  ( $G_{c_{F_{R}}}$ ) and at 5 GHz ( $G_{c_{5GHz}}$ ). The frequency at maximum resistance  $F_{R}$  of the FSA was selected as the reference frequency to measure the other factors instead of the resonance frequency because not all designs properly resonated at the first useful resonance of the FSA. This means that  $X_{F_{R}}$  is not zero in some designs, although there is a proximity to resonate. To provide clarity about the CBFSA resonance, a plot of impedance vs. frequency (3 GHz - 6 GHz) is presented in Figure 4-1. The red line corresponds to the reactance and the violet line corresponds to the reactance.

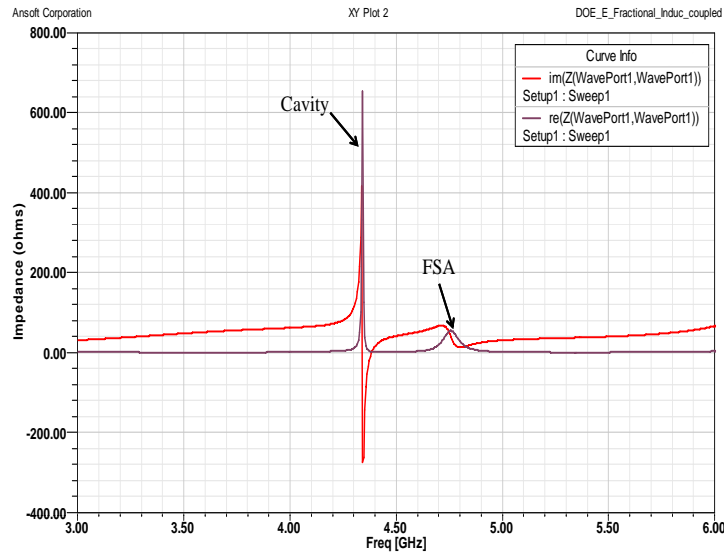


Figure 4-1: Input impedance of a CBFSA vs Frequency (3 GHz - 6 GHz).

In Figure 4-1 two peaks are observed in resistance plot, which correspond to responses of the cavity and the FSA. The peak at 4.3 GHz corresponds with the cavity resonance for the  $TE_{101}$  mode calculated and presented in Table 3-2. Additionally, the impedance bandwidth of this peak is very narrow, which is characteristic of a high Q devices such as cavities. The peak around 4.76 GHz corresponds to the FSA

response. The maximum resistance is  $56 \Omega$  and the reactance is close to be zero at 4.8 GHz. A close view around the FSA peak is shown in Figure 4-2.

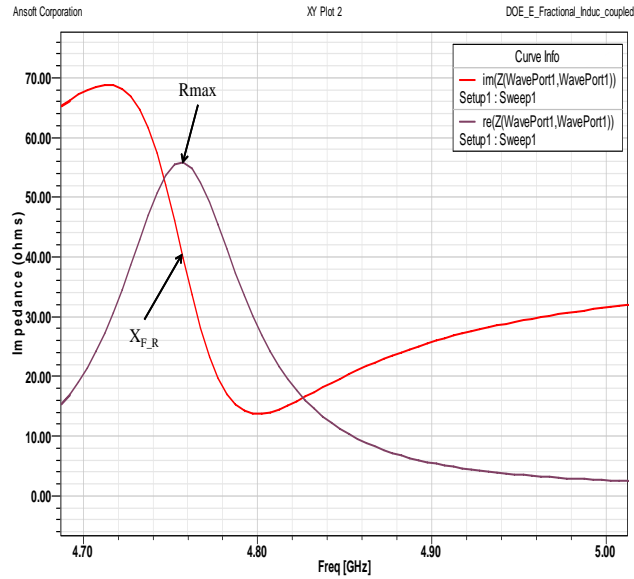


Figure 4-2: Input impedance of a CBFSA vs Frequency (4.7 GHz - 5 GHz).

Although the reactance of the FSA is not zero in the frequency range (4.7 GHz - 5 GHz), a typical response of a FSA is observed. The magnitude of the reflection coefficient is 0.3 at 4.76 GHz, which means that the criteria  $VSWR < 2$  is accomplished at this frequency. Thus, information about the matching of the antenna could be obtained by studying  $\Gamma_{F,R}$ , although there is no information the resonance frequency.

Figure 4-3, shows the reference plane position in the CBFSA, in which the measurement of the responses are performed. This point is selected because it is near to the FSA. In simulations, this position is reached by de-embedding the port from the connector position to the ending of the CPW transmission line.

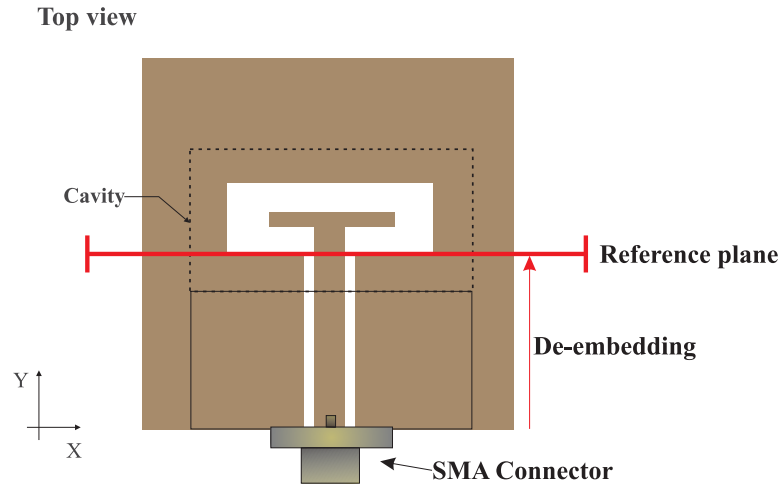


Figure 4-3: Reference plane for measurements.

#### 4.1.1 DOE I simulation results

Table 4-1 presents the simulation results for the designs proposed in DOE I, as well as the maximum and minimum values of the responses of interest obtained with this structure. These results, together with the coded factors of the DOE I (table 3-4), are used by the statistical software Minitab V.15<sup>®</sup> to determine the effect that the factors  $Wa_2$ ,  $Wa_1$ ,  $Wa_3$  and  $Sa$  have on the interest responses  $R_{max}(\Omega)$ ,  $F_{-R}$  (GHz),  $X_{F_{-R}}(\Omega)$ ,  $\Gamma_{F_{-R}}$ ,  $\Gamma_{5GHz}$ ,  $G_{s_{F_{-R}}}$  (dB),  $G_{c_{F_{-R}}}$  (dB),  $G_{s_{5GHz}}$  (dB) and  $G_{c_{5GHz}}$  (dB).

Table 4–1: Simulation results for DOE I ( $2_V^{5-1}$  fractional factorial design)

Design	Rmax	$X_{F_R}$	$F_R$	$\Gamma_{F_R}$	$\Gamma_{5GHz}$	$Gs_{F_R}$	$Gc_{F_R}$	$Gs_{5GHz}$	$Gc_{5GHz}$
E	55.84	39.84	4.75	0.35	0.92	4.84	-13.58	1.57	-17.57
A	10.44	24.69	5.53	0.71	0.97	4.95	-12.19	-4.56	-17.73
B	342.92	41.60	5.57	0.74	0.96	5.06	-13.04	1.52	-15.73
ABE	87.03	64.52	5.03	0.48	0.65	5.57	-12.95	5.50	-13.28
C	80.54	28.13	5.13	0.30	0.85	4.99	-12.77	4.53	-13.58
ACE	14.57	35.27	4.61	0.67	0.97	4.63	-12.50	-7.24	-27.02
BCE	238.67	30.65	4.77	0.65	0.62	52.86	-13.10	5.24	-14.78
ABC	124.82	41.76	5.32	0.47	0.93	5.49	-12.34	3.72	-13.92
D	89.07	32.83	5.51	0.35	0.97	4.88	-12.40	-0.11	-15.66
ADE	18.21	32.82	4.88	0.60	0.89	5.17	-12.64	3.89	-16.19
BDE	190.75	47.49	5.00	0.60	0.60	5.40	-12.94	5.48	-13.63
ABD	118.79	40.87	5.66	0.45	0.97	5.41	-12.54	0.46	-16.44
CDE	78.17	16.52	4.51	0.25	0.95	4.78	-13.00	1.09	-19.84
ACD	13.19	33.62	5.18	0.69	0.96	5.21	-12.46	2.23	-13.92
BCD	237.88	64.19	5.24	0.67	0.92	5.36	-13.53	4.01	-12.90
ABCDE	97.86	53.37	4.85	0.45	0.60	5.63	-13.47	5.36	-14.18
Max	342.92	64.52	5.66	0.74	0.97	5.63	-12.19	5.50	-12.90
Min	10.44	16.52	4.51	0.25	0.60	4.63	-13.53	-7.24	-27.02

The effects that factors have on the responses of interest are estimated graphically through normal probability plots of the effects. These plots are obtained through the statistical software Minitab V.15<sup>®</sup>. In this plot type, the effects that are negligible, are normally distributed with mean zero and variance  $\sigma^2$  and will tend to fall along a straight line [26]. The effects that are significant have mean different from zero and they will not tend to fall along the line. Thus, for each DOE proposed there will be nine normal probability plots, one for each interest response.

Additionally, regression models, which can be used to express the interest response as a linear function of the coded factors, are also presented for each interest response in DOE I, DOE II, DOE III and DOE IV.

Due to DOE I, DOE II, DOE III and DOE IV are single replicate factorial designs, there is no internal estimate of the error and normal plots of the residuals could not be generated. Therefore, a model adequacy checking is not possible. To overcome this limitation and to obtain information about the residuals, the factors that appear with negligible effect in the normal probability plot of the effects, will be discarded from the experiment, and a new experiment with replicas is obtained. The conclusions obtained with both the original and the new design with replicas, must remain unaltered. For example in a  $2^4$  full factorial design with one negligible factor, this factor might be discarded and the design becomes in a  $2^3$  full factorial design with two replicas.

In the rest of this chapter, the influence that the factors have on the specific interest response for DOE I, DOE II, III and IV is discussed.

### DOE results for Rmax

The maximum and minimum values of Rmax are  $342.92 \Omega$  and  $10.44 \Omega$ , respectively. Figure 4-4 shows the normal probability plot of the effects for Rmax.

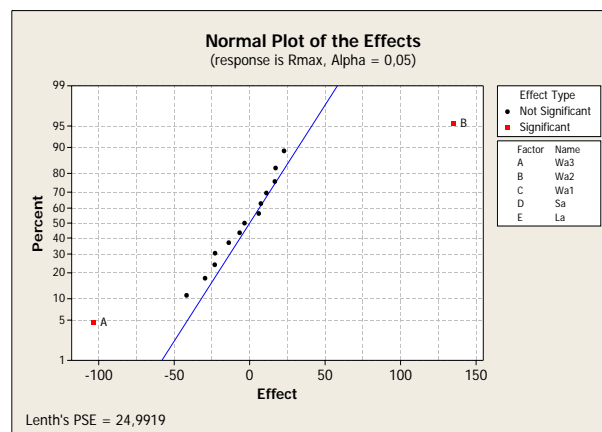


Figure 4-4: Normal probability plot of the effects for the maximum resistance in DOE I.

According to the Figure 4-4, the coded factors that affect the maximum resistance are A and B, which correspond to  $Wa_3$  and  $Wa_2$ , respectively. However, these factors influence the maximum resistance in different manner because they are located at a different side of the normal distribution line. The factor  $Wa_3$ , which is at the left, negatively affects the maximum resistance and the factor  $Wa_2$ , which is at the right, positively affects the maximum resistance. Thus, for decreasing the maximum resistance it is necessary to maintain  $Wa_3$  in its high level and  $Wa_2$  in its low level.

The fact that  $Wa_3$  affects negatively the maximum resistance of the CPW-inductively fed CBFSAs has also been observed for a CPW-fed FSA [27], in which was found that increasing  $Wa_3$  decreases the resistance of the FSA. Regarding the positive effect of  $Wa_2$  on the maximum resistance [1], it is known for a CPW-fed FSA, that increases  $Wa_2$  decreases the resonance frequency of a FSA and consequently increases the input impedance of a FSA.

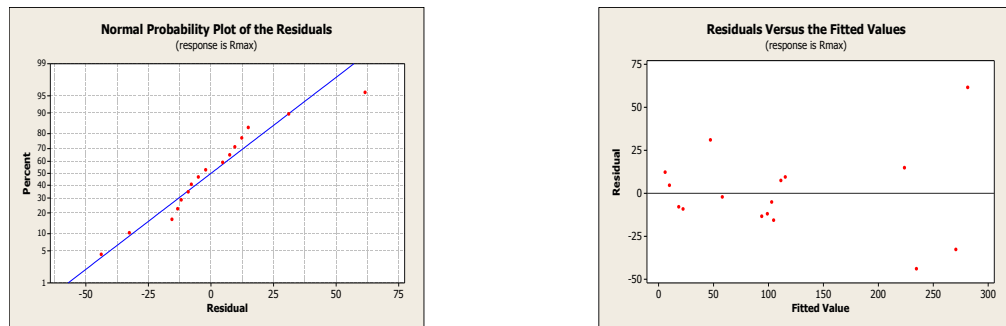
The Rmax regression model obtained through Minitab V.15<sup>®</sup> is given by:

$$Rmax(model) = 112.42 - 51.81A + 67.42B \quad (4.1)$$

In Equation (4.1), A and B are the coded factors that corresponds to  $Wa_3$  and  $Wa_2$ , respectively. The first term in the equation corresponds to the average of the observations and the coefficients are one-half of the corresponding factor effect value.

In order to verify the accuracy of the regression model given by Equation (4.1), the DOE I design is projected into another one with replicas for obtaining the normal plot of residuals and the residuals versus predicted values plot. This projection is achieved by discarding  $Sa$ , the factor with negligible effect on the Rmax model. Thus, a new design with two replicas is obtained.

Figure 4-5(a) and 4-5(b) show the normal probability plot of the residuals and the residuals versus the predicted values plot. It is observed that the residuals follow a normal distribution and appear structureless, which is required for considering that the regression model accurate. Additionally, outliers are not present in the plots. Outliers are residuals much larger than the others and revision should be considered for this specific run or treatment if they are observed in the plots.



(a) Normal plot of residuals.

(b) Residuals versus predicted values.

Figure 4-5: Normal plot of residuals and residuals versus predicted values for Rmax model of DOE I: (a) Normal plot of residuals ; and (b) Residuals versus predicted values.

To preserve the clarity along the chapter, the plots used for accuracy checking of the remaining models of DOE I and those of DOE II, DOE III and DOE IV, are presented in Appendix A. The analysis of the plots is the same as presented previously. Additional discussion about the plots will be included in this Chapter if non-linearities or outliers are found for a specific treatment.

### DOE results for $F_R$

Table 4-1, shows that the maximum and minimum frequencies at Rmax corresponds to 4.51 GHz and 5.66 GHz, respectively. Figure 4-6, shows that the factors

that mostly influence the frequency at maximum resistance are:  $La$ ,  $Wa_1$ ,  $Wa_2$  and  $Wa_3$ . The interaction of the factors that also influence  $F_R$  are  $Wa_2La$  and  $Wa_1La$ . Among the factors mentioned,  $La$  is the factor that have the strongest effect on  $F_R$ , which could be explained because an increment in the antenna length produces an increment in the antenna perimeter or  $\lambda_g$  and consequently a decrement in the frequency. Another factor that negatively affect the frequency is  $Wa_1$  and the factors that positively affect it are  $Wa_3$ ,  $Wa_2$  and the interactions  $Wa_2La$  and  $Wa_1La$ .

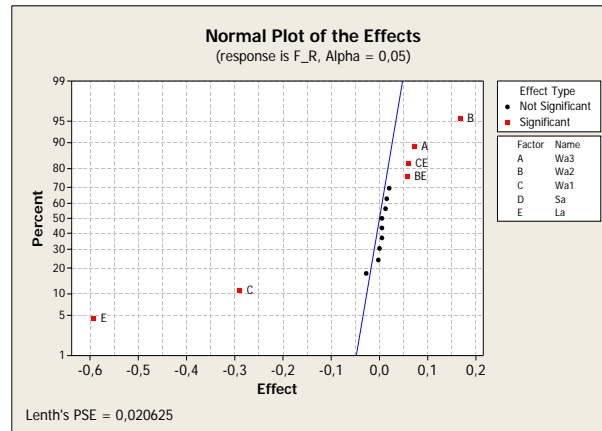


Figure 4–6: Normal probability plot of the effects for the frequency at maximum resistance in DOE I.

The  $F_R$  regression model is given by:

$$\begin{aligned}
 F_R(model) = & 5.096 - 0.296E - 0.145C + 0.083B + 0.036A \\
 & + 0.030CE + 0.028BE
 \end{aligned}
 \tag{4.2}$$

In Equation (4.2), E, C, B, A, CE and BE are the coded factors that corresponds to  $La$ ,  $Wa_1$ ,  $Wa_2$ ,  $Wa_3$ ,  $Wa_1La$  and  $Wa_3La$  respectively. The factor that is discarded for obtaining the residual plots is  $Sa$ .

Although there is no explicit information about the resonance frequency of the cavity in Table 4-1, note that for all designs this resonance agrees with the calculated resonance frequency for the  $TE_{101}$  mode presented in Table 3-2. However, note that  $R_{max}$  and the resonance resistance of the cavity are altered when  $F\_R$  approaches the resonance frequency of the cavity. This behavior evidences the coupling that exists between the FSA and cavity.

#### **DOE results for $X_{F\_R}$**

According with Table 4-1, the designs of the CPW-inductively fed CBFSA have positive values of reactance. This inductive behavior might be caused by the influence of the inductive-feed to the antenna and the strong coupling between the FSA and the cavity. The maximum and minimum reactances at  $R_{max}$  corresponds to  $64.52 \Omega$  and  $16.52 \Omega$ , respectively.

For providing a visualization of the inductive behavior of the CPW-inductively fed CBFSA some impedance plots are presented. Figure 4-5(a), shows the impedance of the design E, in which there is no resonance and inductive behavior is observed in the range of frequency (3 GHz- 6 GHz). However, although positive values of  $X_{F\_R}$  are observed, that no means that the first useful resonance of the FSA does not occur for all treatments of DOE I. Figure 4-7, presents the impedance of the CDE design, where the red line corresponds to the reactance. Observed that  $X_{F\_R}$  is close to be zero ( $16.52 \Omega$ ) at  $F\_R$ , but undergo the first useful resonance of the FSA.

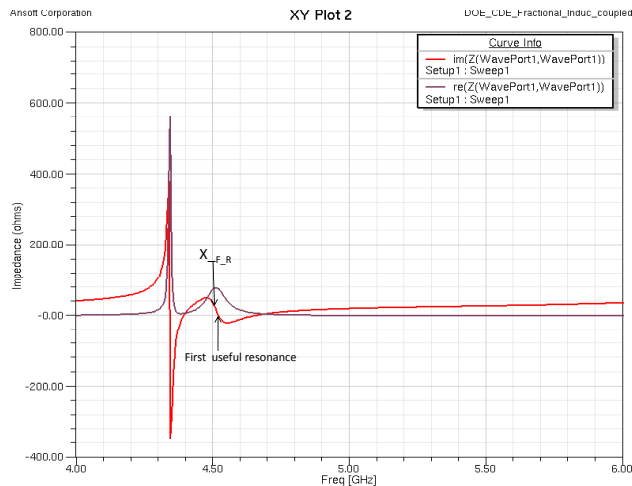


Figure 4–7: Impedance of the CDE design.

Figure 4–8 shows the normal probability plot of the effects for  $X_{F,R}$ . According with the plot, the factor that mostly influence the reactance at  $F_R$  is B, which is the coded factor of  $Wa_2$ . This factor has a positive effect in the reactance. Therefore, if it is desired to decrement  $X_{F,R}$ ,  $Wa_2$  must be set in the low level.

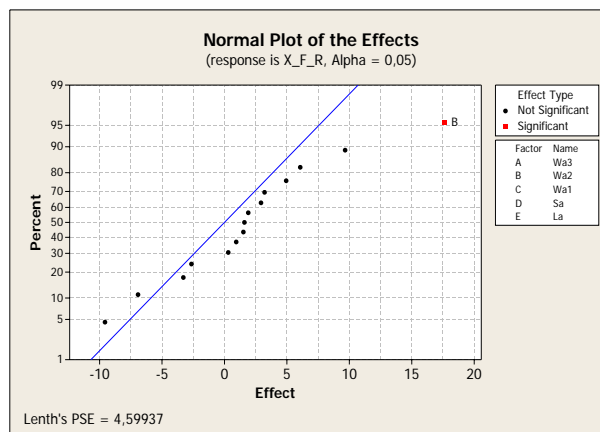


Figure 4–8: Normal probability plot of the effects for the reactance at  $F_R$  in DOE I.

The  $X_{F,R}$  regression model is given by:

$$X_{F\_R}(\text{model}) = 39.261 + 8.796B \quad (4.3)$$

In Equation (4.3),  $B$  is the coded factor that corresponds to  $Wa_2$ . The factor that is discarded for obtaining the residual plots is  $Sa$ .

### DOE results for $\Gamma_{F\_R}$

The minimum and maximum values of the magnitude of the reflection coefficient at  $F\_R$  are 0.25 and 0.64, respectively. These results show that it is possible to achieve the goal of  $\Gamma_{F\_R} < 0.33$ , which means that the antenna could be designed for  $VSWR < 2$ . Note that the most significant effects in the the design are caused by  $Wa_3$  and the interaction  $Wa_3Wa_2$ . To obtain the lowest magnitude of the reflection coefficient it is necessary to maintain  $Wa_3$  in the low level and each factor of the interaction  $Wa_3Wa_2$  simultaneously in the low level.

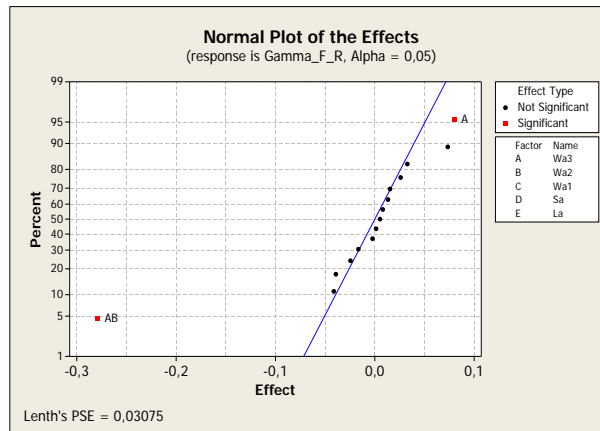


Figure 4–9: Normal probability plot of the effects for the magnitude of the reflection coefficient at  $F\_R$  in DOE I.

The factors that affect the magnitude of the reflection coefficient are the same that affect the resistance and reactance of the antenna. Thus, if  $Wa_2$  is maintained

in the low level, a decrement in the reactance and reflection coefficient could be obtained.

The  $\Gamma_{F_R}$  regression model is given by:

$$\Gamma_{F_R}(model) = 0.5288 - 0.1395BA + 0.0400B + 0.0367A \quad (4.4)$$

In Equation (4.4), B and A are the coded factor that corresponds to  $Wa_2$  and  $Wa_3$ , respectively. The influence of the factor  $Wa_3$  was included in Equation (4.4) because the effect is significant although it was not marked in the Figure 4–9. The factor that is discarded for obtaining the residual plots is  $Sa$ .

#### **DOE results for $\Gamma_{5GHz}$**

The maximum and minimum magnitude of the reflection coefficient at 5 GHz are 0.60 and 0.97. The normal probability plot of the effects of Figure 4–10 shows that  $Wa_2$  and  $La$  and the two-factor interaction  $Wa_2La$ , are the factors that most effect have on  $\Gamma_{5GHz}$ . The plot shows that all factors have negative effect on the response. Thus, for a lowest value of  $\Gamma_{5GHz}$  it is necessary to set  $Wa_2$  and  $La$  in the high level, which guarantee that the interaction  $Wa_2La$  have a negative effect on the response.

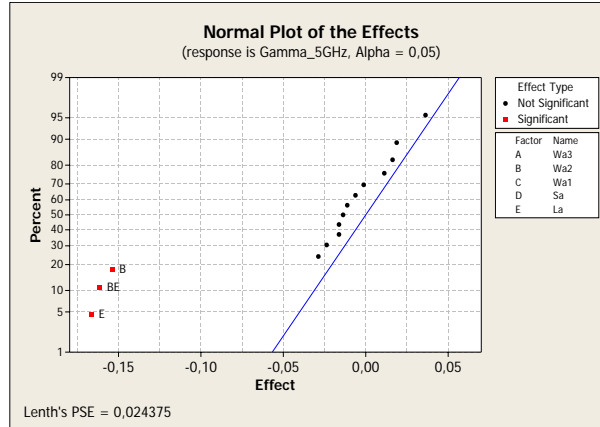


Figure 4–10: Normal probability plot of the effects for the magnitude of the reflection coefficient at 5 GHz in DOE I.

The  $\Gamma_{5GHz}$  regression model is given by:

$$\Gamma_{5GHz}(model) = 0.85813 - 0.7687B - 0.08313E - 0.08063BE \quad (4.5)$$

In Equation (4.5), B and E are the coded factor that corresponds to  $Wa_2$  and  $La$ , respectively. The factor that is discarded for obtaining the residual plots is  $Sa$ .

#### DOE results for $G_{S_{F-R}}$

The maximum and minimum gain values on the substrate side at  $F_R$  are 5.63 dB and 4.63 dB, respectively. The difference of 1dB between the maximum and minimum gain suggests that  $G_{S_{F-R}}$  remain almost constant through all designs considered in DOE I. Figure 4–11, show the that  $Wa_2$  have a positive effect on  $G_{S_{F-R}}$ .

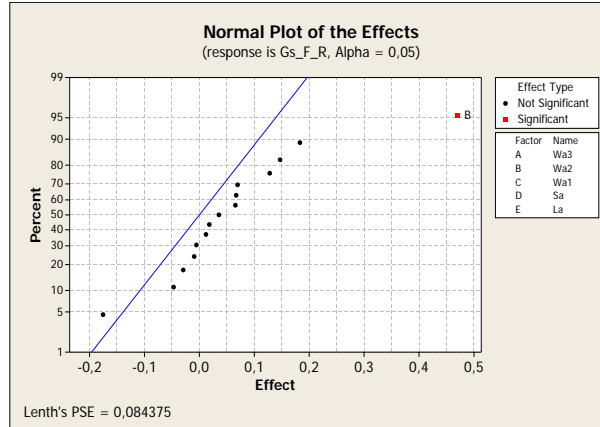


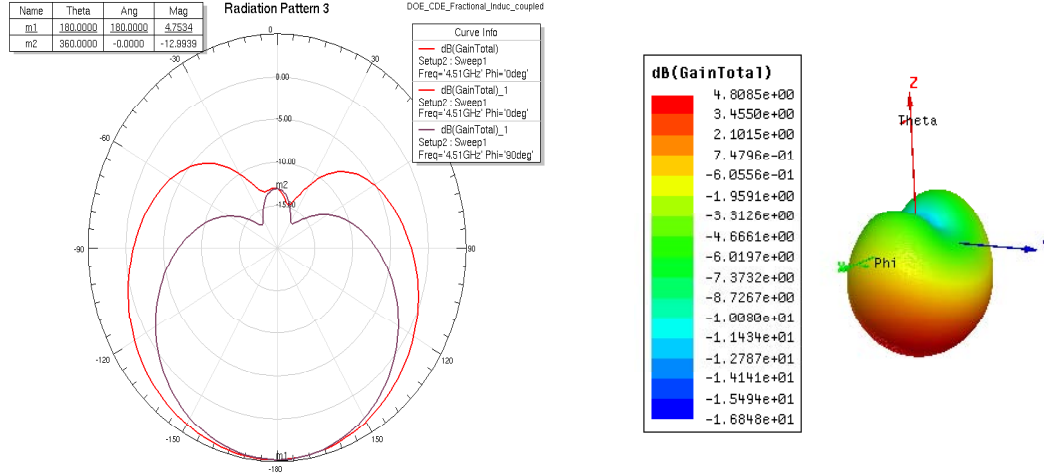
Figure 4–11: Normal probability plot of the effects for the gain in the substrate side at  $F_R$  in DOE I.

The  $G_{s_{F_R}}$  regression model is given by:

$$G_{s_{F_R}}(model) = 5.1660 + 0.2347B \quad (4.6)$$

In Equation (4.6), B is the coded factor that corresponds to  $W_{a_2}$ . The factor that is discarded for obtaining the residual plots is  $Sa$ .

Before continuing with the results for  $G_{c_{F_R}}$ , 2-D and 3-D plots of radiation pattern for the design CDE are presented in Figure 4–12(a) and 4–12(b) for providing an insight about the radiation of the CPW-inductively fed CBFSA. In 4–12, the red line and violet lines corresponds to the radiation pattern measured at  $\phi=0$  and  $\phi=90$ , respectively.



(a) 2-D Radiation pattern plot for CDE design.

(b) 3-D Radiation pattern plot for CDE design.

Figure 4–12: 2-D and 3-D Radiation patterns plots for CDE design: (a) 2-D plot ; and (b) 3-D plot.

In the 2-D plot is observed that the gain on the substrate side for this CBFSA, which employs a shallow cavity, is 4.75 dB. The gain value observed are higher than the ones typically observed for a FSA, which are close to 2 dB. It should be mentioned that the radiation pattern appear broadside for all DOE experiments discussed in this work.

### DOE results for $G_{C_{F-R}}$

The maximum and minimum values obtained for the gain on the cavity side are -12.19 dB and -13.53 dB, respectively. Note that  $G_{C_{F-R}}$  remains almost constant for all designs. The fact that the gain remain constant on the substrate side, as well as on the substrate side, could allow to affirm that the gain and the front to back ratio ( $\approx 17.5$  dB) for the CPW-inductively fed CBFSA do not depend on the FSA dimensions used in DOE I. Low radiation on the cavity side is obtained with this structure that uses a shallow cavity ( $H_w \approx \frac{\lambda_0}{40} \approx \frac{\lambda_d}{22}$ ).

Figure 4-13 shows the normal probability plot of the effects for  $G_{c_{F\_R}}$ . Significant effects caused by the factors on the response are not observed. Therefore, in the regression model of Equation (4.7), all factors are included.

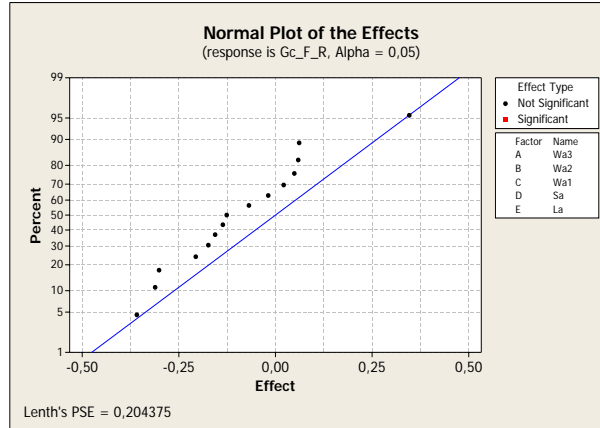


Figure 4-13: Normal probability plot of the effects for the gain in the cavity side at  $F\_R$  in DOE I.

The  $G_{c_{F\_R}}$  regression model is given by:

$$\begin{aligned}
 G_{c_{F\_R}}(model) = & -12.81 + 0.17A - 0.18B - 0.09C - 0.06D - 0.15E \\
 & - 0.01AB + 0.03AC - 0.08AD - 0.10AE - 0.03BC \quad (4.7) \\
 & - 0.07BD + 0.02BE - 0.16CD + 0.03CE + 0.01DE
 \end{aligned}$$

In the last equation, A, B, C, D and E are the coded factors that correspond to  $Wa_3$ ,  $Wa_2$ ,  $Wa_1$ ,  $Sa$  and  $La$ , respectively. In this case, it is not possible to discard any factor for testing the accuracy of the model.

#### DOE results for $G_{s_{5GHz}}$

The minimum and maximum values obtained for  $G_{s_{5GHz}}$  are -7.24 dB and 5.50 dB. The low gain in the substrate side obtained at 5GHz for some designs could be

explained because the impedance bandwidth of the CPW-inductively fed CBFSA is around 120 MHz and the resonance frequency these designs are far from 5 GHz.

Figure 4-14 shows the normal probability plot of the effects for  $G_{s_{5GHz}}$ . Significant effects caused by the factors on the response are not observed. Therefore, in the regression model of Equation (4.8), all factors are included.

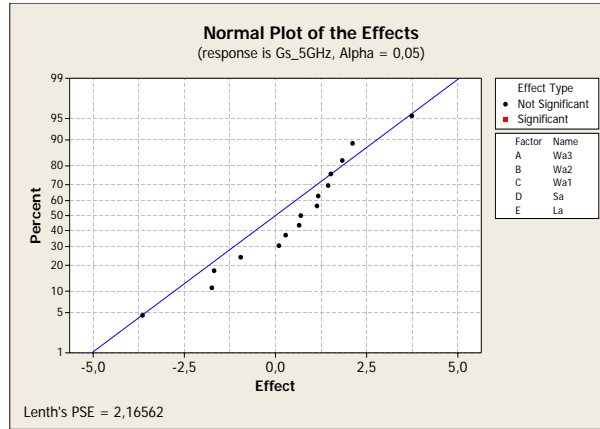


Figure 4-14: Normal probability plot of the effects for the gain in the substrate side at 5 GHz in DOE I.

The  $G_{s_{5GHz}}$  regression model is given by:

$$\begin{aligned}
 G_{s_{5GHz}}(model) = & 2.043 - 0.873A + 1.868B + 0.324C + 0.758D \\
 & + 0.568E - 0.722AB - 0.477AC + 1.057AD \\
 & + 0.139AE + 0.347BC - 0.842BD + 0.916BE \\
 & + 0.047CD - 1.823CE + 0.586DE
 \end{aligned} \tag{4.8}$$

In the last equation, A, B, C, D and E are the coded factors that correspond to  $Wa_3$ ,  $Wa_2$ ,  $Wa_1$ ,  $Sa$  and  $La$ , respectively. In this case, it is not possible to discard any factor for testing the accuracy of the model.

### DOE results for $G_{c_{5GHz}}$

The maximum and minimum values obtained for the gain on the cavity side at 5 GHz are -12.90 dB and -27.02 dB, respectively. Figure 4–15 shows the normal probability plot of the effects for  $G_{c_{5GHz}}$ . Significant effects caused by the factors on the response are not observed. Therefore, in the regression model of Equation (4.9), all factors are included.

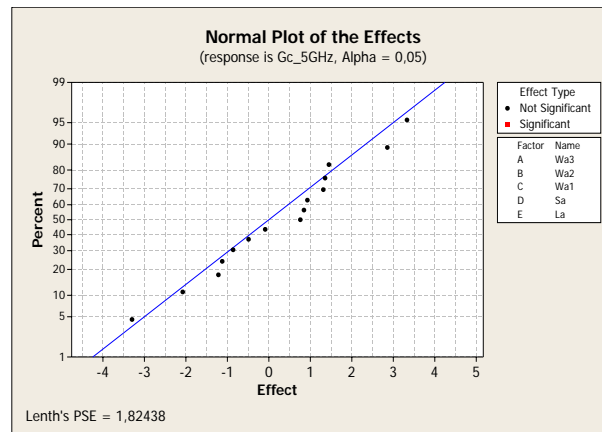


Figure 4–15: Normal probability plot of the effects for the gain in the cavity side at 5 GHz in DOE I.

The  $G_{c_{5GHz}}$  regression model is given by:

$$\begin{aligned}
 G_{c_{5GHz}}(model) = & -16.02 - 0.56A + 1.67B - 0.24C + 0.68D - 1.04E \\
 & + 0.46AB - 0.43AC + 0.72AD - 0.04AE + 0.66BC \\
 & - 0.61BD + 1.43BE + 0.38CD - 1.65CE + 0.42DE
 \end{aligned} \quad (4.9)$$

In the last equation, A, B, C, D and E are the coded factors that correspond to  $Wa_3$ ,  $Wa_2$ ,  $Wa_1$ ,  $Sa$  and  $La$ , respectively. In this case, it is not possible to discard any factor for testing the accuracy of the model.

### Validation of the regression models

The validation consists in performing an additional simulation of the structure by using the central values for the factors. Additionally, the predicted values of each interest response are calculated for the central values by using the regression models. Then, the simulated and predicted responses are compared. The central values are:  $Wa_3 = 0.65\text{mm}$ ,  $Wa_2 = 0.75\text{mm}$ ,  $Wa_1 = 0.75\text{mm}$ ,  $Sa = 0.45\text{mm}$  and  $La = 16\text{mm}$ .

To use the central values into the regression models, these values must be coded. Previously the coding was carried out for the high and low levels of the factors, obtaining 1 for the high level and -1 for the low level. For coding additional dimensions, such as the central values into coded values, the following equation should be used:

$$Value_{coded} = \frac{Value_{phys} - \frac{Value_{phys\_high} + Value_{phys\_low}}{2}}{\frac{Value_{phys\_high} - Value_{phys\_low}}{2}} \quad (4.10)$$

In Equation (4.10),  $Value_{phys\_high}$  and  $Value_{phys\_low}$  correspond to the high and low level of the factor, respectively. In this case,  $Value_{phys}$  corresponds to the central value of the factor. According with Equation (4.10), the central values coded are set to be zero. Therefore, the regression models coincide with the average of the observations, which is the first term of each regression model equation. Table 4-2 presents the predicted and simulated interest responses when central values are used.

Table 4-2: Predicted and simulated interest responses for DOE I

Response	Rmax	$X_{F\_R}$	$F\_R$	$\Gamma_{F\_R}$	$\Gamma_{5GHz}$	$G_{S_{F\_R}}$	$G_{C_{F\_R}}$	$G_{S_{5GHz}}$	$G_{C_{5GHz}}$
Simulated	91.09	38.12	5.08	0.38	0.76	5.41	-12.55	5.32	-13.84
Predicted	112.42	39.26	5.09	0.52	0.85	5.16	-12.81	2.04	-16.02
Percent									
Difference(%)	20.9	2.9	0.19	31.1	11.18	4.73	2.05	89.13	14.60

The best correspondence between the simulated and predicted values is observed for the regression models of  $F_{R}$ ,  $G_{C_{F_R}}$  and  $X_{F_R}$ . Good agreement is obtained for the models of  $G_{S_{F_R}}$  and  $\Gamma_{5GHz}$ . However, differences above 14 % are observed for the rest of models. The model of  $G_{S_{5GHz}}$  has the largest percent difference. The differences observed between the simulated and predicted values could be produced because the lineal model is assumed to represent the factor effects and possible second order effects on the responses were omitted.

#### 4.1.2 DOE II simulation results

Table 4–3 shows the simulation results obtained for the designs proposed in DOE II. The interest responses remain the same as the previous analysis. In this subsection, the effect that the factors  $Wa_3$ ,  $g$ ,  $t$ ,  $m$ ,  $n$ ,  $La$  and  $Sa$  have on each interest response of the CPW-capacitively fed CBFSA is studied.

Table 4–3: Simulation results for DOE II ( $2_{VII}^{7-1}$  fractional factorial design)

Design	Rmax	$X_{F_R}$	$F_R$	$\Gamma_{F_R}$	$\Gamma_{5GHz}$	$G_{S_{F_R}}$	$G_{C_{F_R}}$	$G_{S_{5GHz}}$	$G_{C_{5GHz}}$
G	32.49	15.48	5.54	0.28	0.96	4.97	-12.93	-0.82	-13.73
A	16.80	-21.47	5.60	0.56	0.97	5.04	-12.27	-0.47	-14.14
B	76.64	-21.93	5.68	0.25	0.96	4.54	-13.5	1.30	-13.34
ABG	21.38	-53.8	5.66	0.54	0.97	5.09	-12.35	-0.23	-13.77
C	23.17	1.64	5.55	0.37	0.97	4.53	-13.25	-2.10	-14.48
ACG	4.45	-5.64	5.60	0.84	0.97	4.20	-12.46	-20.65	-22.17
BCG	8.89	-0.83	5.58	0.70	0.97	3.70	-13.38	-4.00	-15.90
ABC	9.77	20.28	5.63	0.71	0.97	-3.89	-18.00	-11.47	-26.48
D	149.77	-17.77	5.60	0.49	0.94	5.03	-12.95	2.65	-12.53
ADG	37.06	-18.92	5.65	0.26	0.96	5.21	-12.19	1.09	-13.32
BDG	106.57	-30.84	5.62	0.39	0.95	5.13	-12.16	2.26	-13.39
ABD	45.24	-27.77	5.69	0.28	0.95	5.12	-11.94	0.92	-13.07
CDG	83.18	3.59	5.58	0.23	0.95	5.00	-12.15	1.59	-13.32
ACD	23.48	1.13	5.64	0.37	0.96	4.95	-12.34	-0.57	-14.64
BCD	63.55	3.85	5.67	0.11	0.96	4.78	-12.67	0.58	-14.20
ABCDG	15.76	-2.41	5.68	0.53	0.97	4.98	-12.02	-1.26	-14.19

Continued ...

Table 4-3: (continued)

Design	Rmax	$X_{F_R}$	$F_R$	$\Gamma_{F_R}$	$\Gamma_{5GHz}$	$G_{S_{F_R}}$	$G_{C_{F_R}}$	$G_{S_{5GHz}}$	$G_{C_{5GHz}}$
E	34.95	19.38	5.50	0.28	0.97	5.02	-11.82	-0.78	-15.72
AEG	9.79	16.11	5.58	0.70	0.97	5.19	-11.48	-2.23	-14.50
BEG	79.79	-19.59	5.62	0.26	0.95	5.14	-12.25	1.94	-12.88
ABE	35.05	-21.93	5.67	0.30	0.96	5.22	-12.25	0.68	-12.89
CEG	23.25	8.75	5.48	0.39	0.97	4.93	-11.90	-1.22	-14.27
ACE	4.82	7.02	5.58	0.83	0.98	4.54	-12.40	-4.98	-15.68
BCE	0.74	33.06	5.52	0.98	0.98	2.97	-15.16	-11.80	-20.68
ABCEG	1.17	23.66	5.67	0.96	0.98	1.27	-15.18	-20.81	-20.51
DEG	138.48	-9.50	5.61	0.46	0.94	5.12	-12.24	2.78	-11.99
ADE	55.79	-11.53	5.66	0.11	0.95	5.27	-12.43	1.73	-12.75
BDE	122.34	-10.98	5.67	0.41	0.94	5.14	-12.53	2.38	-13.36
ABDEG	43.12	-14.49	5.71	0.17	0.96	5.28	-11.77	1.40	-13.22
CDE	107.34	7.44	5.56	0.35	0.95	5.09	-12.28	1.96	-13.47
ACDEG	29.10	8.36	5.65	0.29	0.97	5.18	-11.7	0.00	-13.57
BCDEG	59.61	5.73	5.62	0.09	0.96	5.22	-12.13	0.94	-13.40
ABCDE	20.45	6.52	5.72	0.43	0.96	4.89	-12.32	-0.91	-14.26
F	95.31	-36.48	4.77	0.38	0.92	4.94	-12.7	3.82	-18.37
AFG	19.27	-32.03	4.93	0.58	0.88	5.19	-12.26	5.15	-14.49
BFG	62.71	-36.01	4.83	0.32	0.91	5.06	-12.45	4.17	-16.60
ABF	29.73	-40.60	4.96	0.50	0.69	5.33	-12.33	5.43	-13.84
CFG	17.33	-4.99	4.74	0.48	0.96	4.70	-12.54	0.31	-21.92
ACF	0.79	-3.51	4.80	0.96	0.97	-4.26	-19.78	-3.79	-21.68
BCF	9.15	-12.29	4.81	0.70	0.96	4.73	-12.95	0.47	-22.06
ABCFG	3.45	20.34	4.91	0.88	0.94	-2.11	-14.32	3.05	-14.24
DFG	113.5	-24.32	4.88	0.41	0.77	5.27	-12.86	5.20	-15.12
ADF	35.99	-8.19	4.96	0.18	0.42	5.41	-12.2	5.52	-13.75
BDF	121.69	-35.45	4.93	0.45	0.70	5.35	-12.83	5.39	-14.61
ABDFG	34.58	-25.60	5.03	0.33	0.32	5.43	-11.95	5.54	-12.85
CDF	62.95	43.42	4.79	0.56	0.78	4.96	-12.66	4.54	-16.18
ACDFG	20.35	16.50	4.98	0.47	0.47	5.82	-12.02	5.43	-13.40
BCDFG	42.76	-1.45	4.92	0.08	0.64	5.25	-12.24	5.28	-14.79
ABCDF	15.38	5.85	4.99	0.53	0.63	5.28	-11.96	5.40	-13.15
EFG	93.96	-26.61	4.87	0.34	0.78	5.22	-12.67	5.12	-15.12
AEF	33.18	-13.43	4.96	0.25	0.47	5.36	-12.07	5.51	-13.71

Continued ...

Table 4-3: (continued)

Design	Rmax	$X_{F_R}$	$F_R$	$\Gamma_{F_R}$	$\Gamma_{5GHz}$	$G_{S_{F_R}}$	$G_{C_{F_R}}$	$G_{S_{5GHz}}$	$G_{C_{5GHz}}$
BEF	101.51	-33.36	4.92	0.39	0.71	5.34	-12.71	5.36	-14.32
ABEFG	22.17	-18.44	5.02	0.44	0.45	5.43	-12.25	5.55	-13.29
CEF	36.98	3.97	4.74	0.15	0.93	4.73	-12.32	3.00	-19.84
ACEFG	7.38	5.97	4.94	0.74	0.84	4.64	-12.17	4.72	-14.22
BCEFG	0.63	10.57	4.71	0.97	0.98	0.29	-13.51	-11.47	-22.10
ABCEF	0.53	14.85	4.84	0.98	0.98	1.02	-13.06	-13.26	-18.94
DEF	145.68	-6.81	4.93	0.48	0.60	5.36	-12.97	5.45	-14.60
ADEFG	30.80	36.93	5.00	0.46	0.46	5.51	-13.31	5.51	-13.31
BDEFG	87.59	6.83	4.99	0.27	0.26	5.41	-12.29	5.55	-13.87
ABDEF	25.66	23.35	5.02	0.42	0.50	5.44	-12.00	5.42	-12.50
CDEFG	92.55	22.33	4.90	0.33	0.48	5.24	-12.26	5.29	-14.10
ACDEF	29.74	23.69	4.98	0.37	0.34	5.37	-11.98	5.51	-13.39
BCDEF	59.42	13.31	4.94	0.14	0.34	5.31	-12.21	5.45	-14.01
ABCDEFG	13.80	24.69	5.03	0.64	0.67	5.26	-11.89	5.38	-13.27
Max	149.77	43.42	5.72	0.98	0.98	5.82	-11.48	5.55	-11.99
Min	0.53	-53.80	4.71	0.08	0.26	-4.26	-19.78	-20.81	-26.48

### DOE results for Rmax

Simulation results showed that the maximum and minimum resistance measured at  $F_R$  are  $149.77 \Omega$  and  $0.53 \Omega$ , respectively. The resistance range obtained for this structure is  $332.48 \Omega$  lower than the resistance obtained with the CPW-inductively fed CBFSAs.

The resistance plots obtained with DOE II designs are similar to the plot of Figure 4-7, in which the cavity and FSA peaks are observed.

Figure 4-16, shows the normal probability plot of the effects for Rmax. The factors and two-factors interaction that have negative effect on Rmax are:  $Wa_3$ ,  $t$ ,  $Wa_3m$ ,  $mLa$  and  $gm$ . Otherwise, the factors and two-factors interaction that have positive effect on Rmax are:  $m$  and  $Wa_3t$ .

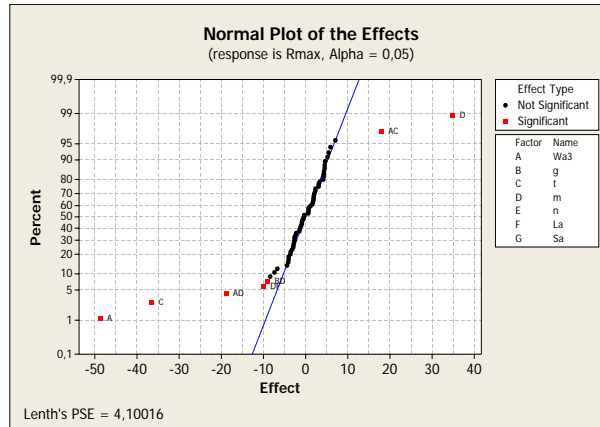


Figure 4–16: Normal probability plot of the effects for the maximum resistance in DOE II.

The Rmax regression model is given by:

$$\begin{aligned}
 Rmax(model) = & 46.10 - 24.35A - 18.23C + 17.44D \\
 & - 9.42AD - 4.99DF - 4.49BD + 9.00AC
 \end{aligned} \tag{4.11}$$

In Equation (4.11), A, B, C, D and F are the coded factors that correspond to  $Wa_3$ ,  $g$ ,  $t$ ,  $m$  and  $La$ , respectively. Since  $Sa$  has negligible effect on Rmax, it will be discarded for obtaining the residual plots.

### DOE results for $F_R$

The maximum and minimum values obtained for  $F_R$  are 5.66 GHz and 4.51 GHz, respectively. Regarding the resonance frequency of the cavity, Figure 4–18 shows that this resonance agrees with the calculated resonance frequency for the  $TE_{101}$  mode presented in Table 3–2 for the B and AB design. The correspondence between the theoretical and simulated resonance frequencies of the cavity for the additional designs was also confirmed

Figure 4–17, shows the normal probability plot of the effects for  $F_R$ .

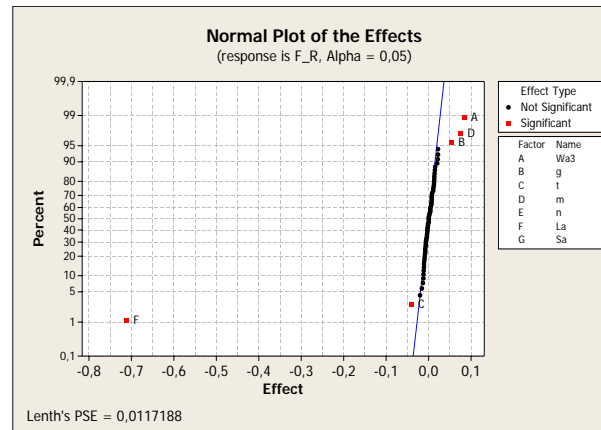


Figure 4–17: Normal probability plot of the effects for the frequency at maximum resistance in DOE II.

The factors that negatively affect  $F_R$  are  $La$  and  $t$ . The factors that positively affect  $F_R$  are  $g$ ,  $m$  and  $Wa_3$ . The influence of the factors  $La$  and  $Wa_3$  on  $F_R$  had also been observed in DOE I for the CPW-inductively fed CBFSA.

Note the similarity between the maximum and minimum values of  $F_R$  obtained with the CPW-inductively and CPW-capacitively fed CBFSA's. This could be explained because for both designs, the factor that has the strongest effect on  $F_R$  is  $La$ . The high and low levels of this factor are the same for both DOE I and DOE II.

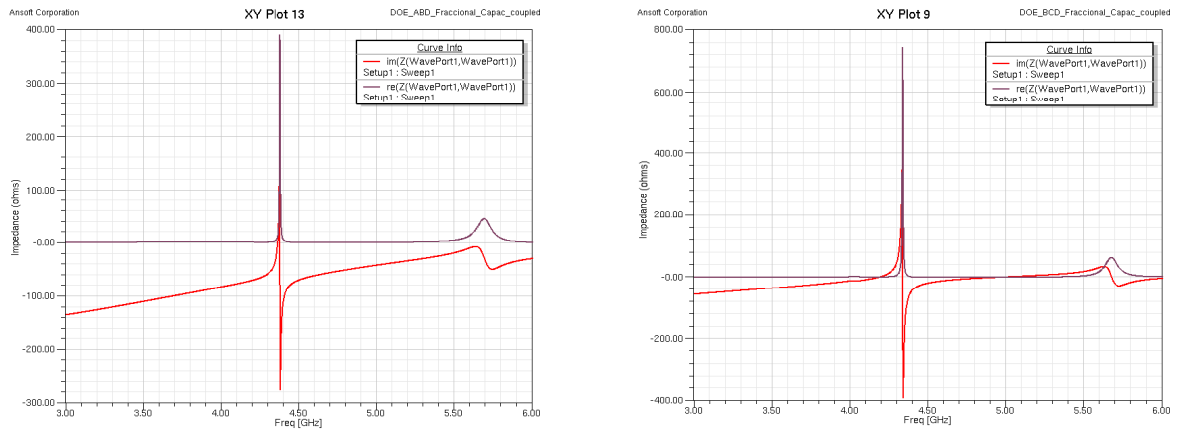
The  $F_R$  regression model is given by:

$$F_R(model) = 5.2627 + 0.0417A + 0.0267B - 0.0205C + 0.0373D - 0.3558F \quad (4.12)$$

In Equation (4.12), A, B, C, D and F are the coded factors that correspond to  $Wa_3$ ,  $g$ ,  $t$ ,  $m$  and  $La$ , respectively. Since  $Sa$  has negligible effect on  $F_R$ , it will be discarded for obtaining the residual plots.

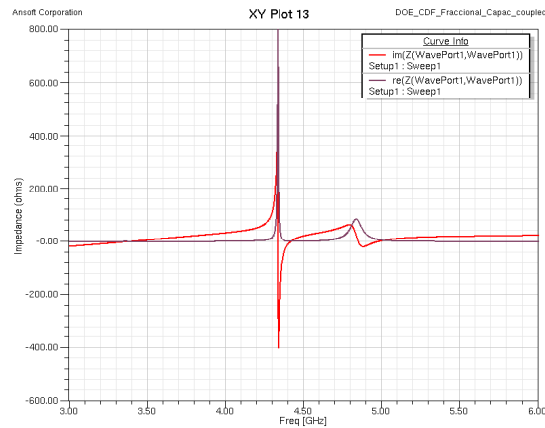
### DOE results for $X_{F\_R}$

Observe from Table 4-3 that positive as well negative reactances are obtained with the CPW-capacitively fed CBFSA, contrary to the CPW-inductively fed CBFSA presented previously, which only presents an inductive behavior. The maximum and minimum values obtained for  $X_{F\_R}$  are  $43.42 \Omega$  and  $-53.80 \Omega$ , respectively. Figure 4-18, shows three impedance plots measured at  $F\_R$  for the ABD, BCD and CDF designs of DOE II.



(a) Impedance plot for the ABD design.

(b) Impedance plot for the BCD design.



(c) Impedance plot for the CDF design.

Figure 4-18: Impedance plots for CDF, BCD and ABD designs of DOE II: (a) Impedance plot for the ABD design; (b) Reactance for the BCD design; and (c) Impedance plot for the CDF design.

It is observed that the CPW-capacitively fed CBFSA could resonate at the first useful resonance or could have an inductive or capacitive behavior, depending on the geometrical dimensions of the design. For this structure note that the influence that the capacitive feed to the antenna have on the antenna impedance and the strong coupling between the FSA and the cavity.

Figure 4–19, shows the normal probability plot of the effects for  $X_{F,R}$ . The three-factor interactions  $gtLa$  and  $gtm$  have negative effects on  $X_{F,R}$ , whereas the factors  $t$ ,  $m$  and  $n$  and the two-factors interactions  $mLa$ ,  $gt$  and  $Wa_3La$  have a positive effect on the the this response.

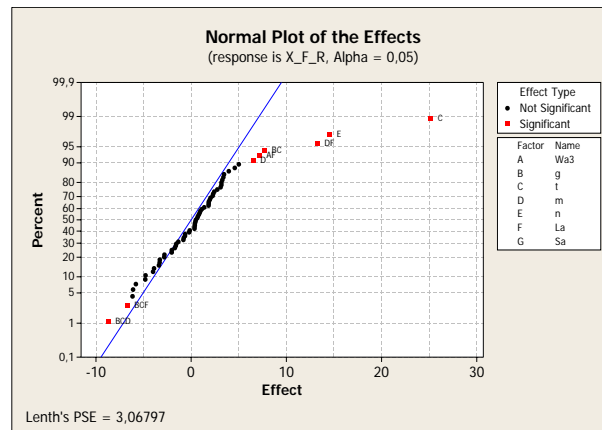


Figure 4–19: Normal probability plot of the effects for the reactance at  $F_R$  in DOE II.

The  $X_{F,R}$  regression model is given by:

$$\begin{aligned}
 X_{F,R}(model) = & -3.037 + 12.581C + 7.282E + 3.271D + 3.867BC \\
 & + 6.639DF + 3.595AF - 3.341BCF - 4.353BCD
 \end{aligned}
 \tag{4.13}$$

In Equation (4.13), A, B, C, D, E and F are the coded factors that correspond to  $Wa_3$ ,  $g$ ,  $t$ ,  $m$ ,  $n$  and  $La$ , respectively. Since  $Sa$  has negligible effect on  $X_{F_R}$ , it will be discarded for obtaining the residual plots.

### DOE results for $\Gamma_{F_R}$

The maximum and minimum values obtained for  $\Gamma_{F_R}$  are 0.08 and 0.98, respectively. It is observed from Table 4-3 that lower values of  $\Gamma_{F_R}$  are obtained with the CPW-capacitively fed CBFSA structure than the ones obtained with the CPW-inductively fed CBFSA. This result is a consequence that low values of either  $R_{max}$  and  $X_{F_R}$  are obtained with this structure.

Figure 4-20, shows the normal probability plot of the effects for  $\Gamma_{F_R}$ .

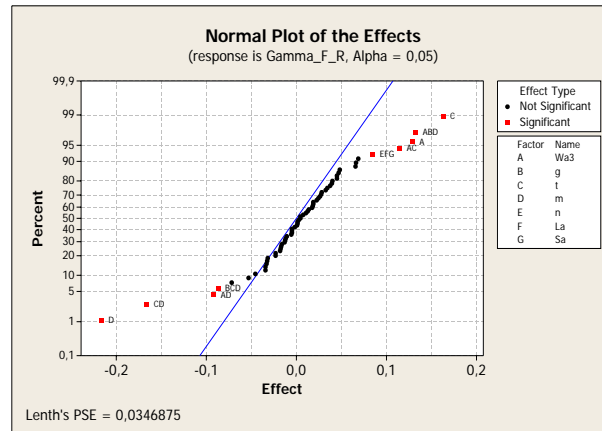


Figure 4-20: Normal probability plot of the effects for the reflection coefficient at  $F_R$  in DOE II.

This plot shows that all factors have influence on  $\Gamma_{F_R}$ . This could be unfavorable because the complexity in the regression model and the design increases. The factors  $m$ ,  $tm$ ,  $Wa_3m$  and  $gtm$  have negative effects on  $\Gamma_{F_R}$ , whereas the factors  $nLaSa$ ,  $Wa_3t$ ,  $Wa_3gm$  and  $t$  have a positive effect on the this response.

The  $\Gamma_{F_R}$  regression model is given by:

$$\begin{aligned} \Gamma_{F.R}(model) = & 0.4547 - 0.1081D - CD0.0831 - 0.0459AD - 0.0434BCD \\ & + 0.0425EFG + 0.0575AC + 0.0663ABD + 0.0816C \end{aligned} \quad (4.14)$$

In Equation (4.14), A, B, C, D, E, F and G are the coded factors that correspond to  $Wa_3$ ,  $g$ ,  $t$ ,  $m$ ,  $n$ ,  $La$  and  $Sa$ , respectively. Since all factors are included in the regression model, it is not possible to discard any factor for performing the residual analysis.

#### DOE results for $\Gamma_{5GHz}$

The maximum and minimum values obtained for  $\Gamma_{5GHz}$  are 0.98 and 0.26, respectively. Note that the minimum value is 0.34 times lower than the one obtained in DOE I, for the CPW-inductively fed CBFSA. According to Table 4-3, the design BDEFG obtain the lowest reflection coefficient at 5GHz. This means that this design achieve the goal  $\Gamma < 0.33$  at 5 GHz.

Figure 4-21, shows the normal probability plot of the effects for  $\Gamma_{5GHz}$ . This plot shows that all factors have influence on  $\Gamma_{F.R}$ . The factors  $La$ ,  $m$ ,  $mLa$ ,  $nLa$ ,  $n$ ,  $Wa_3La$ ,  $Wa_3$ ,  $tmLa$  and  $tm$  have negative effects on  $\Gamma_{F.R}$ , whereas the factors  $gtSa$ ,  $Wa_3nm$ ,  $tLa$  and  $t$  have a positive effect on the the this response.

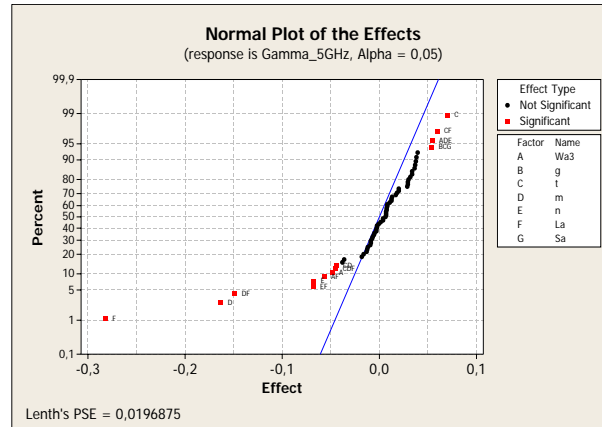


Figure 4–21: Normal probability plot of the effects for the reflection coefficient at 5 GHz in DOE II.

Note that  $La$  is the factor that has strongest effect on  $\Gamma_{5GHz}$ , although there are also influence of all factors. The strong influence that this has on  $\Gamma_{5GHz}$  has also been observed for the CPW-inductively fed CBFSA.

The  $\Gamma_{5GHz}$  regression model is given by:

$$\begin{aligned}
 \Gamma_{5GHz}(model) = & 0.8206 - 0.1409F - 0.0816D - 0.0744DF \\
 & - 0.0341EF - 0.0337E - 0.0284AF - 0.0244A \\
 & - 0.0225CDF - 0.0222CD + 0.0269BCG \\
 & + 0.0272ADE + 0.0297CF + 0.0350C
 \end{aligned} \tag{4.15}$$

In Equation (4.15), A, B, C, D, E, F and G are the coded factor that correspond to  $Wa_3$ ,  $g$ ,  $t$ ,  $m$ ,  $n$ ,  $La$  and  $Sa$ , respectively. Since all factors are included in the regression model, it is not possible to discard any factor for performing the residual analysis.

### DOE results for $G_{S_{F_R}}$

The 2-D and 3-D radiation patterns plots for the CPW-capacitively fed CBFSAs are very similar to the Figures 4-12(a) and 4-12(b), obtained for the CPW-inductively fed CBFSAs. The maximum and minimum values of  $G_{S_{F_R}}$  are 5.63 dB and -4.26 dB, respectively. According to Table 4-3, the designs that obtained the lowest gain values are the same designs that had the lowest resistances  $R_{max}$ . These low resistances are close to be a electric short-circuit. For example, for the design ABC,  $R_{max}$  and  $G_{S_{F_R}}$  are 9.77  $\Omega$  and -3.89 dB, respectively. Also, for the ABC design,  $R_{max}$  and  $G_{S_{F_R}}$  are 0.79  $\Omega$  and -4.26 dB, respectively.

Figure 4-22, shows the normal probability plot of the effects for  $G_{S_{F_R}}$ . Observe that  $t$  is the factor that has negative influence on  $G_{S_{F_R}}$ , whereas  $m$  and  $tm$  have positive effects on this response. The factors  $m$  and  $t$  have also strong influence on  $R_{max}$ , which could explain the results obtained for  $G_{S_{F_R}}$ .

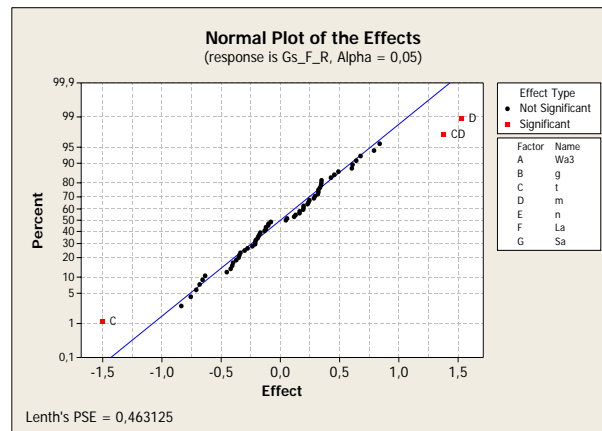


Figure 4-22: Normal probability plot of the effects for the gain in the substrate side at  $F_R$  in DOE II.

The  $G_{S_{F_R}}$  regression model is given by:

$$Gs_{F_R}(model) = 4.4552 - 0.7498C + 0.6905CD + 0.7655D \quad (4.16)$$

In Equation (4.16), C and D are the coded factors that correspond to  $t$  and  $m$ , respectively. Since,  $Sa$  has negligible effect on  $Gs_{F_R}$ , it will be discarded for obtaining the residual plots.

In the normal probability plot of the residuals of Figure 5-9(a), it is observed that there are two residuals that appear separated from the normal line. The residual at the right to the line corresponds to the design ACG, which  $R_{max}$  is  $4.45 \Omega$  and the residual at the left to the line corresponds to ACF, which  $R_{max}$  is  $0.79 \Omega$ . Therefore, the presence of these outliers could be due to those designs which resistance is strongly decreased.

#### DOE results for $G_{C_{F_R}}$

The maximum and minimum values of  $G_{C_{F_R}}$  are -11.48 dB and -19.78 dB, respectively. Therefore, low radiation contribution is obtained from the cavity side of the CPW-capacitively fed CBFSA. The front to back ratios are  $\approx 15$  dB for all designs, which is similar to the values obtained for DOE I. This result show that  $Gs_{F_R}$  and  $G_{C_{F_R}}$  decrease in almost the same proportion for the designs where  $R_{max}$  is strongly decreased.

Figure 4-23, shows the normal probability plot of the effects for  $G_{C_{F_R}}$ . According with the plot, the two-factor interaction  $tm$  has a positive effect on  $G_{C_{F_R}}$ .

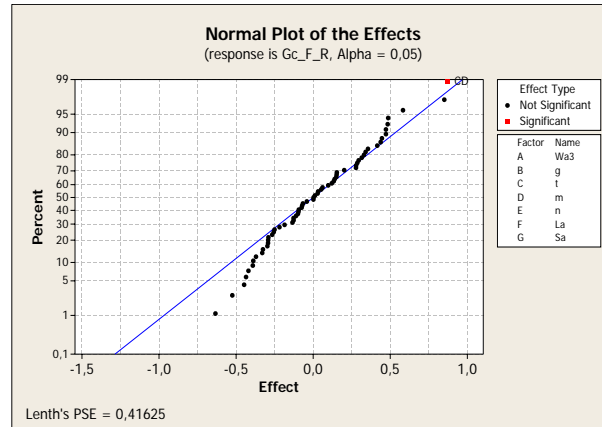


Figure 4–23: Normal probability plot of the effects for the gain in the cavity side at  $F_R$  in DOE II.

The  $G_{C_{F_R}}$  regression model is given by:

$$G_{C_{F_R}}(model) = -12.72 + 0.44CD \quad (4.17)$$

In Equation (4.17), C and D are the coded factors that correspond to  $t$  and  $m$ , respectively. Since  $Sa$  has negligible effect on  $G_{C_{F_R}}$ , it will be discarded for obtaining the residual plots.

Similar to the previous case, in the normal probability plot of the residuals of Figure 5–10(a), the residuals of the ACG and ACF designs appear separated from the normal line.

#### DOE results for $G_{S_{5GHz}}$

The maximum and minimum values of  $G_{S_{5GHz}}$  are 5.55 dB and -20.81 dB, respectively. Figure 4–24, shows the normal probability plot of the effects for  $G_{S_{5GHz}}$ . According with the plot, the factors that most influence  $G_{S_{5GHz}}$  are  $t$ ,  $m$  and  $La$ . Other factors that also have effect on the response are  $gtn$ ,  $gn$ ,  $gt$ ,  $Wa_3$ ,  $gtm$ ,  $Wa_3La$ ,  $gmn$ ,  $Wa_3LaSa$  and  $tm$ .

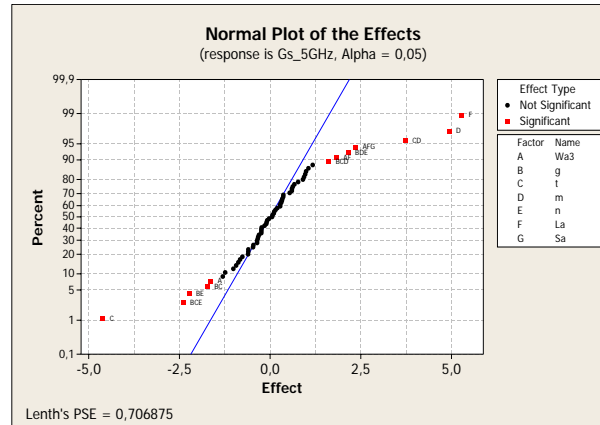


Figure 4-24: Normal probability plot of the effects for the gain in the substrate side at 5 GHz in DOE II.

The  $G_{s5GHz}$  regression model is given by:

$$\begin{aligned}
 G_{s5GHz}(model) = & 0.764 - 2.308C - 1.197BCE - 1.117BE - 0.864BC \\
 & - 0.817A + 0.807BCD + 0.915AF + 1.077BDE \\
 & + 1.180AFG + 1.864CD + 2.467D + 2.642F
 \end{aligned} \quad (4.18)$$

In Equation (4.18), A, B, C, D, E, F and G are the coded factors that correspond to  $Wa_3$ ,  $g$ ,  $t$ ,  $m$ ,  $n$ ,  $La$  and  $Sa$ , respectively. Since all factors are included in the regression model, it is not possible to discard any factor for performing the residual analysis.

#### DOE results for $G_{c5GHz}$

The maximum and minimum values of  $G_{c5GHz}$  are -11.99 dB and -26.48 dB, respectively. Figure 4-25, shows the normal probability plot of the effects for  $G_{c5GHz}$ . The factor that has negative effect on  $G_{c5GHz}$  is  $t$  and the factors that affect positively the response are  $Wa_3La$ ,  $tm$  and  $m$ .

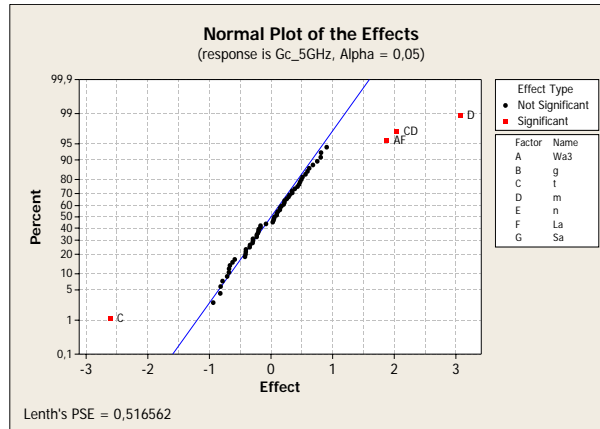


Figure 4-25: Normal probability plot of the effects for the gain in the cavity side at 5 GHz in DOE II.

The  $Gc_{5GHz}$  regression model is given by:

$$Gc_{5GHz}(model) = -15.21 - 1.31C + 0.94AF + 1.02CD + 1.54D \quad (4.19)$$

In Equation (4.19), A, C, D and F are the coded factors that correspond to  $Wa_3$ ,  $t$ ,  $m$  and  $La$ , respectively. Since  $Sa$  has negligible effect on  $Gc_{5GHz}$ , it will be discarded for obtaining the residual plots.

### Validation of the regression models

The central values used for validate the models of the interest responses are:  $Wa_3 = 0.75\text{mm}$ ,  $g = 0.25\text{mm}$ ,  $t = 6.60\text{mm}$ ,  $m = 0.25\text{mm}$ ,  $n = 0.25\text{mm}$ ,  $La = 16\text{mm}$  and  $Sa = 0.45\text{mm}$ .

Table 4-4 presents the predicted and simulated interest responses when central values are used.

Table 4–4: Predicted and simulated interest responses for DOE II

Response	Rmax	$X_{F\_R}$	$F\_R$	$\Gamma_{F\_R}$	$\Gamma_{5GHz}$	$G_{S_{F\_R}}$	$G_{C_{F\_R}}$	$G_{S_{5GHz}}$	$G_{C_{5GHz}}$
Simulated	25.90	-2.34	5.21	0.33	0.91	5.05	-11.73	3.80	-12.25
Predicted	46.10	-3.03	5.26	0.46	0.82	4.45	-12.72	0.76	-15.21
Percent Difference(%)	56.11	25.70	0.96	10.40	32.91	12.63	8.10	130.46	25.08

Good agreement is obtained between the simulated and predicted values for the regression models of  $F\_R$ ,  $\Gamma_{F\_R}$ ,  $\Gamma_{5GHz}$ ,  $G_{S_{F\_R}}$  and  $G_{C_{F\_R}}$ . However, note that the percent difference obtained for each response of interest is greater than the one obtained with the models of DOE I, which could be due to second order effects omitted on the responses. For example for the response  $G_{S_{5GHz}}$ , it is observed in the probability plot of the effects shown in Figure 4-24 that the tails show departures from the fitted line.

#### 4.1.3 DOE III simulation results

Table 4–5 shows the simulation results obtained for the designs proposed in DOE III. The responses of interest remain the same as presented in previous results. In this subsection, the effect that the cavity dimensions  $a$ ,  $b$  and  $Hw$  have on each interest response of the CPW-inductively fed CBFSA is studied.

The port size used in HFSS simulations should be adjusted for each CPW dimension to guarantee that it is coupled to 50  $\Omega$ . For DOE I, DOE II and some designs of DOE III and DOE IV where  $Hw=1.52$  mm, the port size used is constant and the port impedance obtained is 49.9  $\Omega$ . For the designs of DOE III and DOE IV where  $Hw=0.72$  mm, the port size should be re-adjusted to archive that an impedance port coupled to 50  $\Omega$ . The port impedance obtained when the port size is changed was 47  $\Omega$ .

Table 4-5: Simulation results for DOE III ( $2^3$  factorial design)

Design	Rmax	$X_{F\_R}$	$F\_R$	$\Gamma_{F\_R}$	$\Gamma_{5GHz}$	$G_{S_{F\_R}}$	$G_{C_{F\_R}}$	$G_{S_{5GHz}}$	$G_{C_{5GHz}}$
1	7.80	74.48	5.71	0.91	0.94	-10.94	-25.4	2.95	-16.31
A	75.28	58.15	5.34	0.45	0.76	4.47	-13.54	5.41	-12.96
B	51.72	27.33	4.63	0.28	0.97	4.52	-12.29	-1.02	-22.11
AB	316.46	22.61	4.24	0.73	0.94	4.29	-13.87	1.01	-27.65
C	14.54	65.84	5.71	0.81	0.76	3.73	-12.33	3.12	-15.95
AC	159.95	60.07	5.24	0.57	0.67	5.32	-13.06	4.86	-14.15
BC	57.58	27.06	4.58	0.28	0.97	4.74	-12.50	-1.63	-24.16
ABC	305.86	14.48	4.26	0.72	0.93	4.67	-14.89	1.12	-30.74
Max	316.46	74.48	5.71	0.91	0.97	5.32	-12.29	5.41	-12.96
Min	7.80	14.48	4.24	0.28	0.67	-10.94	-25.40	-1.63	-30.74

### DOE results for Rmax

The maximum and minimum values of Rmax are 316.46  $\Omega$  and 7.80  $\Omega$ , respectively. The resistance range is similar to the range obtained for the CPW-inductively fed CBFSA of DOE I, where the cavity dimensions were kept constant for all designs.

Figure 4-26, shows the normal probability plot of the effects for Rmax. This plot shows that  $Hw$  positively affect the resistance Rmax. Therefore, for obtaining low Rmax values,  $Hw$  should be maintained in the low level. Although  $Hw$  is the only factor marked in the plot, observe that the factor  $b$  and the two-factors interaction  $Hwb$  are away from the normal line. Note that the resistance decreases as the cavity thickness increases, which also has been observed by S.Long in [13] for a cavity-backed slot antenna.

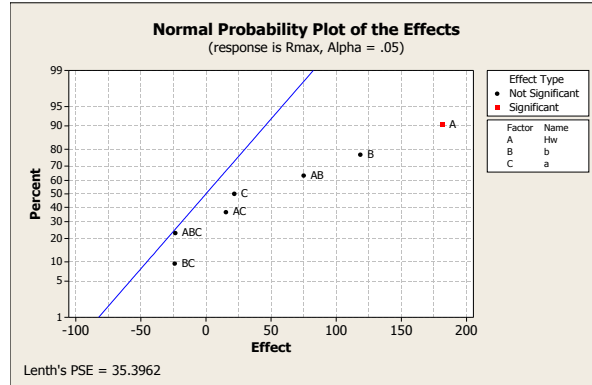


Figure 4–26: Normal probability plot of the effects for the maximum resistance in DOE III.

The Rmax regression model is given by:

$$Rmax(model) = 123.64 + 90.74A + 59.36B + 37.52AB \quad (4.20)$$

In Equation (4.20), A and B are the coded factors that correspond to  $Hw$ ,  $b$  and  $a$ , respectively. Since  $a$  has negligible effect on Rmax, it will be discarded for obtaining the residual plots.

### DOE results for $F_R$

The maximum and minimum values of  $F_R$  are 5.71 GHz and 4.24 GHz, respectively. The frequency range is similar to the ranges observed for the DOE I and DOE II, although in this design the cavity dimensions are varied whereas the FSA dimensions remain constant. Regarding the resonance frequency of the cavity, the impedance plots of Figures 4–28(a) and 4–28(b), show that the resonance frequency of the cavities is around 3.79 GHz, which agrees with the resonance frequency of these designs presented in Table 3–11 for the  $TE_{101}$  mode.

Figure 4–27, shows the normal probability plot of the effects for  $F_R$ . This plot shows that the cavity length  $b$  and the cavity thickness  $Hw$  have negative effects on  $F_R$ . A similar influence of the cavity thickness on the resonance frequency was observed by S.Long in [13] for a cavity-baked slot antenna.

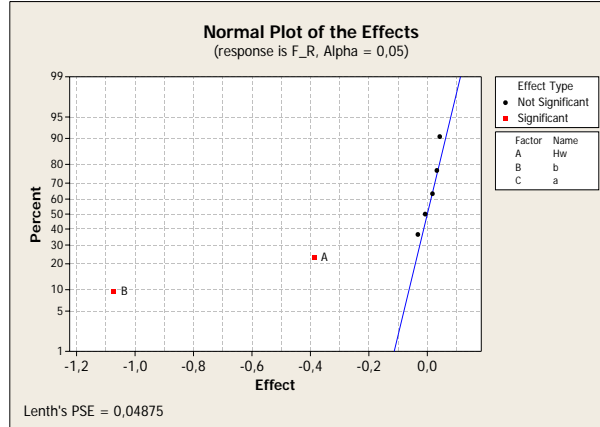


Figure 4-27: Normal probability plot of the effects for the frequency at maximum resistance in DOE III.

The  $F_R$  regression model is given by:

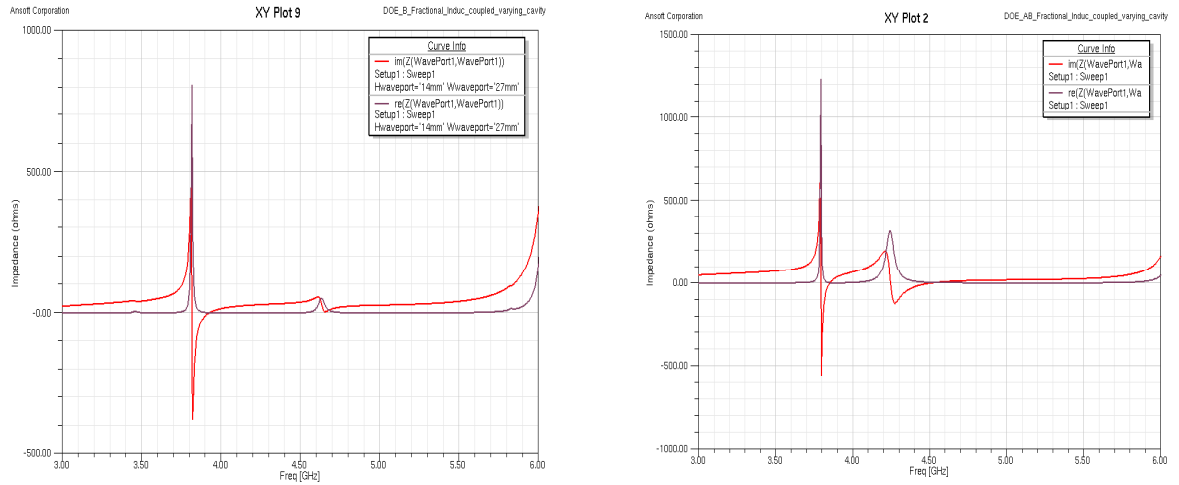
$$F_R(model) = 4.9638 - 0.5362B - 0.1937A \quad (4.21)$$

In Equation (4.21), A and B are the coded factors that correspond to  $Hw$ ,  $b$  and  $a$ , respectively. Since  $a$  has negligible effect on  $F_R$ , it will be discarded for obtaining the residual plots.

#### DOE results for $X_{F_R}$

According with results of Table 4–5, the minimum and maximum values of  $X_{F_R}$  are  $74.48 \Omega$  and  $14.48 \Omega$ , respectively. The reactance is positive for all designs and the range obtained with this design is very similar to the reactance range for DOE I. Therefore, a variation in the cavity dimensions could not has effect on the

inductive behavior of the CPW-inductively fed CBFSA. Figure 4–28, shows the impedance plots for the B and AB designs. An inductive behavior is observed for the B design whereas in the AB design a resonance occurs at 4.25 GHz. Note that the inductive behavior increases when the resistance decreases.



(a) Impedance plot of B design of DOE III.

(b) Impedance plot of AB design of DOE III.

Figure 4–28: Impedance plots of B and AB designs of DOE III: (a) Impedance plot of the B design; and (b) Impedance plot of the AB design.

Figure 4–29, shows the normal probability plot of the effects for  $X_{F\_R}$ . This plot shows that the cavity length  $b$  has negative effect on  $F\_R$ . Although  $Hw$  is not marked as significant, its effect is far from the normal line and it will be included in the regression model of Equation (4.22).

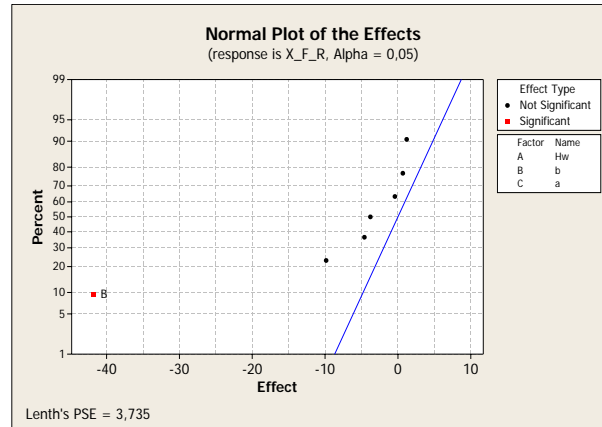


Figure 4–29: Normal probability plot of the effects for the reactance at  $F_R$  in DOE III.

The  $X_{F\_R}$  regression model is given by:

$$X_{F\_R}(\text{model}) = 43.75 - 20.88B - 4.93A \quad (4.22)$$

In Equation (4.22), A and B are the coded factors that corresponds to  $Hw$  and  $b$ , respectively. The factor that is discarded for obtaining the residual plots is  $a$ .

#### DOE results for $\Gamma_{F\_R}$

The maximum and minimum values obtained for  $\Gamma_{F\_R}$  are 0.91 and 0.28, respectively. These results are similar to the ones obtained with DOE I.

Figure 4–30, shows the normal probability plot of the effects for  $\Gamma_{F\_R}$ .

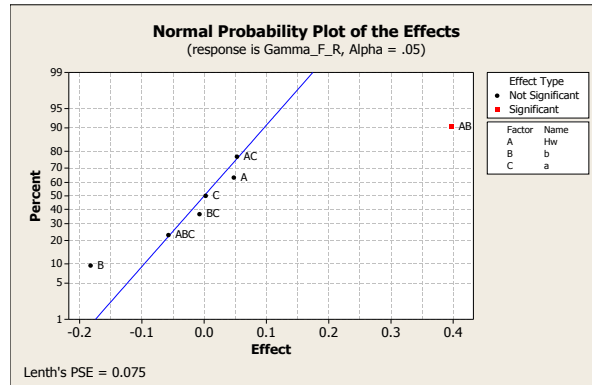


Figure 4–30: Normal probability plot of the effects for the reflection coefficient at  $F_R$  in DOE III.

This plot shows that the factors that have a significant effects on  $\Gamma_{F_R}$  are the same factors that affect  $R_{max}$  and  $X_{F_R}$ . The two-factors interaction  $Hwb$  positively affect the reflection coefficient whereas  $b$  have a negative influence on this response.

The  $\Gamma_{F_R}$  regression model is given by:

$$\Gamma_{F_R}(model) = 0.59375 + 0.19875AB - 0.09125B \quad (4.23)$$

In Equation (4.23), A and B are the coded factors that correspond to  $Hw$  and  $b$ , respectively. The factor that is discarded for obtaining the residual plots is  $a$ .

#### DOE results for $\Gamma_{5GHz}$

The maximum and minimum magnitude of the reflection coefficient at 5 GHz are 0.97 and 0.67, respectively. These results are similar to the ones obtained with DOE I.

Figure 4-31, shows the normal probability plot of the effects for  $\Gamma_{5GHz}$ .

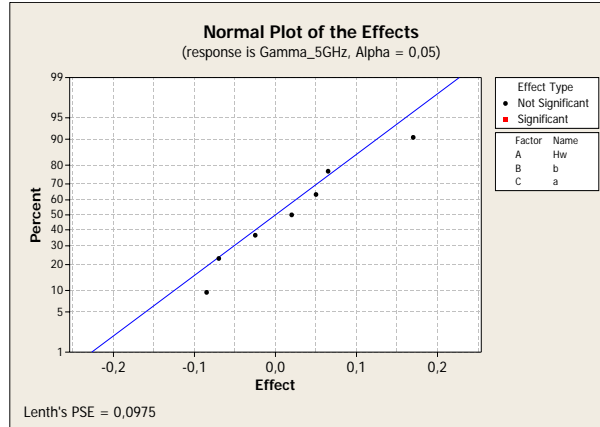


Figure 4–31: Normal probability plot of the effects for the reflection coefficient at 5 GHz in DOE III.

In this plot the effects caused by the factors on the response are not observed. Therefore, in the regression model of Equation (4.24), all factors are included.

The  $\Gamma_{5GHz}$  regression model is given by:

$$\begin{aligned} \Gamma_{5GHz}(model) = & 0.86750 - 0.04250A - 0.08500B - 0.03500C + 0.02500AB \\ & + 0.01000AC + 0.03250BC - 0.01250ABC \end{aligned} \quad (4.24)$$

In Equation (4.24), A, B and C are the coded factor that corresponds to  $Hw$ ,  $b$  and  $a$ , respectively. In this case, it is not possible to discard any factor for testing the accuracy of the model.

### DOE results for $G_{S_{F-R}}$

The shape of the 2-D and 3-D radiation patterns plots for the designs of DOE III are very similar to the Figures 4–12(a) and 4–12(b), obtained for the design CDE of DOE I. The maximum and minimum values of  $G_{S_{F-R}}$  are 5.32 dB and -10.94 dB, respectively. The minimum value is the only negative gain of Table 4–5 and

corresponds to the 1 design, which is characterized for having the lowest  $R_{max}$  ( $7.80 \Omega \approx$  electric short-circuit). This relationship between the resistance and gain was also observed in DOE II.

Figure 4-22, shows the normal probability plot of the effects for  $G_{s_{F_R}}$ . In this plot effects caused by the factors on the response are not observed. Therefore, in the regression model of Equation (4.25), all factors are included.

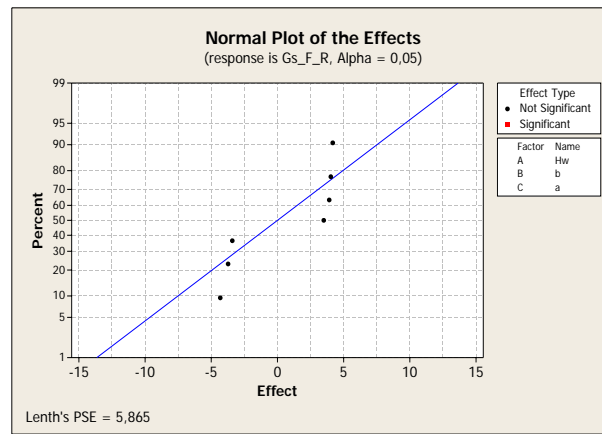


Figure 4-32: Normal probability plot of the effects for the gain in the substrate side at  $F_R$  in DOE III.

The  $G_{s_{F_R}}$  regression model is given by:

$$G_{s_{F_R}}(model) = 2.600 + 2.087A + 1.955B + 2.015C - 2.162AB - 1.707AC - 1.865BC + 1.747ABC \quad (4.25)$$

In Equation (4.25), A, B and C are the coded factors that corresponds to  $Hw$ ,  $b$  and  $a$ , respectively. In this case, it is not possible to discard any factor for testing the accuracy of the model.

### DOE results for $G_{c_{F_R}}$

The maximum and minimum values obtained for the gain on the cavity side are -12.29 dB and -25.40 dB, respectively. Front to back ratios  $\approx 17$  dB are obtained for all designs of DOE III, which is similar to the values obtained for DOE I and DOE II. Note that low radiation on cavity side is obtained with the CPW-inductively fed CBFSA, even when a shallow cavity ( $H_w \approx \frac{\lambda_0}{80} \approx \frac{\lambda_d}{44}$ ) is used.

Figure 4-33 shows the normal probability plot of the effects for  $G_{c_{F_R}}$ . Significant effects caused by the factors on the response are not observed. Therefore, in the regression model of Equation (4.26), all factors are included.

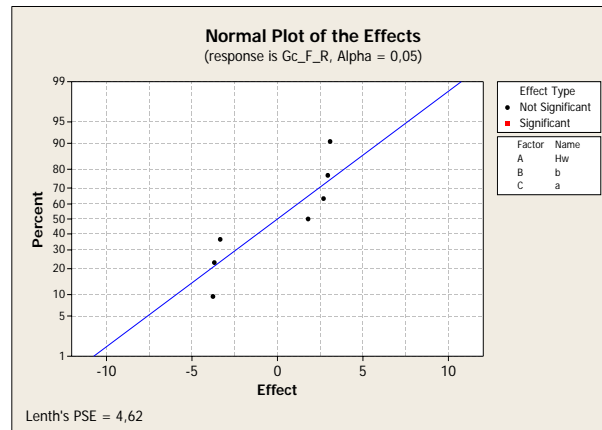


Figure 4-33: Normal probability plot of the effects for the gain in the cavity side at  $F_R$  in DOE III.

The  $G_{c_{F_R}}$  regression model is given by:

$$\begin{aligned}
 G_{c_{F_R}}(model) = & -14.74 + 0.89A + 1.35B + 1.54C - 1.89AB \\
 & - 1.68AC - 1.85BC + 1.47ABC
 \end{aligned} \tag{4.26}$$

In Equation (4.26), A, B and C are the coded factors that corresponds to  $Hw$ ,  $b$  and  $a$ , respectively. In this case, it is not possible to discard any factor for testing the accuracy of the model.

### DOE results for $G_{s5GHz}$

The minimum and maximum values obtained for  $G_{s5GHz}$  are -1.63 dB and 5.41 dB. The maximum value is similar to the maximum obtained with the DOE I and DOE II. However, the minimum gain value in the substrate side at 5GHz is higher than the ones obtained with DOE I and DOE II.

Figure 4-34 shows the normal probability plot of the effects for  $G_{s5GHz}$ . The cavity length  $b$  has a negative effect on  $G_{s5GHz}$  whereas the cavity thickness has a positive effect.

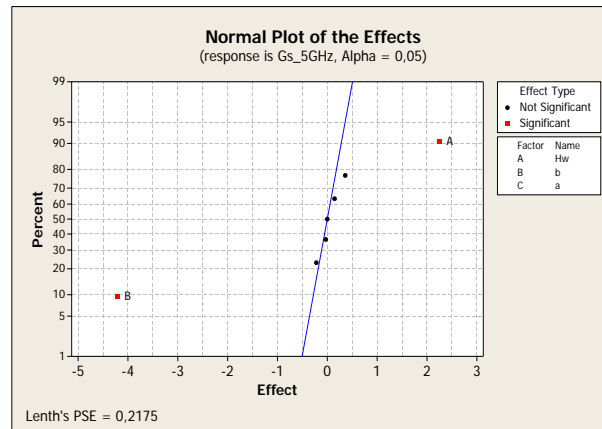


Figure 4-34: Normal probability plot of the effects for the gain in the substrate side at 5 GHz in DOE III.

The  $G_{s5GHz}$  regression model is given by:

$$G_{s5GHz}(model) = 1.978 + 1.122A - 2.107B \quad (4.27)$$

In Equation (4.27), A and B are the coded factors that correspond to  $Hw$  and  $b$ , respectively. The factor that is discarded for obtaining the residual plots is  $a$ .

### DOE results for $Gc_{5GHz}$

The maximum and minimum values of  $Gc_{5GHz}$  are -12.93 dB and -30.74 dB, respectively. This gain range is similar to the one obtained for DOE II. Figure 4–35, shows the normal probability plot of the effects for  $Gc_{5GHz}$ . The factor that has strongest effect effect on  $Gc_{5GHz}$  is  $b$ . Although the two-factor interaction  $Hwb$  is not marked as significant, its effect is far from the normal line.

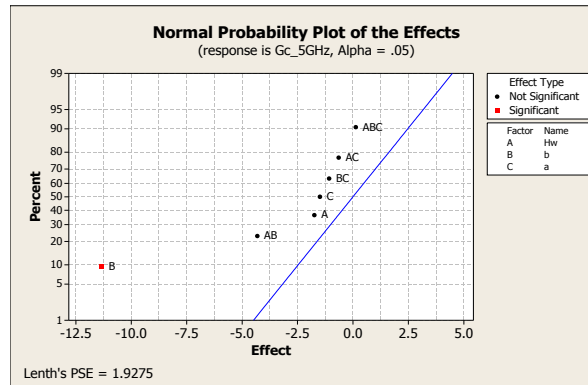


Figure 4–35: Normal probability plot of the effects for the gain in the cavity side at 5 GHz in DOE III.

The  $Gc_{5GHz}$  regression model is given by:

$$Gc_{5GHz}(model) = -20.50 - 5.66B - 2.16AB \quad (4.28)$$

In Equation (4.28), A and B are the coded factors that correspond to  $Hw$  and  $b$ , respectively. The factor that is discarded for obtaining the residual plots is  $a$ .

### Validation of the regression models

The validation of the regression models of DOE III and DOE IV could not be performed by using central values, as done previously, because the CPW feed dimensions do not remain constant when the cavity thickness changes from  $Hw=1.52\text{mm}$  or  $Hw=0.76\text{mm}$  to the central value  $Hw=1.12\text{mm}$ . Therefore, the validation could not be evaluated if the cavity dimensions change as well as the feeding.

#### 4.1.4 DOE IV simulation results

Table 4–6 shows the simulation results obtained for the designs proposed in DOE IV. The responses of interest remain the same as presented in previous results. In this subsection, the effect that the cavity dimensions  $a$ ,  $b$  and  $Hw$  have on each interest response of the CPW-capacitively fed CBFSA is studied.

Table 4–6: Simulation results for DOE IV ( $2^3$  factorial design)

Design	Rmax	$X_{F\_R}$	$F\_R$	$\Gamma_{F\_R}$	$\Gamma_{5GHz}$	$G_{S_{F\_R}}$	$G_{C_{F\_R}}$	$G_{S_{5GHz}}$	$G_{C_{5GHz}}$
1	11.10	-15.13	5.90	0.64	0.86	4.36	-13.16	3.31	-15.53
A	54.94	29.21	5.34	0.27	0.86	5.15	-12.44	4.98	-14.01
B	34.79	-16.60	4.80	0.23	0.97	4.35	-14.30	-0.79	-24.41
AB	154.12	-23.97	4.51	0.52	0.95	4.98	-13.80	0.83	-30.77
C	9.57	29.65	5.81	0.74	0.85	4.61	-12.70	0.88	-18.68
AC	111.52	12.69	5.28	0.38	0.88	5.43	-12.49	3.85	-15.91
BC	55.73	-19.80	4.75	0.21	0.97	4.46	-14.33	-1.28	-25.55
ABC	172.27	-21.06	4.48	0.55	0.95	4.96	-13.88	0.63	-30.10
Max	172.27	29.65	5.90	0.74	0.97	5.43	-12.44	4.98	-14.01
Min	9.57	-23.97	4.48	0.21	0.85	4.35	-14.33	-1.28	-30.77

#### DOE results for Rmax

The maximum and minimum resistance at  $F\_R$  are  $172.27 \Omega$  and  $9.57 \Omega$ , respectively. Table 4–6 shows that Rmax range is similar to the range obtained for DOE II, where the cavity dimensions were kept constant for all designs.

Figure 4–36, shows the normal probability plot of the effects for Rmax. It is observed that although factors  $Hw$  and  $b$  are not marked as significant, their effects are far from the normal line and their effects will be included in the model

of Equation (4.29). Thus, considering this effects it is possible to conclude that the factors  $Hw$  and  $b$  have positively affect on the resistance  $R_{max}$ . Therefore, for obtaining low  $R_{max}$  values,  $Hw$  and  $b$  should be maintained in their low levels.

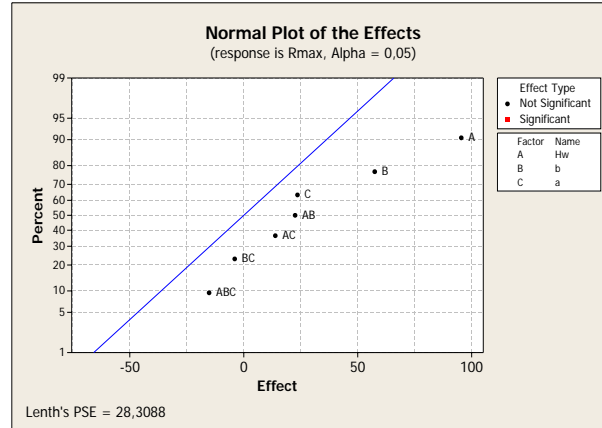


Figure 4-36: Normal probability plot of the effects for the maximum resistance in DOE IV.

It is interesting to note that although similar resistance ranges are obtained with the designs DOE II and DOE IV, which are both CPW-capacitively fed CBFSA's, the regression model obtained for  $R_{max}$  in DOE IV involves less variables, which could facilitate the design of the antenna.

The  $R_{max}$  regression model is given by:

$$R_{max}(model) = 75.505 + 47.707A + 28.722B \quad (4.29)$$

In Equation (4.29), A and B are the coded factors that correspond to  $Hw$  and  $b$ , respectively. Since  $a$  has negligible effect on  $R_{max}$ , it will be discarded for obtaining the residual plots.

### DOE results for $F_R$

The maximum and minimum  $F_R$  are 5.90 GHz and 4.48 GHz, respectively. This frequency range is similar to the one obtained for DOE I, DOE II, DOE III and DOE IV.

Information about the resonance frequency of the cavity for designs B and AB is obtained from the impedance plots of Figure 4-38. This figure shows that the resonance frequencies of design B and AB are in agreement with the theoretical values calculated in Table 3-11 for the  $TE_{101}$  mode. The correspondence between the theoretical and simulated resonance frequencies of the cavity for the additional designs was also confirmed.

Figure 4-37, shows the normal probability plot of the effects for  $F_R$ . According with this Figure, the factors  $Hw$  and  $b$  have negative affect on  $F_R$  whereas the two-factor interaction  $Hwb$  has a positively effect on this response.

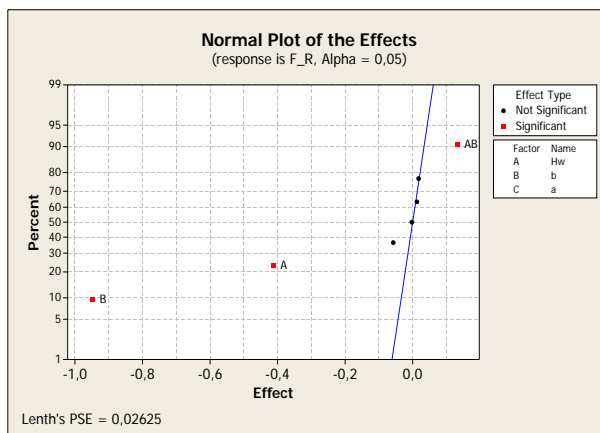


Figure 4-37: Normal probability plot of the effects for the frequency at maximum resistance in DOE IV.

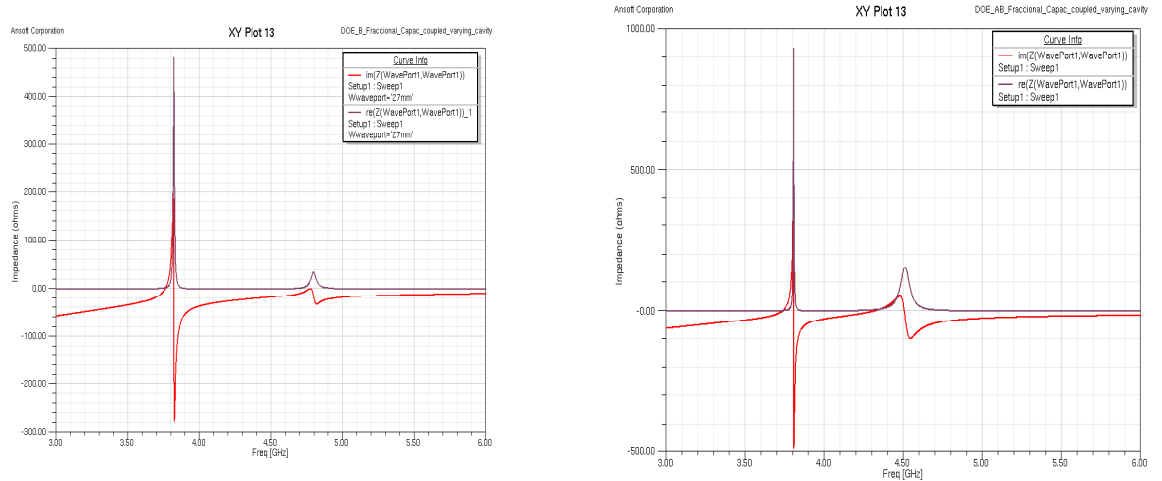
The  $F_R$  regression model is given by:

$$F_{R}(model) = 5.1087 - 0.2062A - 0.4737B + 0.0663AB \quad (4.30)$$

In Equation (4.30), A and B are the coded factors that correspond to  $Hw$  and  $b$ , respectively. Since  $a$  has negligible effect on  $F_R$ , it will be discarded for obtaining the residual plots.

### DOE results for $X_{F_R}$

The maximum and minimum values obtained for  $X_{F_R}$  are  $29.65 \Omega$  and  $-23.97 \Omega$ , respectively. These values are lower than the ones obtained for DOE II. Figure 4–18, shows two impedance plots measured at  $F_R$  for the B and AB design of DOE IV. These plots show an inductive behavior for the B design whereas in the AB design a resonance occurs at 4.5 GHz. It is observed that the capacitive behavior increases when the resistance decreases as observed for DOE II.



(a) Impedance plot of B design of DOE IV

(b) Impedance plot of AB design of DOE IV

Figure 4–38: Impedance plots of B and AB designs of DOE IV: (a) Impedance plot of the B design; and (b) Impedance plot of the AB design.

Figure 4–39, shows the normal probability plot of the effects for  $X_{F_R}$ . Although the factor  $b$  is not marked as significant in this Figure, its effect is far from the normal

line. Therefore it is assumed that this factor negatively affect the reactance at  $F_R$ . In DOE III, also was observed the negative influence that  $b$  has on this response.

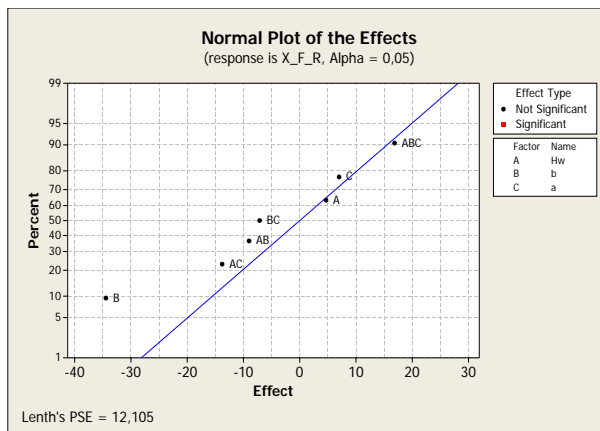


Figure 4–39: Normal probability plot of the effects for the reactance at  $F_R$  in DOE IV.

The  $X_{F_R}$  regression model is given by:

$$X_{F_R}(\text{model}) = -3.13 - 17.23B \quad (4.31)$$

In Equation (4.31), B is the coded factor that corresponds to  $b$ . Since  $a$  has negligible effect on  $X_{F_R}$ , it will be discarded for obtaining the residual plots.

#### DOE results for $\Gamma_{F_R}$

The maximum and minimum values of  $\Gamma_{F_R}$  are 0.74 and 0.21, respectively. Significant differences between the reflection coefficient obtained with the DOE IV design and the designs previously presented are not observed.

Figure 4–40, shows the normal probability plot of the effects for  $\Gamma_{F_R}$ . The two-factors interaction  $Hwb$  have a positive effect on this response as was observed for DOE III.

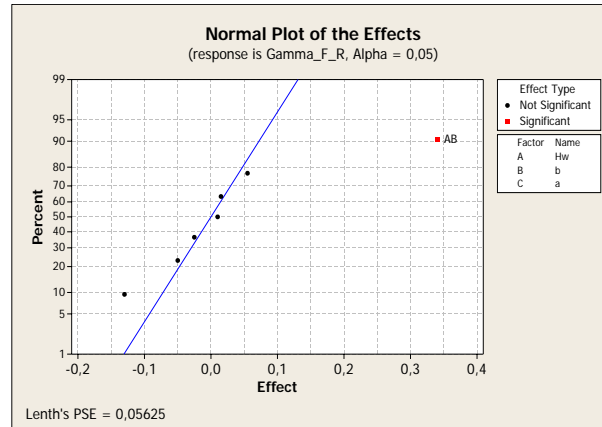


Figure 4–40: Normal probability plot of the effects for the reflection coefficient at  $F_R$  in DOE IV.

The  $\Gamma_{F_R}$  regression model is given by:

$$\Gamma_{F_R}(\text{model}) = 0.44250 + 0.17500AB \quad (4.32)$$

In Equation (4.34), A and B are the coded factors that correspond to  $Hw$  and  $b$ , respectively. Since  $a$  has negligible effect on  $\Gamma_{F_R}$ , it will be discarded for obtaining the residual plots.

#### DOE results for $\Gamma_{5GHz}$

The maximum and minimum  $\Gamma_{5GHz}$  are 0.97 and 0.87, respectively. The minimum value is higher than the one obtained with the others designs presented previously.

Figure 4–41, shows the normal probability plot of the effects for  $\Gamma_{5GHz}$ . In this plot is observed that  $b$  has a positive effect on  $\Gamma_{5GHz}$ . It should be mentioned that although similar values for  $\Gamma_{5GHz}$  are obtained with DOE III and DOE IV, in DOE III the effects caused by the factors on the response are not observed in the normal probability plot of the effects.

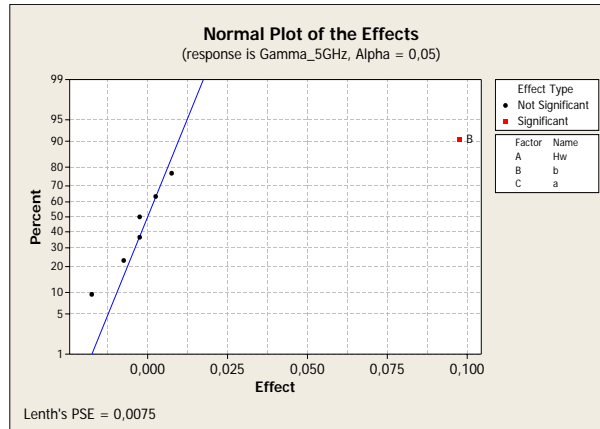


Figure 4–41: Normal probability plot of the effects for the reflection coefficient at 5 GHz in DOE IV.

The regression model for  $\Gamma_{5GHz}$  is:

The  $\Gamma_{5GHz}$  regression model is given by:

$$\Gamma_{5GHz}(model) = 0.911250 + 0.048750B \quad (4.33)$$

In Equation (4.33), B is the coded factor that corresponds to  $b$ . The factor that is discarded for obtaining the residual plots is  $a$ .

#### DOE results for $G_{S_{F-R}}$

The maximum and minimum values of  $G_{S_{F-R}}$  are 5.43 dB and 4.35 dB, respectively and are very similar to the values obtained for the CPW-inductively fed CBFSA of DOE I. This design of experiments did not obtain any negative values as was observed for the DOE II, DOE II and DOE III designs. This could be explained because in this design the resistance values are not as low as observed for DOE II or DOE III. Note that significant gain values are obtained even when shallow cavities are used.

The radiation patterns for this DOE remains the same as presented in Figure 4-12(a) and 4-12(b) for a CPW-inductively fed CBFSA design.

Figure 4-42, shows the normal probability plot of the effects for  $G_{s_{F_R}}$ . The factor that has positive effect on the response is  $Hw$ .

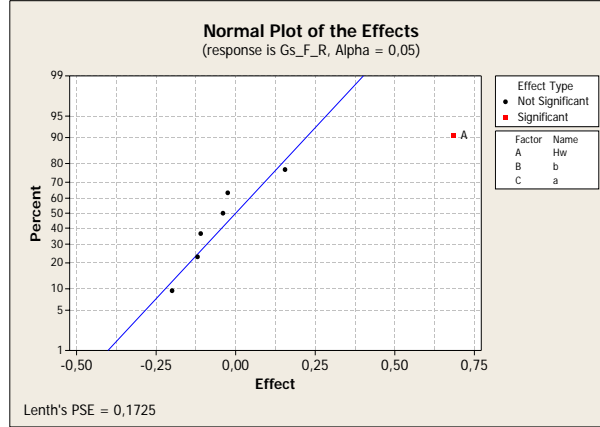


Figure 4-42: Normal probability plot of the effects for the gain in the substrate side at  $F_R$  in DOE IV.

The regression model for  $G_{s_{F_R}}$  is:

The  $G_{s_{F_R}}$  regression model is given by:

$$G_{s_{F_R}}(model) = 4.7875 + 0.3425A \quad (4.34)$$

In Equation (4.34), A is the coded factor that corresponds to  $Hw$ . The factor that is discarded for obtaining the residual plots is  $a$ .

#### DOE results for $G_{c_{F_R}}$

The maximum and minimum values of  $G_{c_{F_R}}$  are -12.44 dB and -14.33 dB, respectively. According with the Table 4-5, note that this design presents front back ratios close to 16 dB even when a shallow cavity ( $Hw \approx \frac{\lambda_0}{80} \approx \frac{\lambda_d}{44}$ ) is used. Similar front to back ratios were obtained all designs considered in this work.

Figure 4–43, shows the normal probability plot of the effects for  $G_{c_{F_R}}$ . The factor that has negative effect on the response is  $b$ .

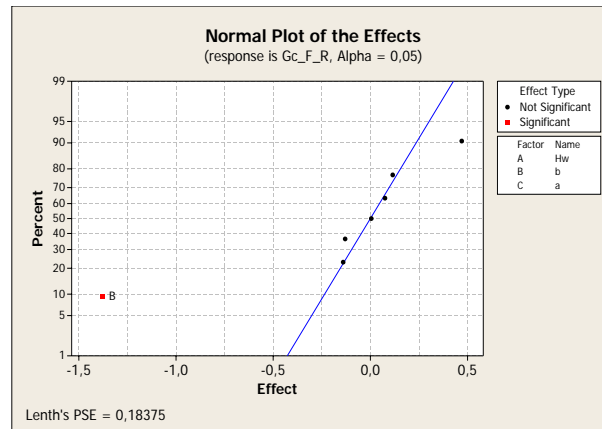


Figure 4–43: Normal probability plot of the effects for the gain in the cavity side at  $F_R$  in DOE IV.

The regression model for  $G_{c_{F_R}}$  is:

The  $G_{c_{F_R}}$  regression model is given by:

$$G_{c_{F_R}}(model) = -13.39 - 0.69B \quad (4.35)$$

In Equation (4.35),  $B$  is the coded factor that corresponds to  $b$ . The factor that is discarded for obtaining the residual plots is  $a$ .

#### DOE results for $G_{s_{5GHz}}$

The maximum and minimum values of  $G_{s_{5GHz}}$  are 4.98 dB and -1.28 dB, respectively. Figure 4–44, shows the normal probability plot of the effects for  $G_{s_{5GHz}}$ . It is observed that the only factor that has effects on the response is  $b$ .

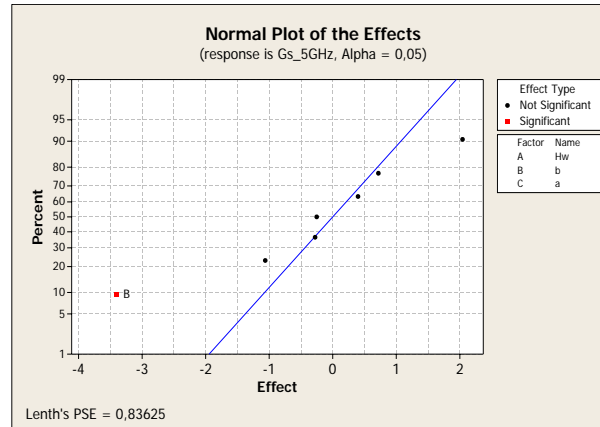


Figure 4–44: Normal probability plot of the effects for the gain in the substrate side at 5 GHz in DOE IV.

The  $G_{s_{5GHz}}$  regression model is given by:

$$G_{s_{5GHz}}(model) = 1.551 - 1.704B \quad (4.36)$$

In Equation (4.36), B is the coded factor that corresponds to  $b$ . The factor that is discarded for obtaining the residual plots is  $a$ .

#### DOE results for $G_{c_{5GHz}}$

The maximum and minimum values of  $G_{c_{5GHz}}$  are -14.01 dB and -30.77 dB, respectively. Figure 4–44, shows the normal probability plot of the effects for  $G_{c_{5GHz}}$ . It is observed that the factor  $b$  negatively affects  $G_{c_{5GHz}}$ .

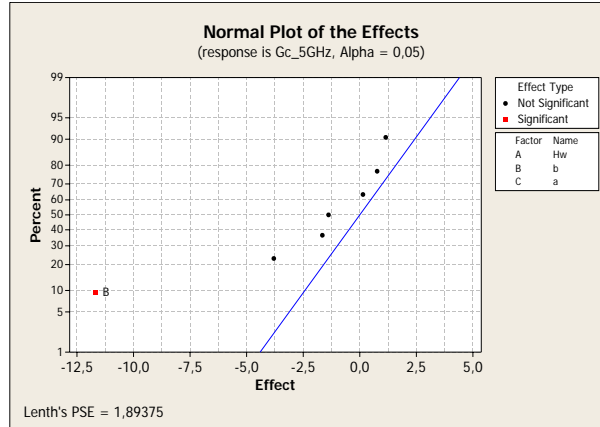


Figure 4–45: Normal probability plot of the effects for the gain in the cavity side at 5 GHz in DOE IV.

The  $Gc_{5GHz}$  regression model is given by:

$$Gc_{5GHz}(model) = -21.87 - 5.84B \quad (4.37)$$

In Equation (4.37), B is the coded factor that corresponds to  $b$ . The factor that is discarded for obtaining the residual plots is  $a$ .

#### 4.2 Examples of CBFSAs designs with $\Gamma < 0.33$ at 5 GHz

Previous simulation results showed that it is possible to design CBFSAs with different geometries that can obtain similar responses. Information about the influence that the geometry of the CBFSA has on these responses were presented in the previous section. One response of interest is the magnitude of the reflection coefficient ( $\Gamma$ ), because gives information about the antenna matching. For example, if a particular antenna obtain  $\Gamma=0$  means that this antenna is perfectly matched. However, in design approaches, usually is accepted that  $\Gamma < 0.33$ . In this section, some examples of the CBFSAs designs that achieved the goal  $\Gamma < 0.33$  at 5 GHz are presented.

The first example is obtained from DOE I. The design ABCDE has  $\Gamma_{5GHz}=0.60$ , which is the lowest value obtained for a CPW-inductively fed CBFSA. Figure 4-46 shows the reflection coefficient versus frequency plot for the ABCDE design.

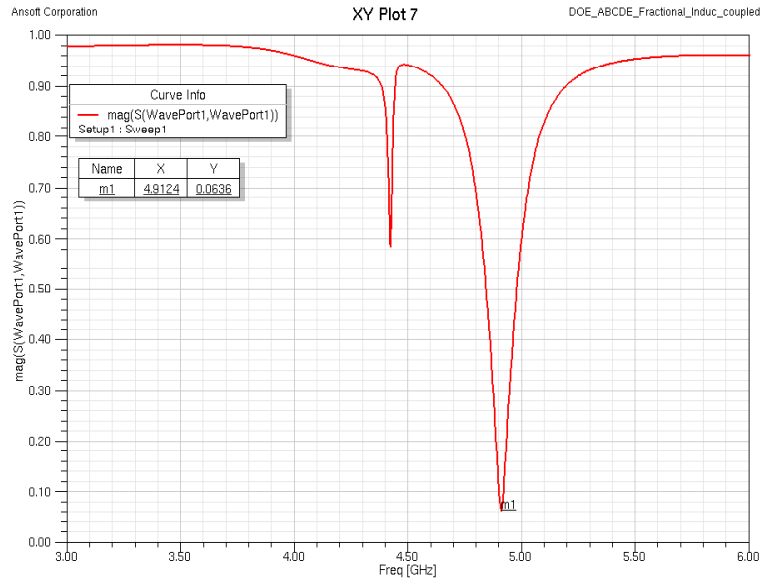


Figure 4-46:  $\Gamma_{5GHz}$  plot for the ABCDE design of DOE I.

In this plot it is observed that the point in which  $\Gamma_{5GHz}=0.60$  do not corresponds to the minimum reflection coefficient of the plot, which is located at 4.91 GHz. This is explained because of the limited impedance bandwidth of the antenna. To shift this point to 5 GHz, the dimension  $Wa_2$  is increased from 1.2 mm to 1.6 mm. The criterion used to shift the frequency was selected based on the model of Equation (4.2) for DOE I, which says that  $F_R$  increases as  $Wa_2$  increases. Figure 4-47 shows the reflection coefficient versus frequency plot for the ABCDE design with  $Wa_2 = 1.6\text{mm}$ .

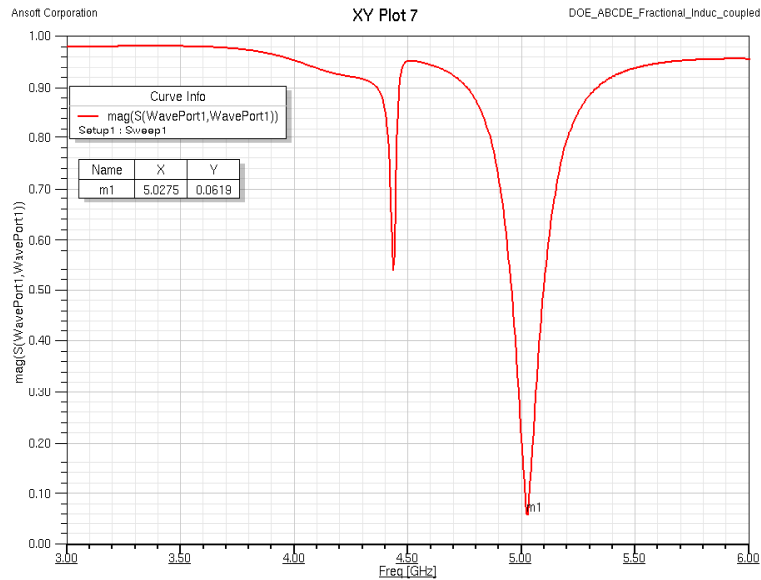


Figure 4-47:  $\Gamma_{5GHz}$  plot for the ABCDE design with  $Wa_2 = 1.6\text{mm}$ .

It is observed from the previous plot that  $\Gamma_{5GHz}=0.0619$ , which means that it was possible to design a CPW-inductively fed CBFSAs that achieve the goal  $\Gamma < 0.33$  at 5 GHz.

The second example is obtained from DOE II. The BDEFG selected has  $\Gamma_{5GHz}=0.26$ , which is the lowest value obtained for a CPW-capacitively fed CBFSAs. In this case it was not necessary to perform any modification to the geometry because the goal is already accomplished. Figure 4-48 presents the reflection coefficient versus frequency plot for the BDEFG design.

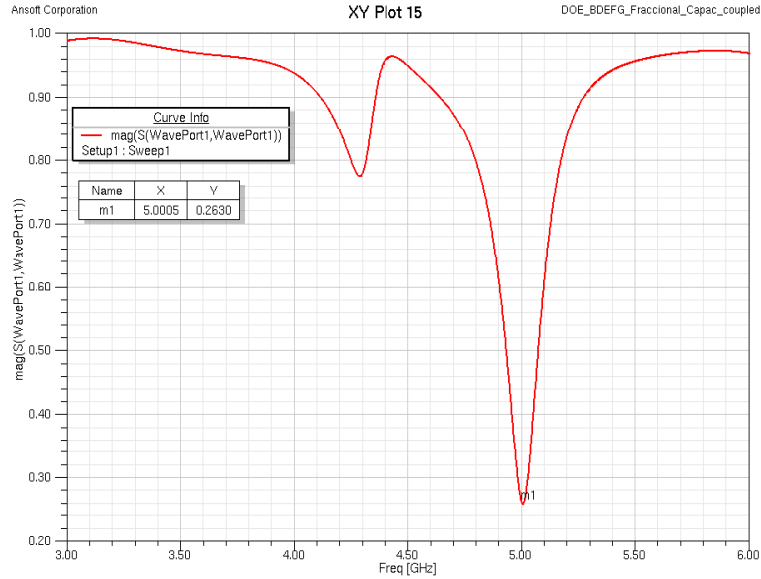


Figure 4–48:  $\Gamma_{5GHz}$  plot for the ABCDE design with  $Wa_2 = 1.6\text{mm}$ .

This plot shows that  $\Gamma_{5GHz}=0.2630$ , which means that it was possible to design a CPW-capacitively fed CBFSA that achieve the goal  $\Gamma < 0.33$  at 5 GHz.

### 4.3 Experimental results

Some CBFSA's were fabricated in order to validate the simulations. The antennas were fabricated by using the wet etching technique and the cavity and dielectric pieces are placed on the FSA's by using silver paint. Three designs were selected, CDE from DOE I, BCDFG from DOE II and AC from DOE III. A picture of the CBFSA's without placing the cavities is presented in Figure 4–49. The CDE, BCDFG, and AC antennas are organized in the picture from the left to the right.

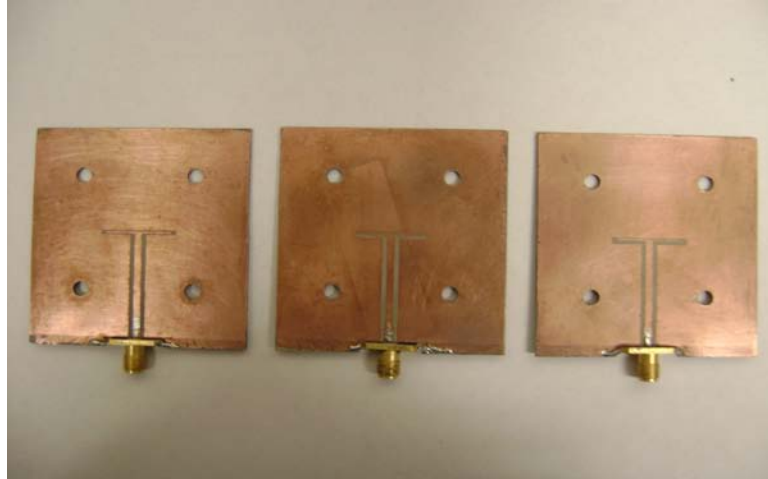


Figure 4-49: CBFSA's fabricated without adding the cavities.

Figure 4-50 shows a picture of the CBFSA's. It is observed that the cavities have already placed on FSA 's. The antennas are organized in the picture as was done in Figure 4-50.



Figure 4-50: CBFSA's fabricated.

Reflection coefficient ( $\Gamma$ ), impedance and radiation pattern measurements were performed for the fabricated antennas.  $\Gamma$  and impedance measurements were carried out in a Vector Network Analyzer (VNA) Agilent 8719ES (50 MHz - 13.5 GHz) and

the reference plane used for measurements is located at the end of the SMA connector. Simulation results are also included in the experimental plots for comparison.

Figure 4-51, 4-52 and 4-53 show the reflection coefficient, resistance and reactance measured and simulated for the CDE design.

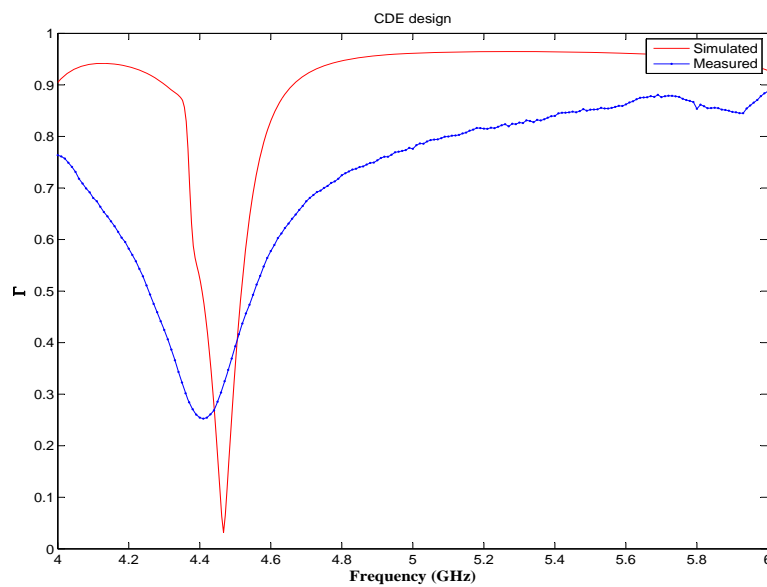


Figure 4-51: Reflection coefficient measured and simulated for the CDE antenna design.

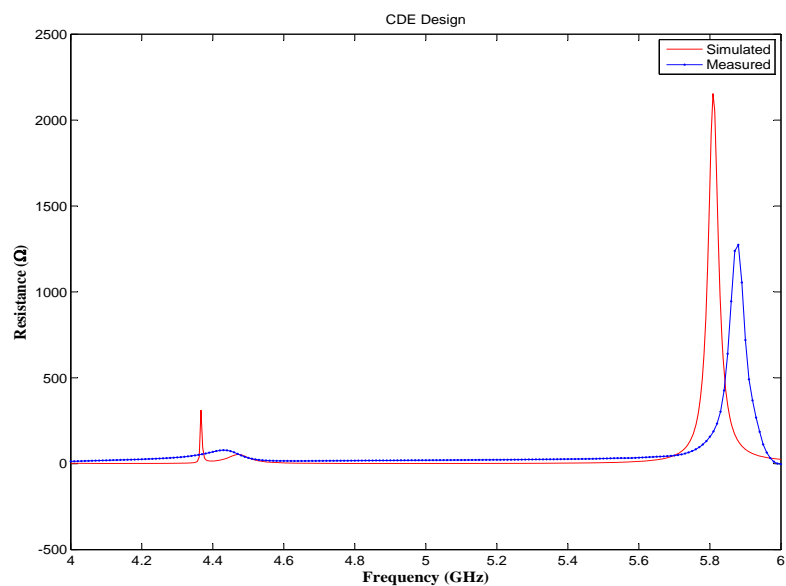


Figure 4-52: Resistance measured and simulated for the CDE antenna design.

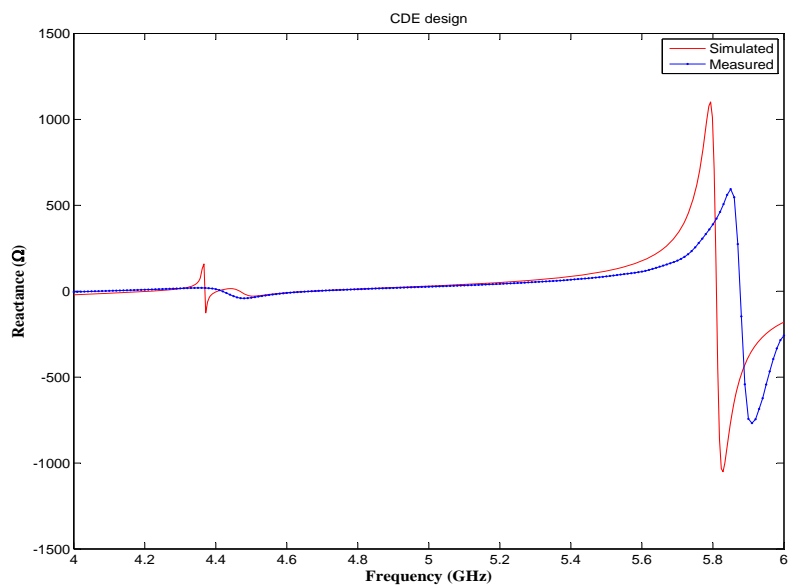


Figure 4-53: Reactance measured and simulated for the CDE antenna design.

Figure 4-54, 4-55 and 4-56 show the reflection coefficient, resistance and reactance measured and simulated for the BCDFG design.

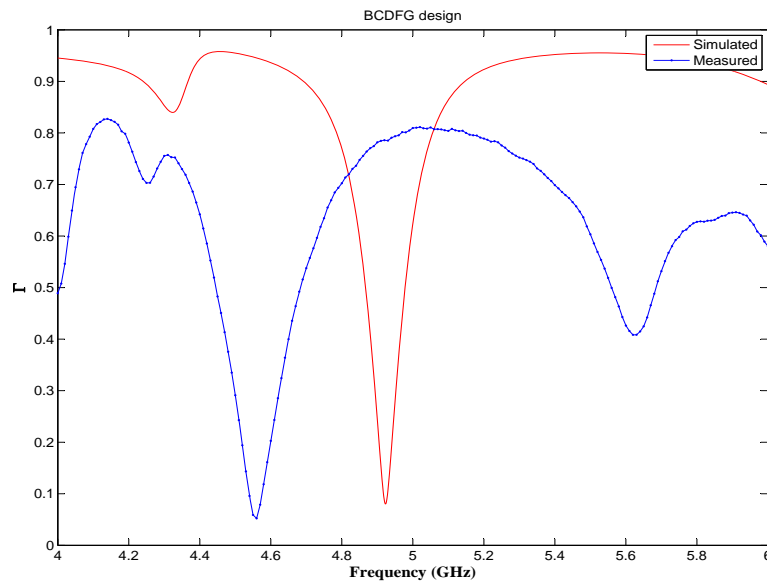


Figure 4-54: Reflection coefficient measured and simulated for the BCDFG antenna design.

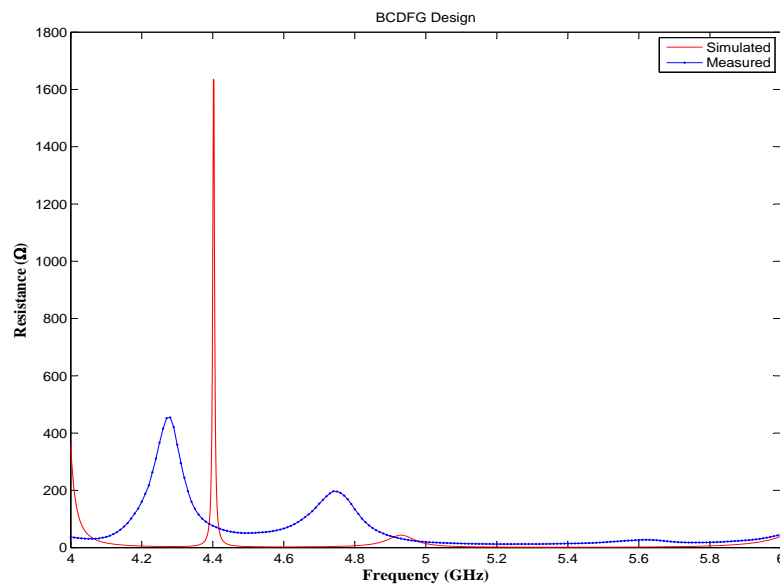


Figure 4-55: Resistance measured and simulated for the BCDFG antenna design.

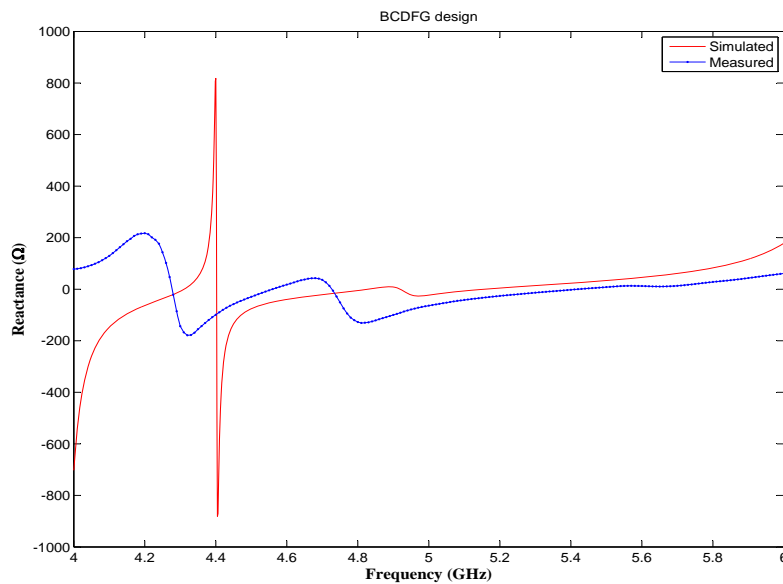


Figure 4-56: Reactance measured and simulated for the BCDFG antenna design.

Figure 4-57, 4-58 and 4-59 show the reflection coefficient, resistance and reactance measured and simulated for the AC design.

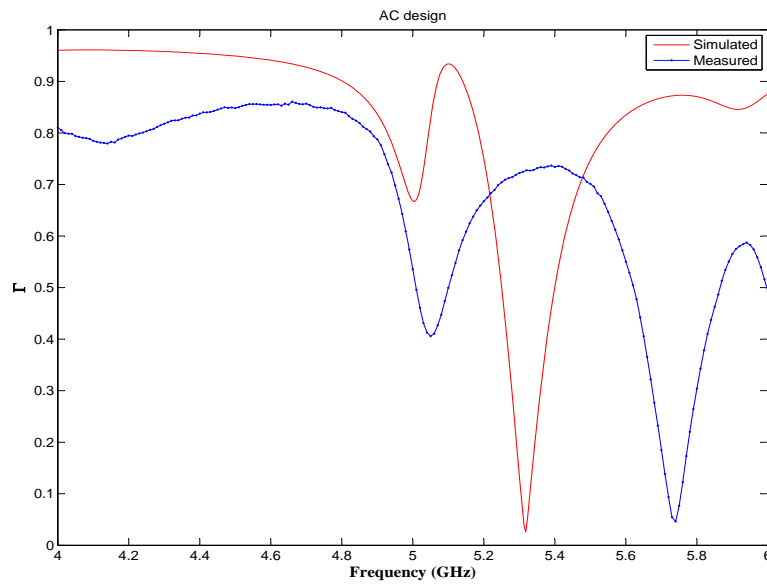


Figure 4-57: Reflection coefficient measured and simulated for the AC antenna design.

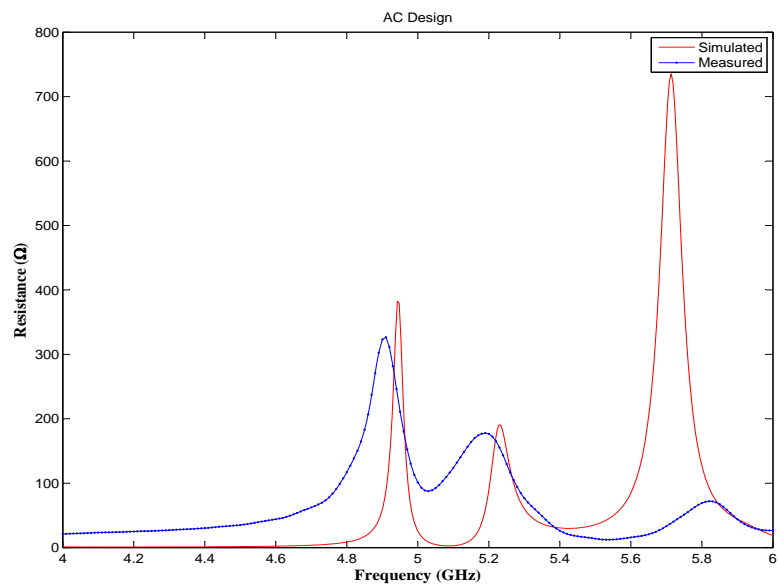


Figure 4-58: Resistance measured and simulated for the AC antenna design.

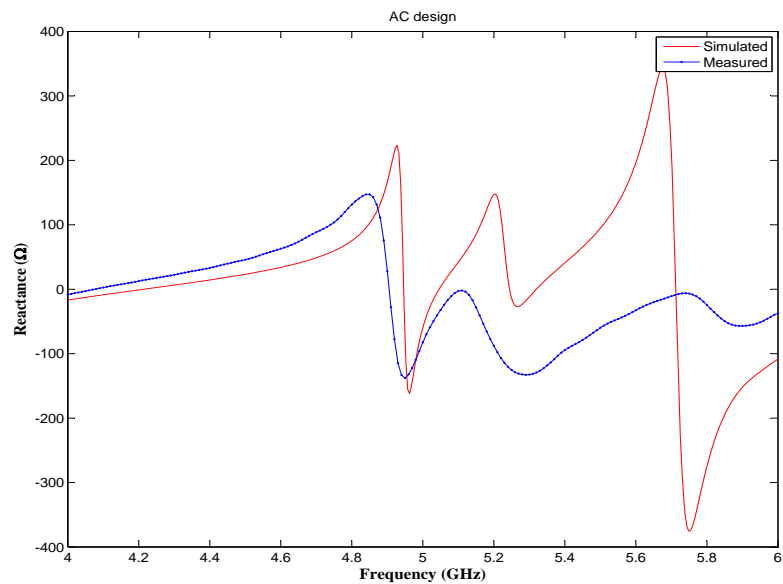
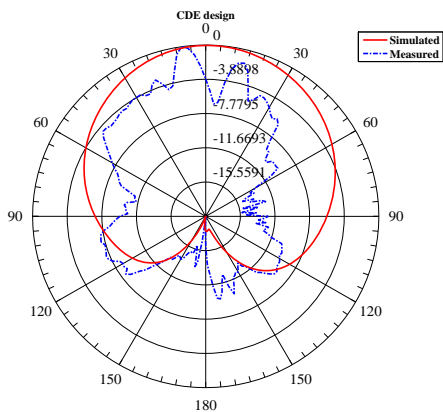


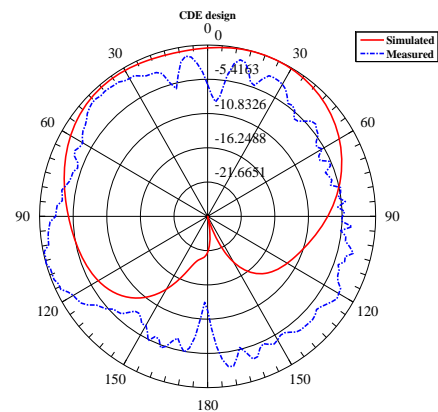
Figure 4-59: Reactance measured and simulated for the AC antenna design.

Note that there is a good agreement between the simulated and measured results, although it is observed a frequency shift in the measured reflection coefficient of the CBFSA's fabricated with the BCDFG and AC designs. The differences observed in the plots could be associated to fabrication errors. Also note that the dimensions of the design are in the order of tenth of millimeters and the fabrication technique employed does not offer a important resolution in this range. However, the most important error source could be associated with the placement of the dielectric piece on the CPW transmission line, which is joined to the SMA connector. The error source resides in the fact that the central pin of the SMA connector has volume, which is not considered in simulations, therefore when the dielectric piece touch this pin, a small air volume ( $\approx 0.1$  mm) is created between the dielectric piece and the CPW transmission line. Additionally, other air volume ( $\approx 0.1$  mm) is also created between the dielectric piece and the SMA connector. This air volume could modify the characteristic impedance of the CPW and consequently the CBFSA responses

Radiation patterns of the CBFSA's at  $\phi=0$  were measured in a spherical anechoic chamber at 4.51 GHz for the CDE design, 4.92 GHz for the BCDFG design and 5.24 GHz for the AC design. These frequencies are the resonance frequencies of each design. Additional measurements at 5 GHz were carried out for all antennas. Figure 4-60, 4-61 and 4-62 show the radiation patterns for the CDE, BCDFG and AC antenna design, respectively.



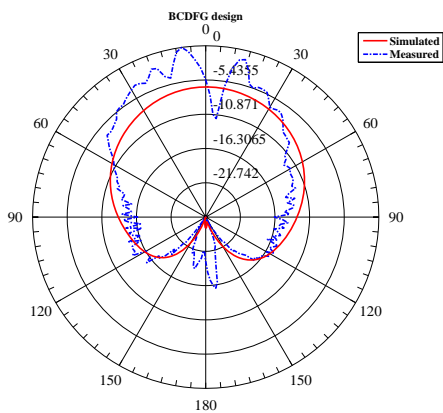
(a) Results at 4.51 GHz



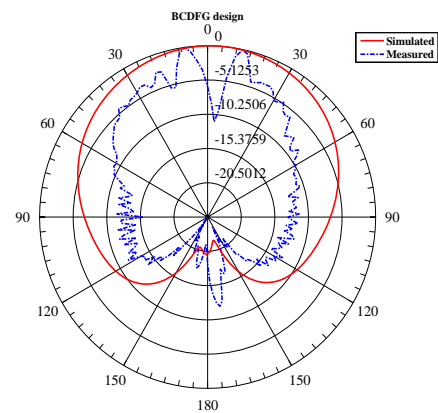
(b) Results at 5 GHz.

Figure 4–60: Radiation pattern measured and simulated for the CDE antenna design:

(a) Results at 4.51 GHz; and (b) Results at 5 GHz.



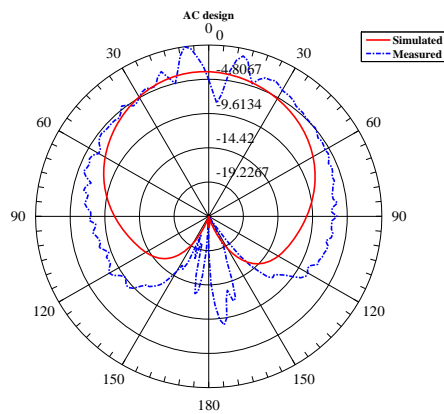
(a) Results at 4.92 GHz



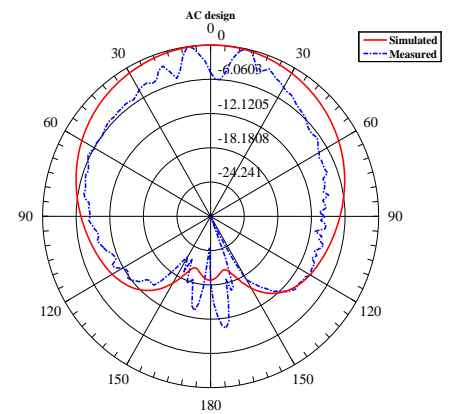
(b) Results at 5 GHz.

Figure 4–61: Radiation pattern measured and simulated for the BCDFG antenna design:

(a) Results at 4.92 GHz; and (b) Results at 5 GHz.



(a) Results at 5.24 GHz



(b) Results at 5 GHz.

Figure 4–62: Radiation pattern measured and simulated for the BCDFG antenna design: (a) Results at 5.24 GHz; and (b) Results at 5 GHz.

It is observed that the simulated and measured results are in agreement. Differences are principally observed in the backward radiation, specially for the measure of the CDE design at 5 GHz.

Gain measurements were performed by using the comparison method which is described by the Equation (4.38) and consists in a comparison between the maximum far fields radiated by the fabricated antennas and the maximum far field radiated with a standard gain antenna. The radiated far fields were obtained through the radiation patterns measurements. In this work the standard antenna used is a standard gain horn with waveguide size WR187. The waveguide size determines the operation frequency range of the antenna (3.95 GHz-5.85 GHz), which is compatible with the operation frequency of the fabricated antennas. The gain provided by the manufacturer for the horn antenna is 10dB.

$$\begin{aligned} \text{Calculated\_AUT\_Gain} &= \text{AUT\_MaxFarField} + \text{SGA\_Gain} \\ &- \text{SGA\_MaxFarField} \end{aligned} \quad (4.38)$$

where *Calculated\_AUT\_Gain* corresponds to the calculated gain of the Antenna Under Test (AUT), *AUT\_MaxFarField* corresponds to the maximum radiated fields measured for the AUT, *SGA\_Gain* is the gain of the Standard Gain Antenna (SGA) and *SGA\_MaxFarField* corresponds to the maximum radiated fields measured for the SGA. In this case, the AUT are the fabricated antennas and SGA is the horn antenna.

Table 4–7, shows the maximum radiated far fields of the standard gain horn antenna as well as the maximum radiated far fields of the fabricated antennas CDE, AC and BCDFG. The measurements were performed at the resonance frequency of each antenna as well as at 5 GHz. The calculated gain through Equation (4.38) and the simulated gain for each antenna are also included in this table.

Table 4–7: Measured Gain and Radiated far fields of the fabricated CBFSA’s

CBFSA	F (GHz)	<i>AUT_MaxFarField</i>	<i>SGA_MaxFarField</i>	<i>Calc_Gain</i>
Design				
CDE	4.51	26.179	31.892	4.287
CDE	5.00	24.432	32.540	1.892
BCDFG	4.92	19.724	32.080	-2.356
BCDFG	5.00	18.541	32.540	-3.999
BCDFG	4.51	26.523	31.892	4.631
AC	5.24	24.536	31.655	2.881
AC	5.00	24.727	32.540	2.187

The dimensions of *AUT\_MaxFarField*, *SGA\_MaxFarField* and *Calc\_Gain* are dB.

Note that the gain obtained for CDE antenna measured at 4.51 GHz and 5 GHz are in agreement with the simulated values of 4.78dB and 1.09 dB, respectively.

According with Table 4-7, it is observed that the gain obtained for the BCDFG antenna at 4.92 GHz and 5 GHz, do not agree with the simulated values. This could be explained through the reflection coefficient plot of Figure 4-54, where it is observed that there is a shift of the measured plot in frequency. Therefore, an additional measurement at the measured resonance frequency of 4.51 GHz is performed and the result is included in the Table 4-7. Now, the gain obtained at this frequency is similar to the simulated gain of 5.25 dB.

Before analyzing the results for the AC design, it should be mentioned that the reflection coefficient measured for this antenna also is shifted in frequency. However, the difference between the measured and simulated values is not so notable as presented by the BCDFG antenna design. According with the Table 4-7, the simulated gain at 5.24 GHz and 5 GHz is 5.32 dB and 4.86 dB, respectively.

## **CHAPTER 5**

# **CONCLUSION AND SUGGESTIONS FOR FUTURE WORK**

CPW-inductively fed CBFSA and CPW-capacitively fed CBFSA were proposed and characterized in this thesis. The characterization was done by using the Design Of Experiments (DOE) techniques. Two designs of experiments were proposed to characterize each antenna. In the first design, the FSA dimensions were varied whereas the cavity dimensions were kept constant, and in the second design, the cavity dimensions are varied whereas the FSA dimensions are kept constant. Thus, a total of four experiments were carried out to study the influence that the FSA and cavity dimensions have on the following responses of the CBFSA's: resistance, frequency, reflection coefficient and gain in the substrate and cavity side. Each response was studied separately for the CBFSA's and linear regression models that intend to predict the responses of the antennas were proposed.

It was observed that the CPW-inductively fed CBFSA shows an inductive behavior, which implies that not all the designs used in the DOE properly resonate at the first useful resonance of the FSA. Regarding the CPW-capacitively fed CBFSA, it was mostly observed a capacitive behavior, although an inductive behavior could also be noted for some designs of the DOE. These inductive/capacitive reactance might be caused by the influence of the inductive/capacitive-feed that goes from the CPW to the antenna and by the strong coupling that exists between the FSA and the cavity.

When the cavity was kept constant, it was found that the resistance of the CPW-inductively fed CBFSA is negatively affected by the on the upper slot dimension and positively affected by the lower slot dimension of the FSA. Thus, if it is desired to decrease the resistance, the upper slot should increases whereas the lower slot should decreases. For the CPW-capacitively fed CBFSA, it was also observed the negative effect that the upper slot has on the resistance. However, it was also noted that two-factors interaction and other three factors also have influence on the resistance model, which could increases the complexity of the model. It was found that the number of factors that have influence on the responses of interest of the CPW-capacitively fed CBFSA is higher than the number of factors that affect the responses of the CPW-inductively fed CBFSA.

When the cavity is varied, it was observed that all responses of interest for both CBFSA's are only affected by the cavity thickness and cavity length. The resistance models of CBFSA's show that the cavity thickness and cavity length have a positive effect on the resistance model. Thus, if low resistance is desired, the cavity thickness and cavity length should be decreased.

It was possible to design through the linear regression models, CPW-inductively fed CBFSA and CPW-capacitively fed CBFSA that achieve the objective proposed of reflection coefficient  $< 0.33$  or VSWR  $< 2$  at 5 GHz. The CBFSA's were able to focus the radiation pattern on one side of the substrate through shallow cavities ( $Hw \approx \frac{\lambda_0}{80} \approx \frac{\lambda_d}{44}$ ) or ( $Hw \approx \frac{\lambda_0}{40} \approx \frac{\lambda_d}{22}$ ). The radiation patterns for all CBFSA's designs appear broadside and Front-to-Back ratios and gains around 15 dB and 5dB, respectively were obtained. Therefore, it can be concluded that the CBFSA's with shallow cavities could be used in applications where uni-directionality and space limitation in designs are required.

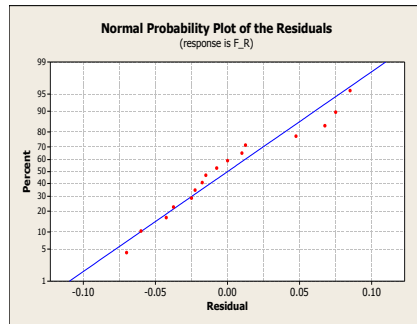
### 5.1 Suggestions for future work

Future work should include the study about mutual coupling of CBFSA's for potential applications of this antenna in arrays such as phase arrays.

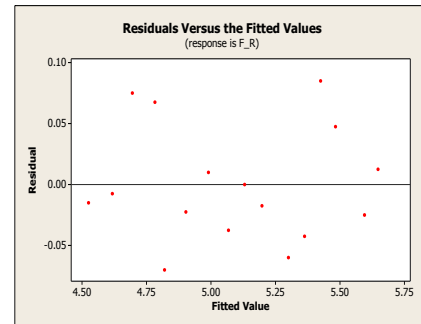
In order to reduce the influence that the feed has on the antenna responses, other feeds such as probe feeds should be proved. Additionally, other feeds for which less design variables are required, could help to reduce the number of factors that affect the antenna responses and therefore it could be possible to perform design of experiments, in which the cavity dimensions as well as the FSA dimensions are varied at the same time.

# APPENDIX A

In this appendix, the normal residual plots and the residuals versus fitted values plots for the interest responses of DOE I, DOE II, DOE III and DOE IV are presented. Information about the analysis of these plots is discussed in Chapter IV.

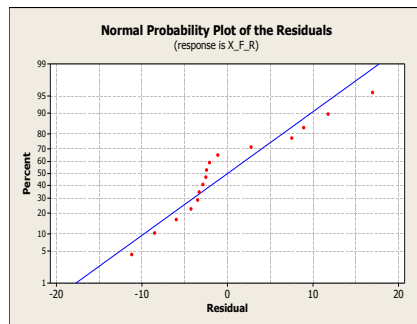


(a) Normal plot of residuals.

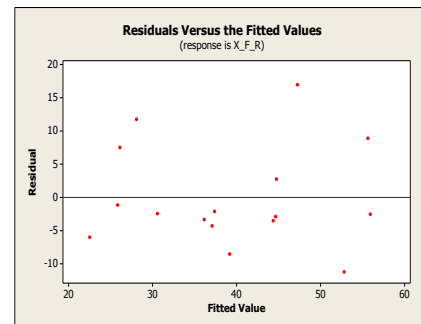


(b) Residuals versus predicted values.

Figure 5–1: Normal plot of residuals and residuals versus predicted values for  $F_R$  model of DOE I: (a) Normal plot of residuals ; and (b) Residuals versus predicted values.

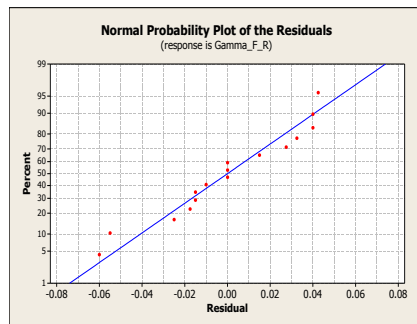


(a) Normal plot of residuals.

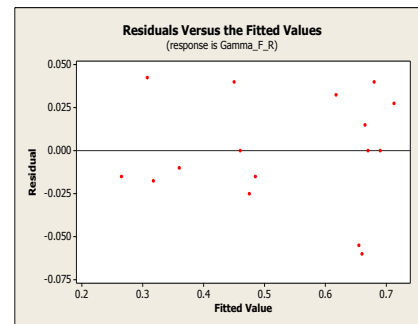


(b) Residuals versus predicted values.

Figure 5–2: Normal plot of residuals and residuals versus predicted values for  $X_{F_R}$  model of DOE I: (a) Normal plot of residuals ; and (b) Residuals versus predicted values.

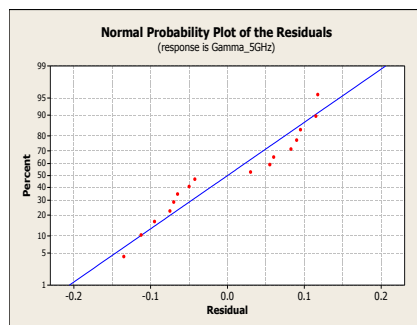


(a) Normal plot of residuals.

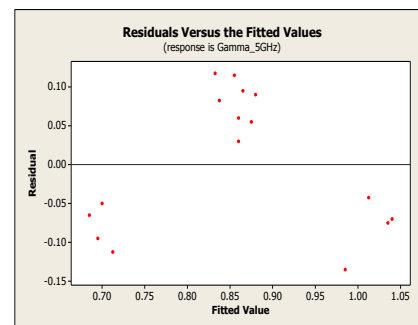


(b) Residuals versus predicted values.

Figure 5–3: Normal plot of residuals and residuals versus predicted values for  $\Gamma_{F_R}$  model of DOE I: (a) Normal plot of residuals ; and (b) Residuals versus predicted values.

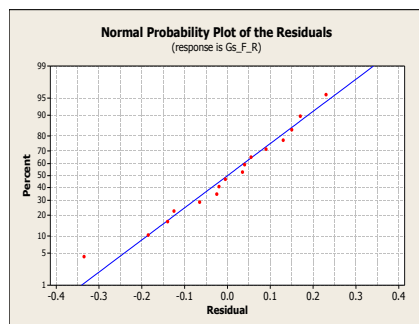


(a) Normal plot of residuals.

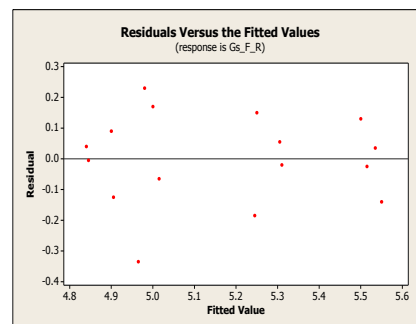


(b) Residuals versus predicted values.

Figure 5–4: Normal plot of residuals and residuals versus predicted values for  $\Gamma_{5GHz}$  model of DOE I: (a) Normal plot of residuals ; and (b) Residuals versus predicted values.

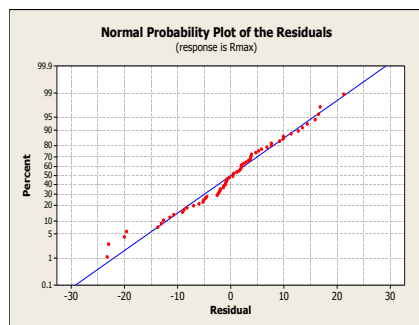


(a) Normal plot of residuals.

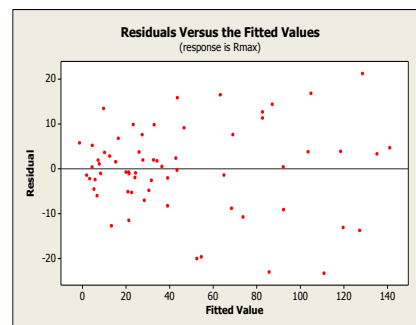


(b) Residuals versus predicted values.

Figure 5-5: Normal plot of residuals and residuals versus predicted values for Gs<sub>F\_R</sub> model of DOE I: (a) Normal plot of residuals ; and (b) Residuals versus predicted values.

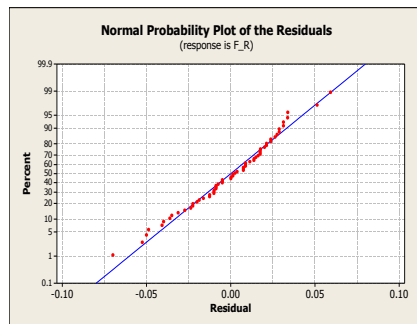


(a) Normal plot of residuals.

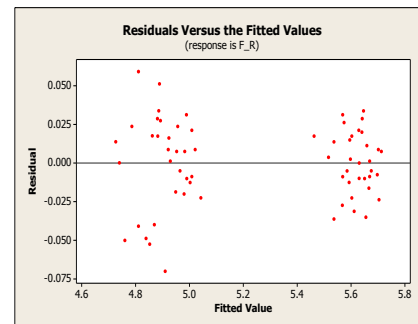


(b) Residuals versus predicted values.

Figure 5-6: Normal plot of residuals and residuals versus predicted values for Rmax model of DOE II: (a) Normal plot of residuals ; and (b) Residuals versus predicted values.

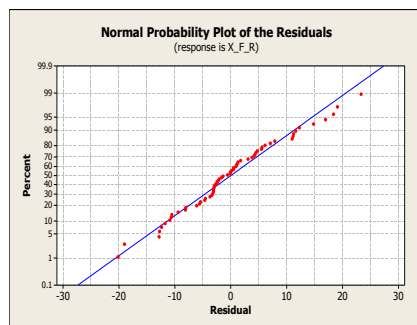


(a) Normal plot of residuals.

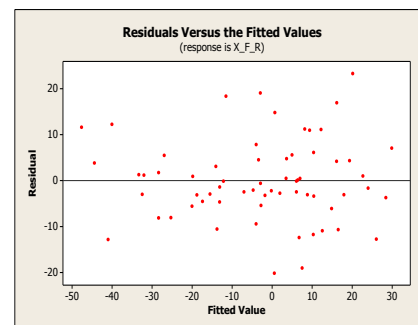


(b) Residuals versus predicted values.

Figure 5-7: Normal plot of residuals and residuals versus predicted values for  $F_R$  model of DOE II: (a) Normal plot of residuals ; and (b) Residuals versus predicted values.

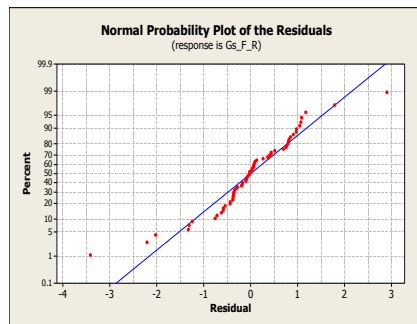


(a) Normal plot of residuals.

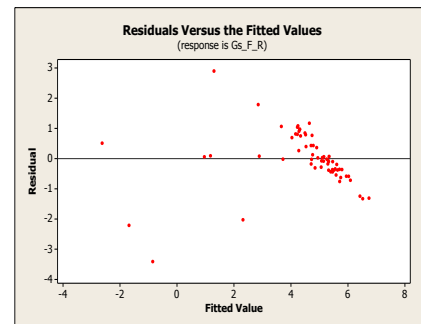


(b) Residuals versus predicted values.

Figure 5-8: Normal plot of residuals and residuals versus predicted values for  $X_{F_R}$  model of DOE II: (a) Normal plot of residuals ; and (b) Residuals versus predicted values.

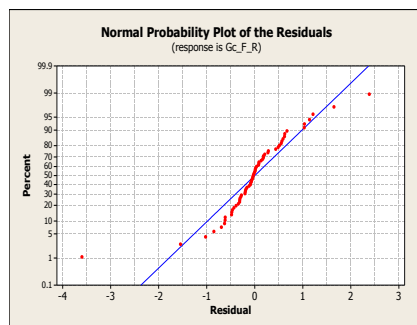


(a) Normal plot of residuals.

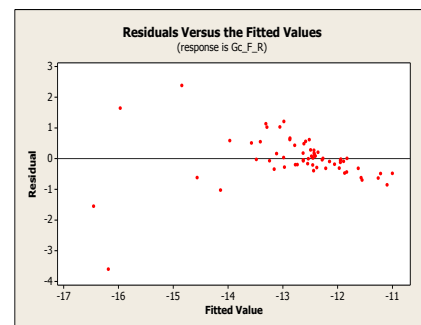


(b) Residuals versus predicted values.

Figure 5–9: Normal plot of residuals and residuals versus predicted values for  $G_{S_{F_R}}$  model of DOE II: (a) Normal plot of residuals ; and (b) Residuals versus predicted values.

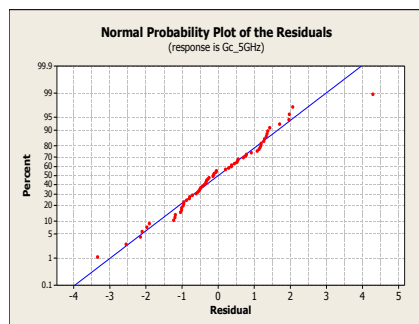


(a) Normal plot of residuals.

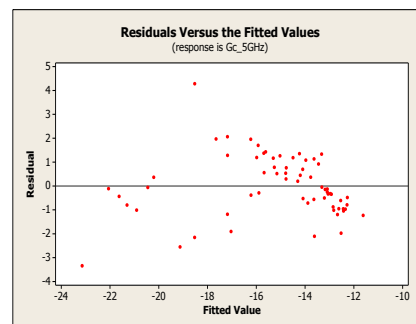


(b) Residuals versus predicted values.

Figure 5–10: Normal plot of residuals and residuals versus predicted values for  $G_{C_{F_R}}$  model of DOE II: (a) Normal plot of residuals ; and (b) Residuals versus predicted values.

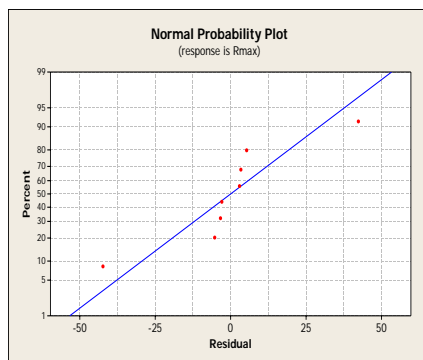


(a) Normal plot of residuals.

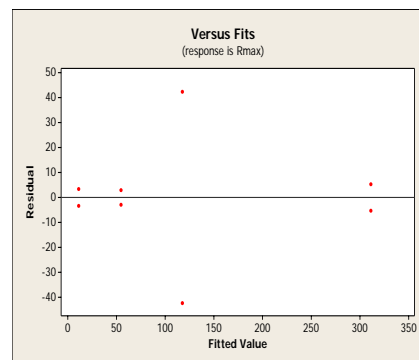


(b) Residuals versus predicted values.

Figure 5–11: Normal plot of residuals and residuals versus predicted values for  $Gc_{5GHz}$  model of DOE II: (a) Normal plot of residuals ; and (b) Residuals versus predicted values.

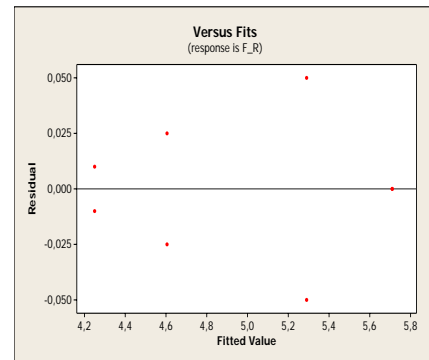
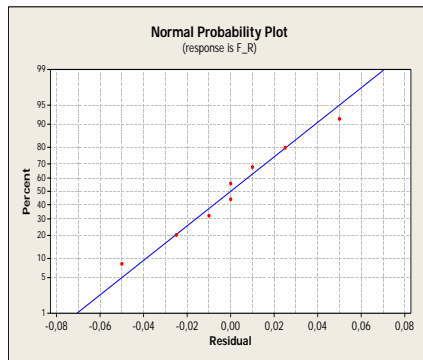


(a) Normal plot of residuals.



(b) Residuals versus predicted values.

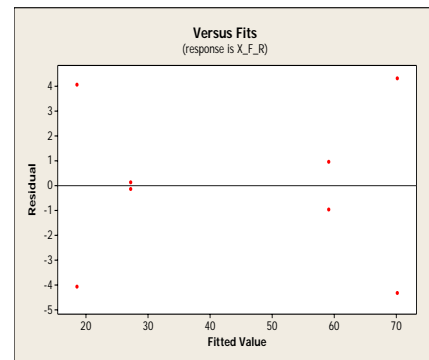
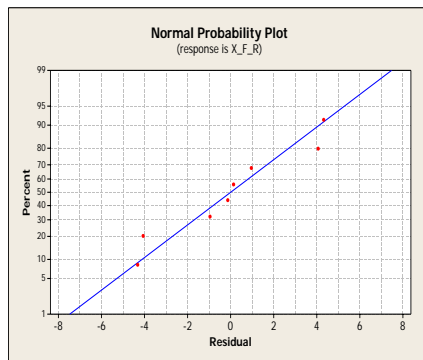
Figure 5–12: Normal plot of residuals and residuals versus predicted values for Rmax model of DOE III: (a) Normal plot of residuals ; and (b) Residuals versus predicted values.



(a) Normal plot of residuals.

(b) Residuals versus predicted values.

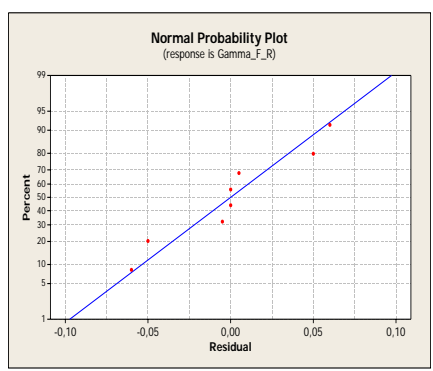
Figure 5–13: Normal plot of residuals and residuals versus predicted values for  $F_R$  model of DOE III: (a) Normal plot of residuals ; and (b) Residuals versus predicted values.



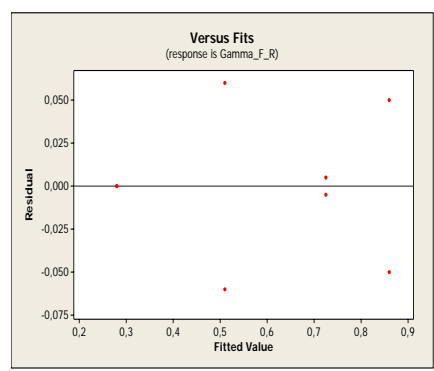
(a) Normal plot of residuals.

(b) Residuals versus predicted values.

Figure 5–14: Normal plot of residuals and residuals versus predicted values for  $X_{F_R}$  model of DOE III: (a) Normal plot of residuals ; and (b) Residuals versus predicted values.

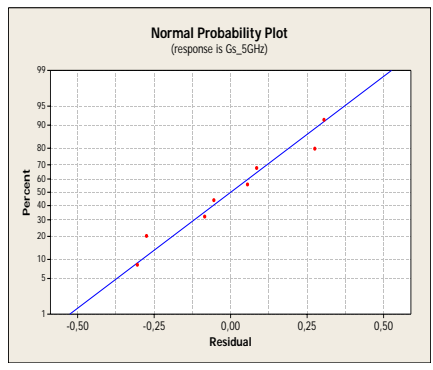


(a) Normal plot of residuals.

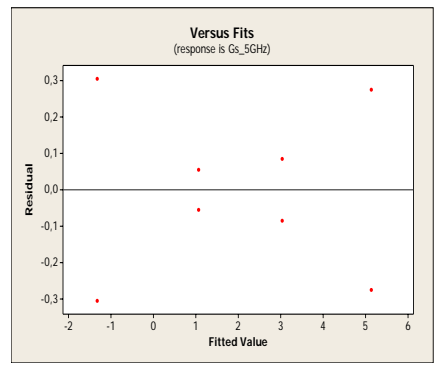


(b) Residuals versus predicted values.

Figure 5–15: Normal plot of residuals and residuals versus predicted values for  $\Gamma_{F\_R}$  model of DOE III: (a) Normal plot of residuals ; and (b) Residuals versus predicted values.

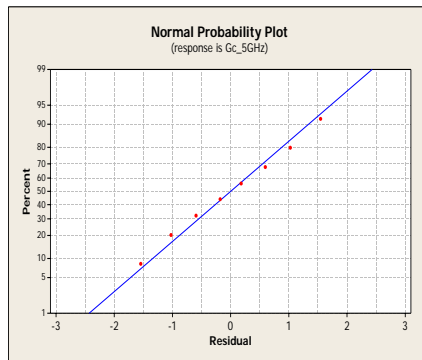


(a) Normal plot of residuals.

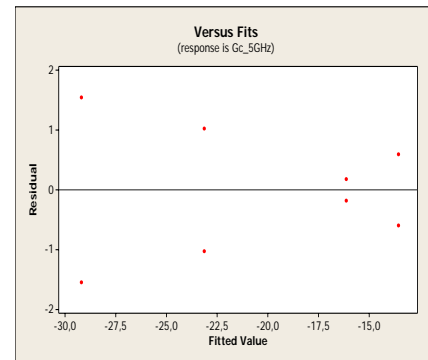


(b) Residuals versus predicted values.

Figure 5–16: Normal plot of residuals and residuals versus predicted values for  $Gs_{5GHz}$  model of DOE III: (a) Normal plot of residuals ; and (b) Residuals versus predicted values.

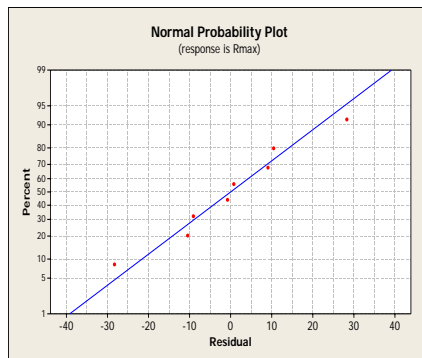


(a) Normal plot of residuals.

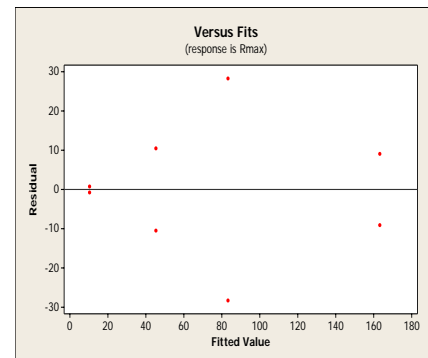


(b) Residuals versus predicted values.

Figure 5–17: Normal plot of residuals and residuals versus predicted values for Gc<sub>5GHz</sub> model of DOE III: (a) Normal plot of residuals ; and (b) Residuals versus predicted values.

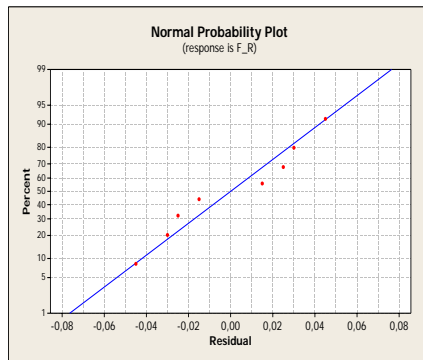


(a) Normal plot of residuals.

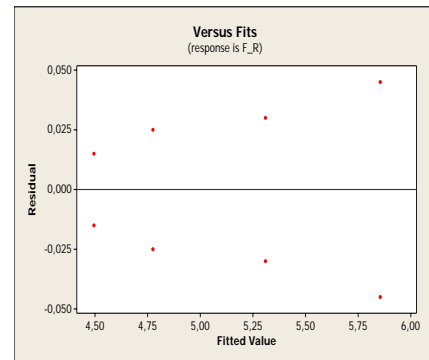


(b) Residuals versus predicted values.

Figure 5–18: Normal plot of residuals and residuals versus predicted values for Rmax model of DOE IV: (a) Normal plot of residuals ; and (b) Residuals versus predicted values.

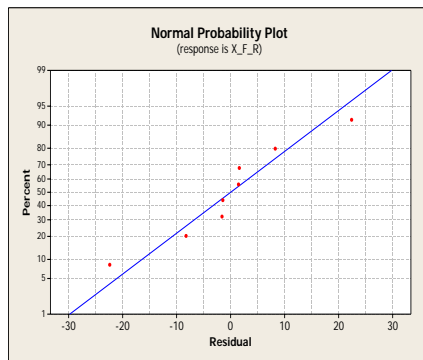


(a) Normal plot of residuals.

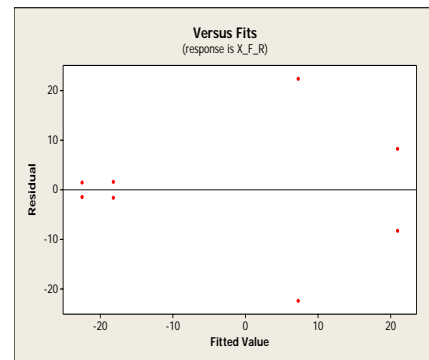


(b) Residuals versus predicted values.

Figure 5–19: Normal plot of residuals and residuals versus predicted values for  $F_R$  of DOE IV: (a) Normal plot of residuals ; and (b) Residuals versus predicted values.

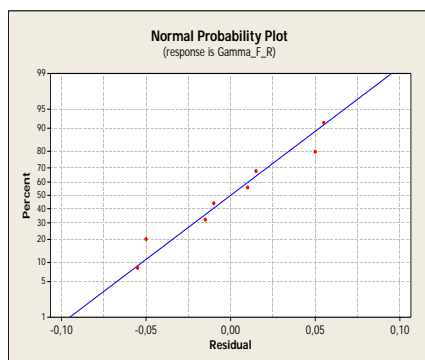


(a) Normal plot of residuals.

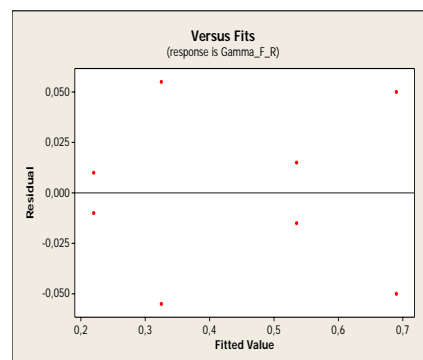


(b) Residuals versus predicted values.

Figure 5–20: Normal plot of residuals and residuals versus predicted values for  $X_{F_R}$  model of DOE IV: (a) Normal plot of residuals ; and (b) Residuals versus predicted values.

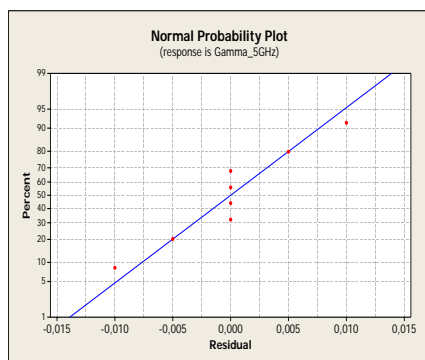


(a) Normal plot of residuals.

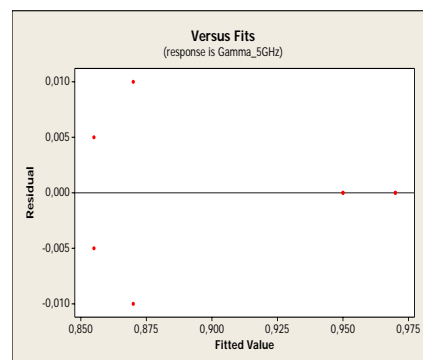


(b) Residuals versus predicted values.

Figure 5–21: Normal plot of residuals and residuals versus predicted values for  $\Gamma_{F\_R}$  model of DOE IV: (a) Normal plot of residuals ; and (b) Residuals versus predicted values.

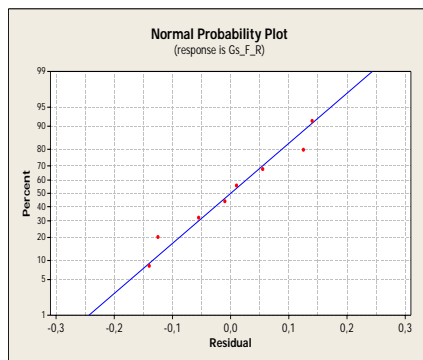


(a) Normal plot of residuals.

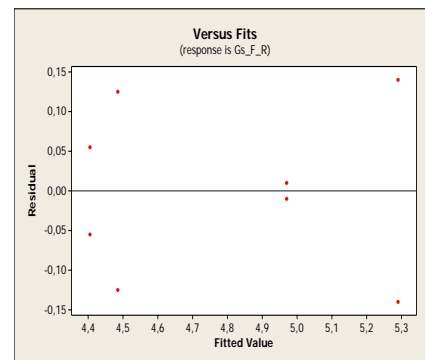


(b) Residuals versus predicted values.

Figure 5–22: Normal plot of residuals and residuals versus predicted values for  $\Gamma_{5GHz}$  model of DOE IV: (a) Normal plot of residuals ; and (b) Residuals versus predicted values.

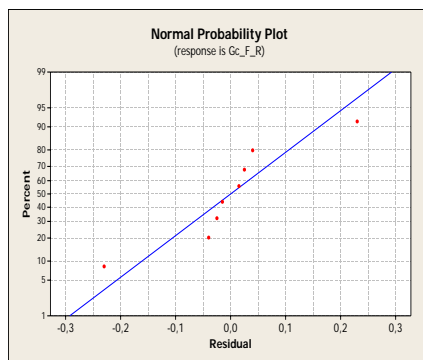


(a) Normal plot of residuals.

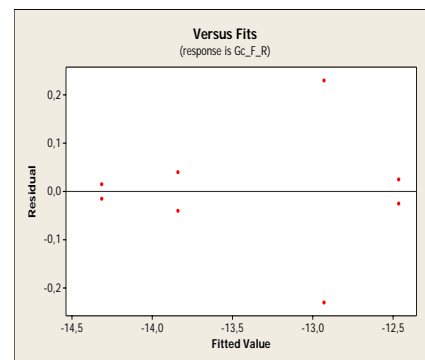


(b) Residuals versus predicted values.

Figure 5–23: Normal plot of residuals and residuals versus predicted values for  $Gs_{F_R}$  model of DOE IV: (a) Normal plot of residuals ; and (b) Residuals versus predicted values.

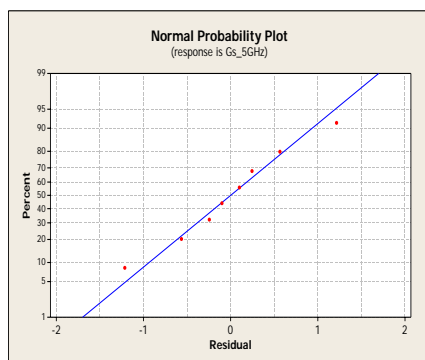


(a) Normal plot of residuals.

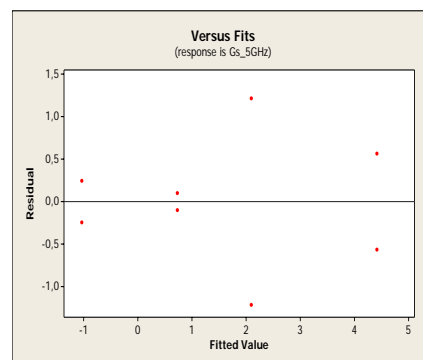


(b) Residuals versus predicted values.

Figure 5–24: Normal plot of residuals and residuals versus predicted values for  $Gc_{F_R}$  model of DOE IV: (a) Normal plot of residuals ; and (b) Residuals versus predicted values.

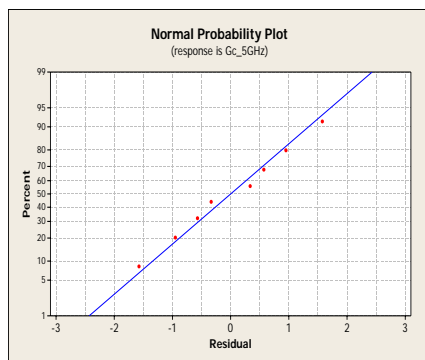


(a) Normal plot of residuals.

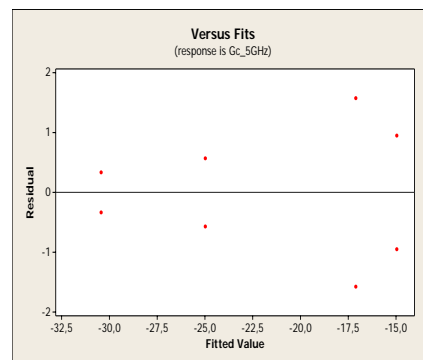


(b) Residuals versus predicted values.

Figure 5–25: Normal plot of residuals and residuals versus predicted values for  $Gs_{5GHz}$  model of DOE IV: (a) Normal plot of residuals ; and (b) Residuals versus predicted values.



(a) Normal plot of residuals.



(b) Residuals versus predicted values.

Figure 5–26: Normal plot of residuals and residuals versus predicted values for  $Gc_{5GHz}$  model of DOE IV: (a) Normal plot of residuals ; and (b) Residuals versus predicted values.

## REFERENCE LIST

- [1] T. Weller, L. Katehi, and G. Rebeiz, "Single and double folded-slot antennas on semi-infinite substrates," *IEEE Trans. Antennas Propag.*, vol. 43, no. 12, pp. 1423–1428, Dec 1995.
- [2] C. Wen, "Coplanar waveguide: A surface strip transmission line suitable for nonreciprocal gyromagnetic device applications," *IEEE Trans. Microw. Theory Tech.*, vol. 17, no. 12, pp. 1087–1090, Dec 1969.
- [3] R. N. Simmons and R. K. Arora, "Coupled slot line field components," *IEEE Trans. Antennas Propag.*, vol. 82, no. 7, pp. 1094–1099, Jul 1982.
- [4] P. B. R. Garg, I. Bahl and K. Gupta, *Microstrip Lines and Slotlines*. Norwood, MA: Artech House, 1996.
- [5] R. N. Simmons, *Coplanar Waveguide Circuits, Components and Systems*. John Wiley and Sons, 2001.
- [6] Q. Li and Z. Shen, "Inverted microstrip-fed cavity-backed slot antennas," *IEEE Antennas Wireless Propag. Lett.*, vol. 1, pp. 98–101, Nov. 1977.
- [7] G. Gauthier, S. Raman, and G. Rebeiz, "A 90-100 ghz double-folded slot antenna," *IEEE Trans. Antennas Propag.*, vol. 47, no. 6, pp. 1120–1122, Jun 1999.
- [8] H.-S. Tsai and R. York, "FDTD analysis of cpw-fed folded-slot and multiple-slot antennas on thin substrates," *IEEE Trans. Antennas Propag.*, vol. 44, no. 2, pp. 217–226, Feb 1996.
- [9] H. Tsai and R. York, "Multi-slot 50- $\Omega$  antennas for quasi-optical circuits," *Microwave and Guided Wave Letters, IEEE*, vol. 5, no. 6, pp. 180–182, Jun 1995.

- [10] N. Lopez-Rivera and R. Rodriguez-Solis, "Input impedance and resonant frequency characterization for folded slot antennas through doe techniques," vol. 2, June 2003, pp. 545–548 vol.2.
- [11] S.-Y. Chen and P. Hsu, "Cpw-fed folded-slot antenna for 5.8 ghz rfid tags," *Electronics Letters*, vol. 40, no. 24, pp. 1516–1517, Nov. 2004.
- [12] J. Galejs, "Admittance of a rectangular slot which is backed by a rectangular cavity," *IEEE Trans. Antennas Propag.*, vol. 11, no. 2, pp. 119–126, Mar 1963.
- [13] S. A. Long, "Experimental study of the impedance of cavity-backed slot antennas," *IEEE Trans. Antennas Propag.*, vol. AP-23, pp. 1–7, Jan. 1975.
- [14] C. Cockrell, "The input admittance of the rectangular cavity-backed slot antenna," *IEEE Trans. Antennas Propag.*, vol. 24, no. 3, pp. 288–294, May 1976.
- [15] D. M. Pozar, *Microwave Engineering*. John Wiley and Sons, 2005.
- [16] D. Rhodes, "On the stored energy of planar apertures," *IEEE Trans. Antennas Propag.*, vol. 14, no. 6, pp. 676–683, Nov 1966.
- [17] S. A. Long, "A mathematical model for the impedance of the cavity-backed slot antenna," *IEEE Trans. Antennas Propag.*, vol. AP-25, pp. 829–833, Nov. 1977.
- [18] A. Hadidi and M. Hamid, "Aperture field and circuit parameters of cavity-backed slot radiator," *Microwaves, Antennas and Propagation, IEE Proceedings H*, vol. 136, no. 2, pp. 139–146, Apr 1989.
- [19] J. Hirokawa, H. Arai, and N. Goto, "Cavity-backed wide slot antenna," *Microwaves, Antennas and Propagation, IEE Proceedings H*, vol. 136, no. 1, pp. 29–33, Feb 1989.
- [20] D. Jackson and N. Alexopoulos, "Gain enhancement methods for printed circuit antennas," *IEEE Trans. Antennas Propag.*, vol. 33, no. 9, pp. 976–987, Sep 1985.
- [21] W. Tan, Z. Shen, Z. Shao, and M. Fujise, "A gain-enhanced microstrip-fed cavity-backed slot antenna," vol. 2, Dec. 2005, pp. 4 pp.–.

- [22] W. Hong, N. Behdad, and K. Sarabandi, "Size reduction of cavity-backed slot antennas," *IEEE Trans. Antennas Propag.*, vol. 54, pp. 1461–1466, May 2006.
- [23] A. Adams, "Flush mounted rectangular cavity slot antennas—theory and design," *IEEE Trans. Antennas Propag.*, vol. 15, no. 3, pp. 342–351, May 1967.
- [24] R. C. Paryani, P. F. Wahid, and N. Behdad, "A wide-band, dual-polarized, differentially-fed cavity-backed slot antenna," *Antennas Applications Symposium*, pp. 132–142, 2008.
- [25] C.A. Balanis, *Advanced Engineering Electromagnetics*. John Wiley and Sons, 1989.
- [26] D. C. Montgomery, *Design and analysis of experiments*. John Wiley Sons, Inc., 2001.
- [27] N. Lopez-Rivera, *Characterization and modeling of folded-slot antennas, Master's thesis*. University of Puerto Rico-Mayaguez, Department of Electrical and Computer Engineering, Mayaguez, Puerto Rico, 2003.
- [28] P. Lozada, *Design and characterization of log Periodic rectangular slot ring antenna, Master's thesis*. University of Puerto Rico-Mayaguez, Department of Electrical and Computer Engineering, Mayaguez, Puerto Rico, 2008.
- [29] A. M. Castro, *Tunable folded-slot antenna with thin film ferroelectrical material, Master's thesis*. University of Puerto Rico-Mayaguez, Department of Electrical and Computer Engineering, Mayaguez, Puerto Rico, 2003.
- [30] C. Jaramillo, *Design and Characterization of Broad Band and Multi-Band Slot Ring, Master's thesis*. University of Puerto Rico-Mayaguez, Department of Electrical and Computer Engineering, Mayaguez, Puerto Rico, 2004.
- [31] A. Amador, *Characterization of asymmetric and annular slot antennas and a design of a tunable asymmetric annular-slot antenna with ferroelectrical material, Master's thesis*. University of Puerto Rico-Mayaguez, Department of Electrical and Computer Engineering, Mayaguez, Puerto Rico, 2006.

- [32] J. Papapolymerou, C. Schwartzlow, and G. Ponchak, “A folded-slot antenna on low resistivity si substrate with a polyimide interface layer for wireless circuits,” *Silicon Monolithic Integrated Circuits in RF Systems, 2001. Digest of Papers. 2001 Topical Meeting on*, pp. 215–218, 2001.
- [33] M. Scardelletti, G. Ponchak, J. Jordan, and S. Merritt, “Reduced size folded slot antennas with capacitive loading,” *Antennas and Propagation Society International Symposium, 2008. AP-S 2008. IEEE*, pp. 1–4, July 2008.

# CHARACTERIZATION OF CAVITY-BACKED FOLDED SLOT ANTENNAS

María Fernanda Córdoba-Erazo

(787) XXX-XXXX

Department of Electrical and Computer Engineering

Chair: Rafael Rodríguez Solís

Degree: Master of Science

Graduation Date: June 2009

In this thesis, two Cavity-Backed Folded-Slot Antennas (CBFSA's) are characterized through the Design Of Experiments technique (DOE) to study the influence that the Folded-Slot Antennas (FSA) and cavity dimensions of each CBFSA have on the following responses: resistance, frequency, reflection coefficient and gain in the substrate and cavity side. The antennas characterized were: the CPW-capacitively fed CBFSA and the CPW-inductively fed CBFSA. Two  $2^k$  factorial DOE's are proposed for performing the characterization of each antenna. The designs proposed in the DOE's are simulated in the High Frequency Structure Simulator (HFSS) and the results obtained were statistically analyzed. Linear regression models for each response of the CBFSA's are presented. Some CBFSA designs were fabricated in order to validate the simulations. The CPW-inductively fed CBFSA achieves gain of 4.28 dB and reflection coefficient  $< 0.33$  or VSWR  $< 2$  at 4.5 GHz, whereas the CPW-capacitively fed CBFSA achieves gain of 4.63 dB and reflection coefficient  $< 0.33$  or VSWR  $< 2$  at 4.5 GHz. The radiation patterns of the antennas are uni-directional and Front-to-Back-Ratio (FBR) about 15 dB is obtained.